

**Design and development of a low-cost high-performance
vehicle mounted UHF RFID system for tracking goods and
inventory**

*This dissertation submitted in fulfilment of the requirements
for the degree of Master of Sciences: Electronic Engineering
in the*

Howard College of Agriculture, Engineering & Science

University of KwaZulu-Natal, Durban - 4041

South Africa.

Student:

Mr. Sheridan Joash Naidoo

Supervisor:

Adv. Dr. Ernest Bhero

Co-supervisor:

Prof. Alwyn Hoffman

05 May 2020

EXAMINER'S COPY

As the candidate's Supervisor I agree to the submission of this thesis.

Adv. Dr. Ernest Bhero  Date 6 October 2020

Table of Contents

Acknowledgements	i
Plagiarism	ii
List of Figures	iii
List of Tables	v
List of Abbreviations	vi
List of Publications	vii
Abstract	viii
1. INTRODUCTION	1
1.1. RFID spectrum	2
1.2. RFID Tags	2
1.3. RFID Reader system	4
1.4. Problem definition	5
1.5. Research questions	5
1.6. Research Work Contribution.....	5
1.7. Organisation of the thesis	5
2. REVIEW OF LITERATURE	7
3. MATERIALS AND METHODS	17
4. CIRCULARLY POLARIZED MICROSTRIP PATCH ANTENNA DESIGN	20
4.1. Introduction.....	20
4.1.1. Metallic patch	22
4.1.2. Dielectric substrate.....	22
4.1.3. Ground plane	22
4.1.4. Feeding techniques	23
4.2. Antenna design and geometry	24
4.3. Results	29
4.4. Discussion	35

5. SIMULATION FOR MONITORING CONTAINARIZED CARGO IN AN UHF-RFID SYSTEM	36
5.1. Introduction.....	36
5.2. Finite Difference Time Domain method.....	36
5.2.1. Maxwell's equations in three dimensions.....	36
5.2.2. Maxwell's equations in two dimensions	39
5.2.3. Maxwell's equations in one dimension.....	40
5.2.4. Yee's algorithm	42
5.2.5. gprMax software.....	54
5.3. Simulation.....	55
5.3.1. Modelling.....	55
5.3.2. Testing procedure	59
5.3.3. Validation	68
5.3.4. Discussion.....	69
5.4. Practical results	70
5.4.1. Component selection.....	70
5.4.2. Testing procedure in a container	72
5.4.3. Results in shipping container.....	80
5.4.4. Testing procedure in free space	85
5.4.5. Results in free space.....	89
5.4.6. Discussion.....	95
6. DISCUSSION AND CONCLUSION	100
6.1. Research work objectives	100
6.2. Summary of all results and validation	100
6.3. Research contribution.....	102
6.4. Recommendations.....	102
6.5. Future research work.....	103
7. REFERENCES.....	105

Acknowledgements

Firstly, I wish to express my deepest gratitude to my supervisor Adv. Dr. Bhero and co-supervisor Prof A. Hoffman for their support and guidance in this research. I would also like to offer a special thank you to Adv. Dr. Bhero for his continuous mentorship during the course of this thesis and always making himself available when I needed support. I wish to acknowledge the support from Dr P. Kumar who assisted me in the development of the antenna.

Secondly, I would like to thank my family for their support whilst working on this thesis. No matter what difficulties I faced, they provided unwavering support. This thesis is dedicated to them.

Thirdly, this thesis would also not have been possible without the assistance from Mr. Craig Beer and his company Taggit. I would like to sincerely thank him for the equipment he provided to conduct the tests in this thesis and his advice on the practicality of undertaking a project like this.

Lastly, I would like to thank The Almighty for providing me with the strength, knowledge and wisdom to embark on this research work. Without His guidance this work would have not been possible.

Plagiarism

I SHERIDAN JOASH NAIDOO declare that:

- (i) The research reported in this dissertation/thesis, except where otherwise indicated, is my original research.
- (ii) This dissertation/thesis has not been submitted for any degree or examination at any other university.
- (iii) This dissertation/thesis does not contain other persons' data, pictures, graphs or other information, unless specifically acknowledged as being sourced from other persons.
- (iv) This dissertation/thesis does not contain other persons' writing, unless specifically acknowledged as being sourced from other researchers. Where other written sources have been quoted, then:
 - a) their words have been re-written but the general information attributed to them has been referenced;
 - b) where their exact words have been used, their writing has been placed inside quotation marks, and referenced.
- (v) Where I have reproduced a publication of which I am author, co-author or editor, I have indicated in detail which part of the publication was actually written by myself alone and have fully referenced such publications.
- (vi) This dissertation/thesis does not contain text, graphics or tables copied and pasted from the Internet, unless specifically acknowledged, and the source being detailed in the dissertation/thesis and in the References sections.



Sheridan Joash Naidoo (05 May 2020)

List of Figures

Figure 1: RFID systems used in logistics [2].	1
Figure 2: Components used in a passive UHF RFID tag [6].	2
Figure 3: Overview of the implementation of the mobile RFID setup [21].	9
Figure 4: Breakdown of the vehicle Terminal Equipment [15].	9
Figure 5: Workflow of the three modes [15].	10
Figure 6: Tracking of vehicle [15].	11
Figure 7: ECTS flow diagram [18].	12
Figure 8: Experimental space used, with the blue dots representing the data points [23].	13
Figure 9: Plot of the transponder with null zones [23].	14
Figure 10: Geometries for patches [26].	22
Figure 11: Geometry of the proposed square patch antenna.	24
Figure 12: Equivalent circuit.	28
Figure 13: Fabricated antenna top view.	28
Figure 14: Fabricated antenna side view.	29
Figure 15: S11 parameter of the antenna.	29
Figure 16: VSWR of the antenna.	30
Figure 17: Radiation patterns at (a) 886MHz (b) 891 MHz (c) 903MHz (d) 924 MHz. ...	31
Figure 18: Directivity and gain versus frequency.	32
Figure 19: Radiation efficiency versus frequency.	32
Figure 20: Axial ratio of the antenna.	33
Figure 21: Axial ratio vs. theta for varying frequencies.	33
Figure 22: FDTD Yee cell displaying the electric (red) and magnetic (green) fields [67].	42
Figure 23: FDTD Yee cell displaying the electric (red), magnetic (green) and zeroed out fields (grey) [67].	55
Figure 24: Geometry of the scenario to be investigated.	56
Figure 25: Location of position 1 and position 2 within the container.	56
Figure 26: Propagation of EM waves inside a steel, (a) time step = 1, (b) time step = 2, (c) time step = 3, (d) time step = 4.	60
Figure 27: Graph of thickness vs power (dBm) for steel.	61
Figure 28: E-field pattern for a thickness value of 1 (2 mm) for steel.	62
Figure 29: E-field pattern for a thickness value of 10 (20 mm) for steel.	62
Figure 30: Graph of thickness vs power (dBm) for plastic.	63

Figure 31: E-field pattern for a thickness value of 1 (5 mm) for plastic.....	64
Figure 32: E-field pattern for a thickness of 10 (50 mm) for plastic.	65
Figure 33: Graph of thickness vs power (dBm) for wood.	66
Figure 34: E-field pattern for a thickness of 1 (20 mm) for wood.....	67
Figure 35: E-field pattern for a thickness of 10 (200 mm) for wood, (a) time step = 1, (b) time step = 2, (c) time step = 3, (d) time step = 4.	67
Figure 36: Experimental setup [71].....	68
Figure 37: Readability of the RFID tag at different thicknesses of mild steel (a) 1 mm thick mild steel, (b) 1.5mm thick mild steel [23].....	69
Figure 38: Practical testing setup inside the steel container.	73
Figure 39: Alien ALR-9680 commercial 4-port RFID reader [61].....	74
Figure 40: Alien RFID graphical user interface.	74
Figure 41: Placing of the UHF RFID antenna connected to a 50-ohm cable.....	75
Figure 42: Master's student (Mr S.J Naidoo) placing the RFID tag mount.	75
Figure 43: Master's student supervisor (Adv. Dr. E. Bhero) placing the RFID tag mount.	76
Figure 44: Plastic RFID tag mount with a RFID tag affixed to it.	77
Figure 45: Plastic container located inside the truck's container during testing.....	78
Figure 46: Materials used, steel (left), plastic (middle), wood (right).	79
Figure 47: Side view of thickness for each material.....	79
Figure 48: Hardware setup using an Alien RFID reader and a laptop.	86
Figure 49: Sample space used to perform the free space experiments.	86
Figure 50: Placement of UHF RFID antenna with a 50-ohm connector cable.....	87
Figure 51: Investigate the effects of wood on the RFID system.....	88
Figure 52: Readability probability for plastic.	95
Figure 53: Readability probability for wood.....	96
Figure 54: Graph of RFID tag orientation vs readability percentage for steel.....	97
Figure 55: Graph of RFID tag orientation vs readability percentage for plastic.	97
Figure 56: Graph of RFID tag orientation vs readability percentage for wood.....	97
Figure 57: Graph of distance vs material using a paper RFID tag in a horizontal orientation.....	98
Figure 58: Graph of distance vs material using a paper RFID tag in a vertical orientation.	98
Figure 59: Directivity of the proposed antenna.	99

List of Tables

Table 1: Comparison between passive and active RFID tags based on various criteria [8].	3
Table 2: Advantages and disadvantages of a microstrip patch antenna [31].	20
Table 3: Comparison of the different feeding techniques and their characteristics [50].	23
Table 4: Dimensions of patch antenna.	27
Table 5: Main lobe and angular width for varying frequencies.	31
Table 6: Comparison of antennas.	34
Table 7: Cost analysis.	34
Table 8: Thickness values of the materials used.	59
Table 9: Locations of the positions to be investigated inside the steel container.	73
Table 10: Readability of a metal RFID tag using steel inside steel container.	80
Table 11: Readability of a paper RFID tag using steel inside steel container.	81
Table 12: Readability of a metal RFID tag using plastic inside steel container.	82
Table 13: Readability of a paper RFID tag using plastic inside steel container.	83
Table 14: Readability of a metal RFID tag using wood inside steel container.	84
Table 15: Readability of a paper RFID tag using wood inside steel container.	84
Table 16: Readability of a metal RFID tag using steel in free space.	89
Table 17: Readability of a paper RFID tag using steel in free space.	90
Table 18: Readability of a metal RFID tag using plastic in free space.	91
Table 19: Readability of a paper RFID tag using plastic in free space.	92
Table 20: Readability of a metal RFID tag using wood in free space.	93
Table 21: Readability of a paper RFID tag using wood in free space.	94

List of Abbreviations

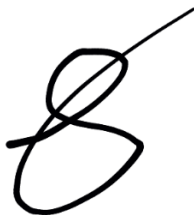
Abbreviations	Full form
UHF	Ultra High Frequency
RFID	Radio Frequency Identification
EM	Electromagnetic
AR	Axial Ratio
CST	Computer Simulation Technology
ITU	International Telecommunication Union
IC	Integrated Circuit
TOM	Tag Operation Module
GSM	Global System for Mobile
GPRS	General Packet Radio Service
GPS	Global Positioning System
TE	Terminal Equipment
ECTS	Electronic Cargo Tracking System
TC	Tansit Checkpoint
NLOS	Non-Line of Sight
RF	Radio Frequency
PCB	Printed Circuit Board
FDTD	Finite Difference Time Domain
GUI	Graphical User Interface
SMA	SubMiniature version A
WLAN	Wireless Local Area Network
VSWR	Voltage Standing Wave Ratio
TEM	Transverse Electromagnetic
GPIO	General Purpose Input/Output
API	Application Programme Interface
RAM	Random Access Memory
EIRP	Effective Isotropic Radiated Power

List of Publications

DETAILS OF CONTRIBUTION TO PUBLICATIONS that form part and/or include research presented in this dissertation (include publications in preparation, submitted, *in press* and published and give details of the contributions of each author to the experimental work and writing of each publication)

1. "Naidoo, S.J., Bhero, E., Hoffman, A. & Kumar, P., 2020, 'A Low Cost Circularly Polarized Microstrip Patch Antenna with Low Axial Ratio for UHF RFID Applications, International Journal of Microwave and Optical Technology (IJMOT), Manuscript Id: IJMOT-2020-2-11909, 9 pages. <https://www.ijmot.com/VOL-15-NO-3.aspx>" Chapter 4 (Accepted on the 22nd April 2020) (Accredited). The candidate was responsible for developing the simulation model of the antenna, analysing and presenting the data. The candidate was also responsible for writing the complete manuscript. Dr. P. Kumar assisted the candidate during the simulations, fabrication and testing processes of the antenna. Adv. Dr. E. Bhero is the candidate's supervisor and Prof A. Hoffman is the candidate's co-supervisor.

2. "Naidoo, S.J., Bhero, E. & Hoffman, A., 2020, 'Performance of an UHF-RFID System in Monitoring Containerized Cargo, International Journal of Radio Frequency Identification Technology and Applications (IJRFITA), Manuscript Id: IJRFITA-287183, 9 pages." Chapter 5 (Submitted on the 30th March 2020) (Accredited). The candidate was responsible for developing the simulation model, analysing and presenting the data. The candidate was also responsible for writing the complete manuscript. Adv. Dr. E. Bhero is the candidate's supervisor and Prof A. Hoffman is the candidate's co-supervisor.



Sheridan Joash Naidoo (05 May 2020)

Abstract

This research work investigates how to design and implement a low-cost high-performance vehicle mounted ultra-high frequency (UHF) radio frequency identification (RFID) system to keep track of cargo whilst in transit. The vehicle mounting include – inside or on cargo vehicle enclosures, the shipping containers, and so forth. In order to achieve a low-cost system, a low cost circularly polarized microstrip patch antenna, which also had a low axial ratio (AR) was designed. Since multiple antennas will be used, the cost factor will be reduced substantially if the cost of each antenna was reduced as compared to reducing the cost of a single RFID reader.

The proposed antenna design, measuring 200mm x 200mm x 6.4mm, utilized the corner-truncated technology with a thicker substrate and larger ground plane. Two independent simulations were done as well as empirical work. One of the simulations used Computer Simulation Technology (CST) studio suite software and the other used gprMax simulation software. The investigations aimed at determining how different materials (steel, plastic, and wood) worsen the performance of the UHF RFID system inside a steel container as well as in free space. The investigation involved placing these materials onto the RFID tag and then varying the thickness of the material.

The simulation results showed that the proposed antenna has a reflection coefficient of less than -10dB from 886.23 MHz to 924.96 MHz with a bandwidth of 38.73 MHz. The antenna provides the AR less than 3 dB for the frequency range from 915 MHz to 919 MHz. The designed and fabricated antenna has a bandwidth of 57.527 MHz and achieves a minimum reflection coefficient of -27.97 dB at 914.045 MHz. These results were then compared to other similar antenna designs. The antenna designed in this research achieved a lower axial ratio while still offering a respectable amount of gain, directivity and bandwidth. Previous papers showed that there was always a notably trade-off between having a low axial ratio and a high gain, directivity or bandwidth. The results for the simulation tests indicated that wood performs the best, followed by plastic and then steel. Wood and plastic were still detected by the RFID reader's antenna at their maximum thickness of 20cm and 5cm respectively. It was further found out that the RFID system performs better inside a steel container than in free space.

In conclusion the design of a low-cost high-performance circularly polarized microstrip patch antenna allows the cost of the overall UHF RFID system to be reduced, making it a more cost-effective solution for tracking containerized cargo. The antenna also achieved circular polarization which is beneficial to the performance of the UHF RFID system. A

circularly polarized antenna allows the UHF RFID reader to detect RFID tags in almost any orientation. The simulation results emulate the data obtained when a horizontally orientated paper RFID tag was used. The results obtained showed the use of steel performed optimally when it is placed directly in line with the receiver. When using plastics, placing them directly in line with the receiver at a distance of 2.36 m, does not offer the best performance. If the plastic material is placed 3 m to the side of the receiver, it is best to use thicker material. The power increased by 3.73 dBm when the thickness of the plastic, increased from 5 mm to 50mm. The system's performance increased with wood when the RFID tag is in line with the receiver at a distance of 2.36 m, and as the thickness was increased from 20 mm to 200 mm. When the RFID tag was placed 3 m to the side of the receiver, the system's performance decreased as the thickness was increased from 20 mm to 200 mm.

1. INTRODUCTION

Radio frequency identification (RFID) systems utilize electromagnetic (EM) fields in order to identify items automatically. Data is stored such as, an identification number of an item, within a microchip. This microchip is then attached to the item. The data on the microchip can then be retrieved by using a reader. An RFID system comprises of three fundamental components. The first component is an RFID tag or transponder, that holds the data and is affixed to the item. The second component is the RFID reader or interrogator, which retrieves the data on the RFID tag by scanning it. The third component is the computer that then controls the flow of the incoming data from the RFID reader and converts it into meaningful data that the user can then interpret [1]. The focus of this thesis is broken down into two investigations. The first investigates whether a low-cost high-performance circularly polarized microstrip patch antenna can be designed in order to reduce the cost of the overall system. The cost and performance of the antenna was benchmarked against a commercial 8dBi UHF Poynting antenna and prior literature, respectively. The second investigates what effect will the interference caused by different materials have on the performance of the UHF RFID system inside a metal enclosure (shipping/steel container).

The results from these investigations will be used to ascertain if goods can be tracked inside a shipping container that is in transit. Tracking of goods and inventory on a shipping container is a labor-intensive task. This is mainly due to the user manually scanning each item before it is loaded onto a container, which is affixed with an RFID tag using a UHF RFID reader. Also, this process is costly. Another problem with this system is security. From Figure 1, it can be shown that the inventory is only recorded, using a RFID portal/gate, when the truck leaves the warehouse and when it arrives at the intended destination. Hence the contents of the truck are most vulnerable during the transportation stage. If the contents of the truck are stolen during transit, i.e., the distribution part, there is no way of promptly detecting this theft of goods until the truck arrives at its destination. In addition, it will be time-consuming for the company to go through the contents of the container to see what goods are missing. This will, in turn, delay the process of reporting the theft of goods to the authorities due to the company not having an accurate report on the exact goods stolen.

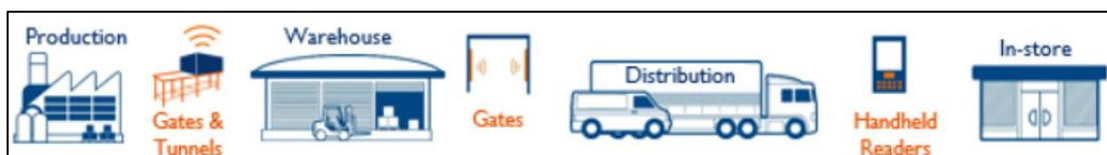


Figure 1: RFID systems used in logistics [2].

1.1. RFID spectrum

The radio frequency or RF spectrum forms part of the EM spectrum. The frequency band within which the RF spectrum belongs to is from 30Hz to 300GHz. The use of this spectrum is strictly regulated by national laws, which are all overseen by the International Telecommunications Union (ITU) [3]. This is also locally overseen by the Independent Communications Authority of South Africa (ICASA). RFID technology utilizes this spectrum. Each band is used for a specific application when used in conjunction with the RFID technology. There exist four frequency bands namely; low frequency, high frequency, ultra-high frequency and super high frequency. This thesis however focuses on the ultra-high frequency band. This frequency band is from 300-3000MHz. The UHF band was chosen because unlike the other bands, it offers faster read rates as compared to the low and high frequency. The UHF band also offers a greater read range as compared to low and high frequency bands. In addition, its performance is still good in a metal environment and is inexpensive as compared to the super-high frequency band [4].

1.2. RFID Tags

RFID tags are attached to various objects. These tags are made of two parts as shown in Figure 2. The initial part is the antenna, which accepts the radio-frequency waves and the second part is an integrated circuit (IC). An IC was utilised to perform three tasks; process data, store data and to modulate and demodulate radio waves that are transmitted or received by the RFID tag's antenna [5].

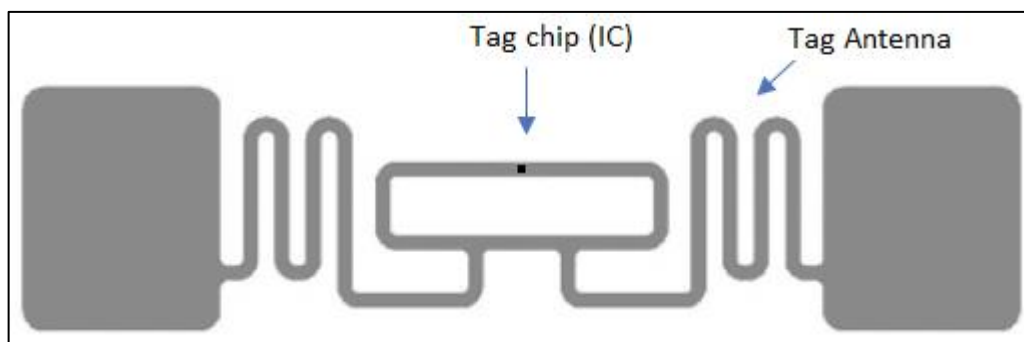


Figure 2: Components used in a passive UHF RFID tag [6].

There are two types of RFID tags, namely, passive and active. Passive RFID tags only consist of an internal antenna and an IC. This type of tag uses the RFID reader's transmitted radio waves to power it. It does this by utilising the transmitted radio-waves, which induces a current in the tag's antenna. The advantages of using passive tags are long life span due to the absence of internal battery, and it is small, inexpensive and lightweight. One of the shortcomings is that the RFID tags can only be read in close

proximity with its RFID reader [7]. Active tags are comparable to passive tags, but these tags have an internal power supply such as a battery. The internal power supply allows active RFID tags to be read from a far more significant distance when compared to passive RFID tags. However, having an internal power supply does compromise on other critical aspects of the active RFID tag, such as the lifespan is reduced, cost increases, footprint increases, and maintenance are also required. Table 1 compares the passive RFID tag to an active RFID tag.

Table 1: Comparison between passive and active RFID tags based on various criteria [8].

	Passive RFID tag	Active RFID tag
Application	Keep track of goods in a specific area.	Keep track of goods throughout an entire building.
Range	1-5m	> 30m
Cost	Inexpensive	Expensive
Battery life	Battery free	3-5 years
Environment constraints	Easy to seal, hence more robust and hard wearing.	Difficult to seal due to internal batteries, hence less robust and wears quicker than passive tags.

The reliability of RFID technology in terms of the RFID tag depends on the readability of the tags. Hence, in order for the RFID tag technology to be successful, the readability has to be maximized. Some of the technical challenges faced by RFID tags include maximizing collected energy for passive RFID tags, tag and antenna size, anti-collision protocols, reading rate and battery life for active tags.

Even though this technology has been implemented commercially, there still exists limitations of this technology. Some of these limitations include the following [9]:

1) *Standardization*

The selection of RFID tags is based on the application and the environment. However, there is still some freedom of choice when it comes to a choice of communication protocols and its format and the amount of information that is stored on the tag.

Standards are essential when it comes to companies sharing their applications with other companies. If standards do not exist, the products offered by these companies will encounter conflicts. Some of the standards that need to be agreed on are communication protocols, signal modulation types, data transmission rates, data encoding and frames and collision handling algorithms.

2) *Collision*

Reading many RFID tags at once will cause signal collision at the RFID reader's side. In addition, data will also be lost. In order to resolve this issue, anti-collision algorithms can be employed. Anti-collision algorithms are designed to sort and individually select RFID tags. The quantity of tags that can be read is dependent on two factors, namely the protocol used and the frequency. High frequencies (HF) typically range from 50 tags/s, and Ultra High frequencies typically range from 200 tags/s [10].

3) *Security and privacy issues*

RFID tags in relation to the supply chain will contain information that may or may not be sensitive data. In the case of RFID tags containing sensitive data, security systems need to be put in place. These security systems will prevent any unauthorised personnel from accessing the contents of the package, modify or corrupt the data contents and duplicating the data from the RFID tag. The following three scenarios could take place in a supply chain, namely industrial sabotage, industrial espionage and counterfeiting [11].

1.3. RFID Reader system

RFID readers typically work by transmitting a pulse of radio-waves towards the RFID tag. The RFID reader then listens and waits for the response. The response is transmitted by the RFID tag. The reader then uses the response to acquire valuable information such as the serial number. In more advanced RFID readers, the transmitted pulse will allow the reader to read or write memory onto a RFID tag or to transmit commands and passwords [12].

A more detailed operation of how a RFID reader works is as follows. A RFID reader consists of a radio frequency module. This module contains a transmitter, receiver and a microprocessor. The transmitter is further broken down into four components, namely an oscillator, modulator, amplifier and an antenna. The oscillator is used to generate a carrier signal. Once the carrier signal has been generated, the modulator is used to impose an input signal on it. The modulated signal is finally amplified using the amplifier. The receiver on the other hand only consists of two parts, namely a demodulator and amplifier. The demodulator is used to retrieve information from the modulated carrier wave. The demodulated signal is then amplified. The amplified signal is then sent for processing. The processing of data occurs in the microprocessor [13].

Some of the limitations of the RFID reader include the following [14]:

1) *Equivalent Isotropic Radiated Power (EIRP)*

This is used to determine the power of the signal transmitted by the RFID reader in the direction of the RFID tag.

2) *Sensitivity*

This is defined as the minimum level of the tag signal which the RFID reader can detect and resolve. It is defined with respect to the signal-to-noise ratio at the receiver's end.

1.4. Problem definition

Two problems were identified in this research. Firstly, certain papers do investigate the performance of an RFID system in the presence of materials that degrades the performance of the RFID system [15, 16, 17, 18] . Unfortunately, limited research was done to investigate the performance of the RFID system when these materials are placed inside a metal enclosure (shipping/steel container). Secondly, the existing systems put forward in these papers rely on RFID equipment that are already on the market which are expensive. Hence limited research was done on how to implement a more cost-effective RFID solution in order to track goods and inventory whilst it is in transit.

1.5. Research questions

This research work will investigate how to answer the following questions:

1. Whether a low-cost high-performance circularly polarized UHF microstrip patch antenna can be designed?
2. What effect will the interference caused by different materials such as steel, plastic and wood have on the RFID system inside a metal enclosure?

1.6. Research Work Contribution

The following contributions are made to the field of RFID:

1. By designing a low-cost high-performance circularly polarized UHF microstrip patch antenna, it will reduce the cost of the overall system that is applied in the tracking of goods and inventory industry.
2. Implementation of this system will help companies to keep track of their goods whilst these are in-transit.

1.7. Organisation of the thesis

Chapter 2: - presents the literature review for this research work. This chapter looks at the previous work that has been done by other researchers in the field of radio frequency identification.

Chapter 3: - discusses the materials and method that was used to determine the feasibility of employing a UHF RFID system inside a steel container. The method followed in this thesis is discussed.

Chapter 4: - focuses on the design of a low-cost high-performance UHF circularly polarized microstrip patch antenna. The antenna was first simulated with the aid of a software tool. Once the simulated results achieved the specifications for the design, the antenna was then fabricated and tested. A cost analysis was then undertaken that compared it to a commercial UHF circularly polarized microstrip patch antenna.

Chapter 5: - details the simulation of practical testing of the performance of an UHF RFID system in monitoring containerized cargo. The aim was to determine how the interference caused by different materials such as steel, plastic and wood have on the RFID system inside a shipping container. The performance was first simulated with the aid of a software tool. The simulated results were then presented and discussed. The practical testing of the performance was then carried out using specialised UHF RFID equipment inside a shipping container and in free space. The performance of the RFID system in both environments was then recorded for each material and the results were then discussed.

Chapter 6: - lastly concludes the work from this thesis and recommends future scope of work.

2. REVIEW OF LITERATURE

This chapter reviews past research papers that apply RFID technology in tracking goods that are in transit. RFID based tracking systems allows for continuous monitoring of goods in real time. Prior research papers were sourced in order to ascertain what has been done in this field. The findings of the prior research papers are discussed below. First, prior research was studied that was relevant to the application of RFID technology in the logistical field and transportation of goods. This was necessary in order to ascertain what systems have already been developed to track goods. Secondly, this literature review then focuses on prior research papers that investigated how the interference caused by different materials affects the performance of a UHF RFID system.

The application of using RFID technology in a logistical environment was discussed by Xiaozheng *et al*, [19]. The aim of the paper was to utilize RFID technology in supplementing the barcode system used in identifying goods. The reason why RFID technology was not fully utilized was due to its cost at that time. If the RFID tags are to be placed on individual items within a pallet this could increase amount of the goods that are lower in cost. Therefore, to avoid the scenario, a more financially achievable way was to use a transitional approach. The pallets will utilise the RFID tags and the goods inside the pallets will use barcodes. Another problem that was raised was the barcodes attached to the items were not compatible with the RFID readers. In addition, it was also found that when acquiring information of a pallet, all the data on the RFID tag must be read. However, this brings about inefficiencies because reading a 2kB RFID tag entirely would take around 5 seconds. It was concluded that this would be too expensive to devote this much time reading RFID tags that for instance were empty or had no information on them. To solve this issue the conception of a Tag Operation Module (TOM) was introduced. TOM is a method that makes use of the index in order to manage the data on the RFID tags. The implementation of this module is not relevant to this research hence an in-depth analysis of this module was not needed. Another paper by Jun'e *et al*, [20], looked at three applications of using RFID technology in inventory management. The first application was placing RFID tags onto goods that enter the warehouse. By affixing goods, boxes or components with RFID tags it allows for electronic data to be transferred without direct contact thus achieving automatic identification of goods. The system also acquires additional data such as, making records of the goods that have entered and exited the warehouse. This allows the warehouse employees to pick up any errors that may have occurred at the previous pick up point, it also avoids goods that may have been delivered incorrectly and lastly reduce managerial cost and labour cost. The second application is

using RFID technology inside the warehouse. Once the correct goods have been selected to be stored in the warehouse, the employees can easily determine the position by using RFID technology in the form of a warehouse management system. RFID readers are located on the shelves, which detects the electronic data of the goods from the RFID tags and thus replaces the manual inspection previously used. In addition, this technology can also automatically identify and return the relevant information to the warehouse management system and also update the goods new position if required. Lastly the third application is using RFID technology to track goods leaving the warehouse. The process is similar to the first application in Jun'e *et al*, [20], where goods entered the warehouse. The RFID readers identify the goods, boxes or components leaving the warehouse and compares it with the pickup order. In conclusion the paper found that the full utilization of RFID technology in inventory management, dramatically improved the efficiency of the inventory levels and labour costs. In addition, the use of RFID technology played a pivotal role in the process to achieve rapid, real-time, standardization of collecting and processing of logistic units.

However, the main issue with using RFID technology was the cost of installing this infrastructure was relatively high at that time. Hence the use of RFID technology was only financially justified if there was a high yield of goods to be identified or tracked. A paper by Holmqvist *et al*, [21], in collaboration with Volvo, the car manufacturer presented a paper on using mobile RFID reader to address the cost issue. They evaluated the usability, productivity and operational reliability of a mobile RFID reader. In addition, this system used cellular networks and Global System for Mobile (GSM)/ General Packet Radio Service (GPRS) with web technology. The mobile RFID proposed solution consisted of a cellular phone that was attached to a RFID reader. The use of the cellular phone allowed data to be transferred between the cellular phone and the back-end system in real time. Once the RFID tag was within range of the mobile RFID reader the cellular phone then executes the predetermined functions i.e. arrival inspection or loading inspection, shown in Figure 3. The arrival inspection objective is the recording of the delivered goods. This in turn improves data gathering, in addition to status reporting. The loading operation assigns goods to specific cargo containers. In the past, all of these operations were done manually. One of the biggest drawbacks of this system is the cost of a mobile RFID reader in comparison to a single static RFID reader and multiple antenna design in today's market. In addition, in order to ensure all RFID tags are recorded and continuously monitored effectively, multiple mobile RFID readers are needed. This will in turn increase the cost of the implemented system.

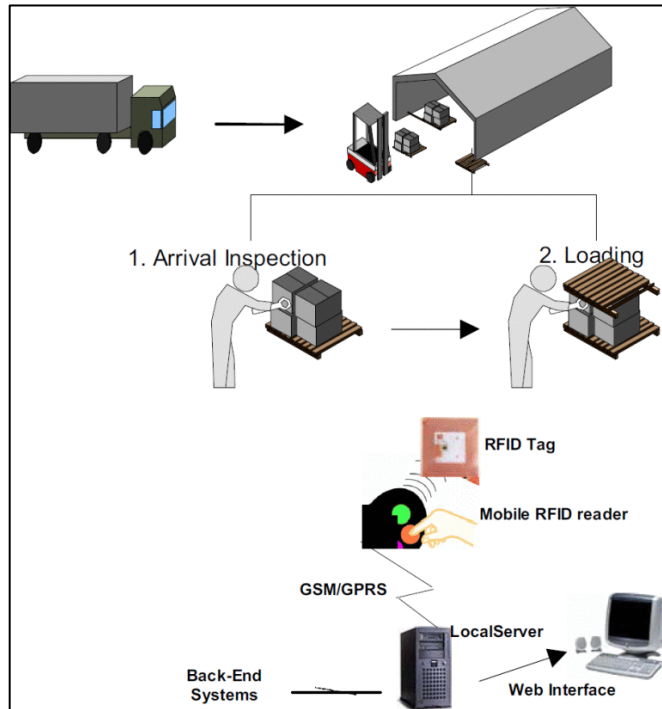


Figure 3: Overview of the implementation of the mobile RFID setup [21].

RFID technology was also applied in the transportation of dangerous goods. A paper by Yu *et al*, [15], developed a system which monitors dangerous goods and tracks the position of the vehicle in real-time. In order to achieve this RFID and Global Position System (GPS) technology was used. The operation principle of the system was broken down into three modes namely; transportation start, transportation process and transportation end. Transportation start comprises of firstly loading the vehicle's Terminal Equipment (TE), see Figure 4, into the vehicle.

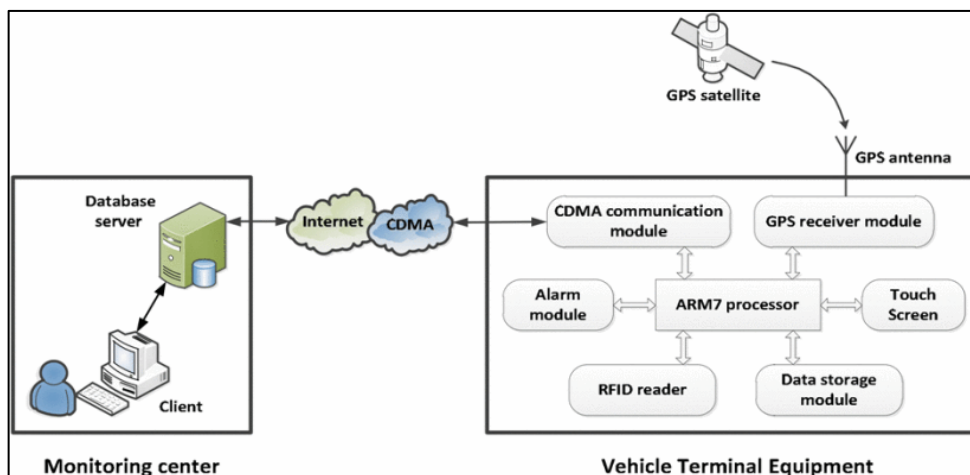


Figure 4: Breakdown of the vehicle Terminal Equipment [15].

The vehicle TE then receives data such as the vehicle, drivers, and the dangerous goods to be loaded into the vehicle. This information is then transmitted to the monitoring centre. Only when the monitoring centre validates this information and submit a unique identification can employees begin loading the vehicle. The RFID reader scans the vehicle and recognizes the RFID tags fixed to the dangerous goods. This data is also transmitted to the monitoring centre in real-time. Once the loading of the vehicle is completed, the vehicle TE enters the transportation mode. This mode will then send information such as, the vehicle position using the GPS module and the dangerous goods in the vehicle using the RFID module. In addition, the vehicle TE has an “Emergency Alarm” function in the event for example the dangerous goods are unloaded along the way without the approval of the monitoring centre. The monitoring centre would then mark this on the map. Lastly the transportation end mode is reached when all the dangerous goods are unloaded in their designated locations. Figure 5 shows the workflow of these modes.

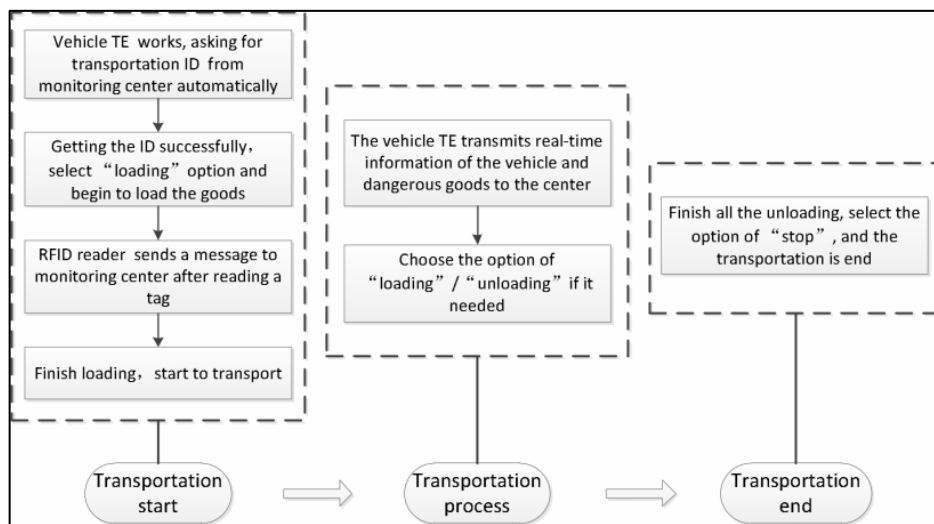


Figure 5: Workflow of the three modes [15].

This system was also tested in the field and the following results was determined, the vehicle TE subsystems successfully collected all the relevant data using the GPS and RFID modules. It also successfully transmitted this data to the monitoring centre. In addition, it was also found that the GPS module accurately analysed and extracted the vehicle’s position. This information was then displayed on an electronic map, shown in Figure 6. The red track depicts the vehicle travel route while the red star is the current position of the vehicle. This system also formed the backbone of other research papers in [16] and [17]. The main drawback from these papers are, firstly these papers do not expand on what vehicle was used during testing and how exactly the RFID system was setup in the vehicle i.e. how was the RFID reader mounted, where was the RFID reader

mounted in relation the RFID tags, what materials was the RFID tags affixed too. As such not much detail was put into investigating and testing the RFID system in actual real-world applications.

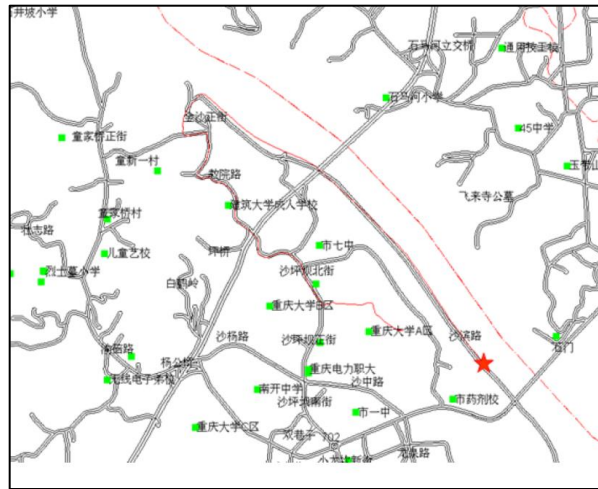


Figure 6: Tracking of vehicle [15].

A study by Siror *et al*, [18], also investigated how RFID technology can be useful in preventing the removal of goods in an illegal manner during transportation or falsely declaring goods that are in transit in order to evade taxes. Previous methods of securing in transit goods involved the mechanical locks and personal accompanying the vehicles. These methods showed to be ineffective. Other factors that also lead to criminal activity was; collusion within the law enforcement agencies, inadequate technological and physical infrastructure and high levels of taxation. In order to solve these existing issues an RFID based Electronic Cargo Tracking System (ECTS) was developed. This system utilised a variety of RFID technologies such as; RFID tamper proof vehicle tags, active RFID electronic seals, outdoor RFID readers, low frequency micro readers and handheld readers. The RFID readers were located on the gates of the ports and at container freight stations. The active RFID electronic seals or E-seals resembles a physical lock. These E-seal locks are used to lock the door of the container. When the E-seals are armed it generates a random identification number. This identification number will remain the same throughout the journey unless if it is tampered with. Over and above the tamper detection, the E-seal also records data such as arming, opening, closing, reading and sensory events. These sensory events are recorded with the aid of tilt and vibration sensors to detect when the door of the container is removed from its hinges. The mode of operation of the ECTS is shown in Figure 7.

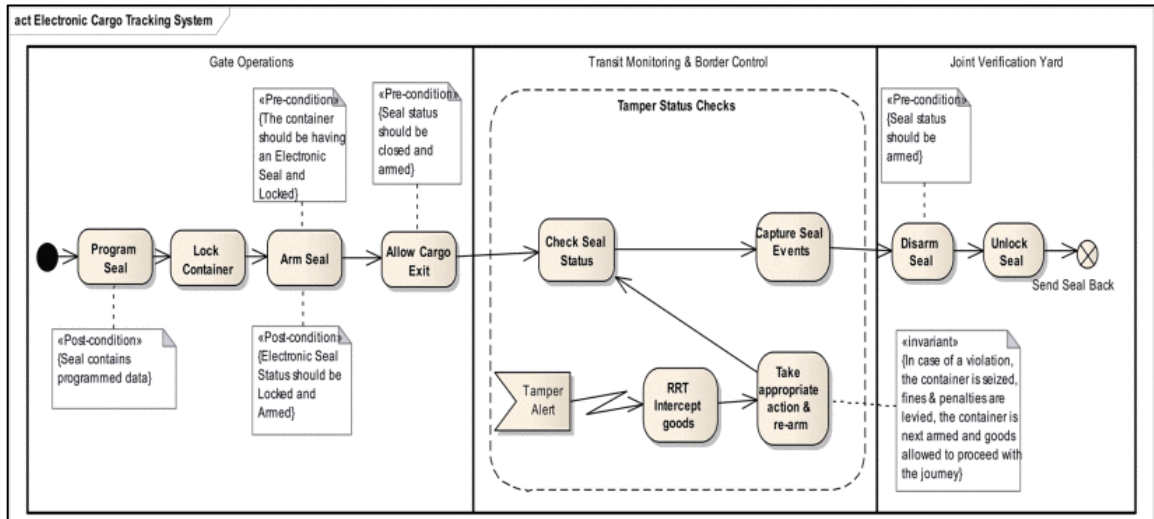


Figure 7: ECTS flow diagram [18].

The system was also tested, and certain problems were noted. Whenever the communication link was unavailable at the Transit Checkpoint (TC) a false alert would have been generated at the next TC because the “cargo appears without notification”. The reason for this false alert was due to the delay between the central database and the ECTS. Another problem experienced included issues such as duplicate reads of the RFID tags. For instance, if an E-seal of the truck’s container came into the TC and was interrogated by the outdoor RFID readers, the details of the E-seal would have been read with the time stamp at which the event occurred. After this interrogation, the truck would then exit the TC, and this is indicated by the E-seal not been in range of the RFID reader. The departure time would have been logged of the truck. However sometimes a truck can still be in the TC but out of range from the outdoor RFID. Therefore, in reality the truck and its contents did not exit the TC. Another issue related to this is while the truck was stationary or parked, when leaving the TC, it may then come within range of the outdoor RFID reader again. Therefore, multiple reads would have been logged for the same truck and its E-seal. In order to solve this issue, the middleware was reconfigured to filter out multiple readers and duplicate entries. In conclusion the benefits of this system included; an increase in government revenue that was lost to crime, improvement in the turnaround time and reduced bribery because there is now minimal contact between the truck drivers and the TC officials. Some limitations noted was; the system was unable to detect the removal of goods; delays can exist due to the limitations in the range of the RFID readers and the system is not suitable for wet or bulky cargo, see Section V (5) in [18].

In reality the performance of an UHF RFID system will degrade when real world factors are introduced. According to Dobkin *et al*, [22], these factors include the placement of a

RFID tag on various materials, such as metal surfaces, liquids, plastics and the radio frequency noise. Hence, it is imperative that these factors are included in any simulation work and the results. This allows a better understanding of how the system will behave in real world conditions.

A paper by Arora *et al*, [23], investigated the effect of placing three different metals in front of a transponder (RFID tag) in a complex metal environment. The three metals used were brass, aluminium and mild steel. In addition, the paper also studied the effects of using these metals when the thickness of the metal was varied. The testing space used measured in at $90\text{cm} \times 90\text{cm} \times 21\text{cm}$. This space was then discretized in the x and z direction with 3cm increments and in the y direction with 5cm increments. Hence it gives a total of 3780 testing points. Figure 8 shows the setup of the experiment. The blue dots represent the 3780 testing points identified for the RFID reader's antenna to move through. In addition, the transponder was placed 160cm from the ground and was affixed to a $30\text{cm} \times 30\text{cm}$ sheet of metal. It was also noted that the minimum distance between the RFID reader and transponder was 5cm . Hence the setup allowed both the near and far field to be observed. In order to get precise and repeatable results, it was also noted that a Fanuc M-16i B/T robot was used. The RFID reader's antenna was affixed to the robot by using an end effector, which was made of Perspex. The RFID reader's antenna was also circularly polarized.

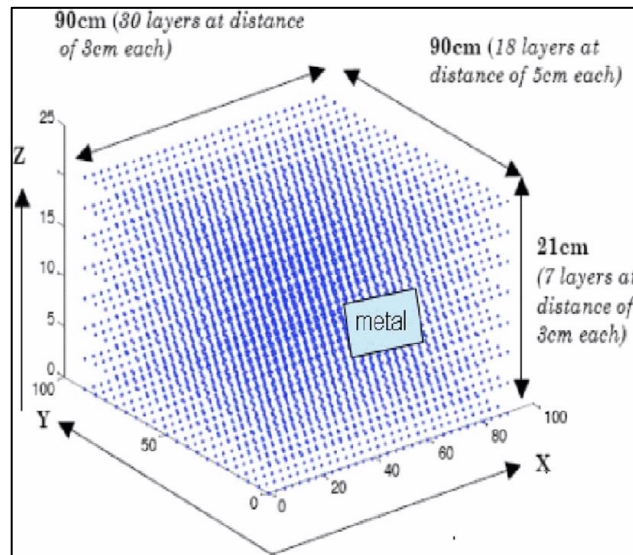


Figure 8: Experimental space used, with the blue dots representing the data points [23].

The outcome from the experiment was broken down into three components namely; the interference caused due to different metals, effects of the thickness of the metal and the orientation sensitivity. In terms of the interference caused by different metals, it was firstly

noted that non-ferrous metals had a similar readability pattern in the near field. In addition, ferrite magnetic substances have a high relative magnetic permeability that usually exceeds unity and have a high specific electrical resistance. These properties reduce the magnetic field of the reader's antenna when it was placed near the transponder. This, however, does not occur for non-ferromagnetic materials. The effect in the far field region showed that the read range was different for each metal. Since brass had the maximum electrical conductivity, it experienced the worse radiation losses. It was also concluded that the more conductive a metal is, the more reflective properties it will have and hence it will therefore cause the most interference of the RF waves. Hence, brass greatly reduces the performance of the RFID system. A maximum range of 50cm was achieved and only 15% of the total data points was able to be detected by the RFID reader's antenna. Aluminium achieved a range of 95cm with 43% of the data points been read. Lastly mild steel showed to offer the best performance. The range exceeded the size of the testing space and 77% of the data points was read. The non-black spots in Figure 9 indicates where the reader's antenna could read the transponder, with the lighter spots indicating the reader's antenna could read the transponder at a greater attenuation. In addition, the null zones shown in Figure 9 indicated that the reader could not detect the transponder because the RF waves destructively interfered with each other due to multipath interference.

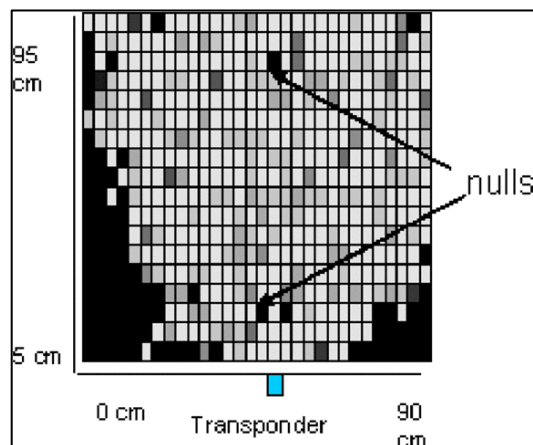


Figure 9: Plot of the transponder with null zones [23].

The experiments for the effect of the thickness of metal involved the use of two thickness of mild steel. The two thicknesses chosen was 1mm and 1.5mm, the results from this experiment concluded that the thicker mild steel further reduced the performance of the RFID system. With the thicker mild steel only 45% of the total data points was read as compared to 77% for the thinner mild steel. Lastly the orientation sensitivity was tested by rotating the RFID reader's antenna by 45° through its vertical axis. It was noted that

the reader could only detect the transponder when the reader's antenna faces it. This was due to an increase in the RF waves that were incident on the transponder. Hence it was concluded that the positioning of the transponder with respect to the reader's antenna does decrease the performance of the RFID system.

In Mercer *et al*, [24], two materials were tested, namely, liquid and metal. It was shown that these two materials decrease the performance of an UHF RFID system significantly [25]. The UHF RFID system was tested on liquid materials by using, a 24 pack 0.5 litre bottled water. Their results showed that when passive RFID tags were placed on the water bottles and had non-line of sight (NLOS) with the UHF RFID reader's antennas, the overall performance of the UHF RFID system decreased because the detection rate of the RFID tag decreased and performance inconsistency when the tests were recurrent. These issues were attributed to factors such as an amalgamation of multipath interference, too many RFID tags in close proximity and radio frequency (RF) absorption by the bottled water. It was noted that the performance of the UHF RFID system increased when the RFID tag was affixed towards the top of the bottled water. In conclusion the findings in [24] showed that in order to have a successful UHF RFID system, when the material that the RFID tag is placed on is liquid, strategic placement was required. This is accomplished by placing a RFID tag so that there was no obstacle between the RFID reader's antenna and the RFID tag. Secondly if strategic placement of the RFID tag was not possible, a semi-passive RFID tag was required or RFID tags that were better suited to that specific material must be used. However, the trade off to this was cost. The second material consisted of plastic door handles that had metal and metallic paint in them. Their results showed that even when the RFID tags were placed beneath the parts, a 100% read rate was attained. This 100% read rate was also achieved regardless of the positioning of the door handle with respect to the RFID reader's antenna. However, their test did not see if the performance of the system decreased if the number of tags was increased.

In conclusion, the papers discussed above details the use of a RFID system in supporting and improving various logistical needs in order to optimise the tracking of goods. In addition, other papers also looked at how different materials impact the performance of a RFID system. As highlighted in the above papers, there were instances that presented some form of limitations.

Such limitations included:

1. The cost of implementing a RFID system was too expensive;

2. They do not expand on what vehicle was used during testing and how exactly the RFID system was setup in the vehicle;
3. In the case of [18], some limitations included the system was unable to detect the removal of goods, delays can exist due to the limitations in the range of the RFID readers and the system is not suitable for wet or bulky cargo; and
4. Limited research was done in determining the effect of the interference caused by different materials on the UHF RFID system inside a metal enclosure, [23].

Hence, this research aims to address these limitations in the following ways:

1. To address the cost issue a low-cost high performance circularly polarized microstrip patch antenna was designed, see Section 4.3;
2. This thesis details out the setup used in obtaining the relevant data;
3. This thesis investigates the performance of the UHF RFID system inside a metal enclosure and investigates the effect of the interference caused by different materials inside a metal enclosure; and
4. This system will also add to the work of [18], because it allows us to now detect what goods have been removed from the container.

3. MATERIALS AND METHODS

This research had two main objectives; the first objective was to design a low-cost high performance circularly polarized microstrip patch antenna. This is required in order to reduce the overall cost of the UHF RFID system. The second objective is to investigate how the interference caused by different materials affects the performance of the UHF RFID system inside a metal enclosure when passive RFID tags were used. The static RFID tags were then placed in free space and the performance of the UHF RFID system was then measured. These results in free space were then used to benchmark the performance of the UHF RFID system.

Since multiple antennas will be used in this system it was imperative that the cost of these antennas was reduced. In order to achieve this a low-cost high performance circularly polarized microstrip patch antenna was designed. A circularly polarized antenna was chosen because it allows the RFID tag to be read at almost any orientation. The design of the antenna was carried out using a simulation tool. In order to achieve circular polarization, the design utilised corner truncated technology along with a thicker substrate and large ground plane. This also enhanced the gain of the antenna. The substrate material used was FR-4 printed circuit board (PCB) material which achieved a low-cost design. This thesis then focuses on how the interference caused by different materials when placed inside a metal enclosure affects the performance of the RFID system and the effect of the metal enclosure has on the UHF RFID system. This investigation was carried out using a simulation tool. The simulated results were then analysed and discussed. Practical testing was then conducted to verify the simulated results. The results were then compared to the simulated results and discussed. Finally, a conclusion was drawn in order to determine if the metal enclosure reduces the performance of the UHF RFID system.

In order to achieve these objectives, the following steps were taken:

1. First objective

- Research was conducted on how to develop a circularly polarized microstrip patch antenna. This research included how to achieve circular polarization using varying techniques, what feedline can be used, what effects does a thicker substrate have on the performance of the antenna and what effect will a larger ground plane also have on the performance of the antenna.
- The proposed antenna was then simulated using the CST Studio Suite software. This software allows us to design and gauge the performance of the antenna by

using the axial ratio, gain and the reflection coefficient results. These results were then discussed.

- Once the antenna meets the specifications set out, the antenna was then fabricated and tested. The results were discussed and compared to the simulated results. In addition, the designed antenna was also benchmarked against other antennas previously researched in terms of the performance. The fabricated antenna was also compared to a commercial circularly polarized patch antenna in terms of the cost.

2. Second objective

- The simulations were done using the gprMax software. This software uses the Finite Difference Time Domain (FDTD) method to solve EM problems by simply discretizing Maxwell's equations in both space and time with central difference approximations. First the boundary of the metal enclosure was set up in the software. The boundary setup was made of steel.
- Two antennas were then placed inside the steel enclosure. One antenna was used as the static transmitter antenna (static RFID tag) while the other antenna was the receiver antenna (reader's antenna).
- Two positions of the transmitting antenna were investigated. The first position was to the far side of the receiver i.e. the furthest distance from the receiver (position 1) and the second position was directly in line of the receiver (position 2), see Figure 25. Position 1 is considered the worst-case scenario because it is located the furthest away from the RFID reader's antenna. Position 2 is the best-case scenario because it is located directly in line with the RFID reader's antenna.
- The transmitting antenna was then sandwiched in between a plastic RFID tag mount and the material to be investigated, see Figure 24. The materials to be investigated was then placed at position 1 and at each thickness the electric and magnetic field recorded. This process was repeated at position 2.
- Once the data is collected, the poynting vector was then applied to calculate the power that was received by using the electric and magnetic field for each material thickness. The data was then analysed and discussed.
- The practical testing involved two types of testing. One was performed inside a steel container while the second test was in free space. A similar approach was used as done in the simulation testing.

- A total of six positions were used in the practical testing, see Figure 38 instead of using two positions. The reason why these six positions were not investigated in the simulations was due to memory related issues.
- The results were recorded using the Alien RFID kit. The graphical user interface (GUI) shows the identification of a RFID tag when it is detected. Therefore, the results obtained was either if the RFID tag was detected or not at the six different positions being investigated. The same approach was also used in the free space testing.
- The data was then analysed and discussed.

4. CIRCULARLY POLARIZED MICROSTRIP PATCH ANTENNA DESIGN

4.1. Introduction

Microstrip patch antennas became popular in the 1970's [26]. However, the original idea of this antenna dated back to 1953 [27] and then later patented in 1955 [28]. The expression "patch" comes from the shape of the radiating element on the antenna. The shape is traditionally rectangular or circular and is usually made up of copper. This type of antenna is from the printed antenna category. As such designing such an antenna follows the printed circuit manufacturing process, hence a low cost of production can be achieved [29]. The frequency used in this design belongs to the UHF EM spectrum. The UHF range was chosen because it offers a much greater read range compared to other types of passive RFID tags such as low and high frequency tags and it also has the ability to read many tags per seconds [30]. Table 2 elaborates on the advantages and disadvantages associated with designing a microstrip patch antenna.

Table 2: Advantages and disadvantages of a microstrip patch antenna [31].

Advantages	Disadvantages
Low cost	Narrow bandwidth
Ease of integration	Low efficiency
Good radiation control	Low gain
Circular and linear polarization	Polarization purity is hard to achieve
No cavity backing is required	The feed structure of arrays has large ohmic losses
Dual and triple frequency capabilities	Surface waves excitation

Some of the methods researched over the years to reduce the disadvantages include: using different patch geometries, varying the thickness, removal of segments in the patch geometry such as slots, altering the shape of the patch or ground plane [30, 32]. The dual band [33], triple band [34], ultra-wideband [35, 36], dual polarization [36, 37, 38], circular polarization [39], wearable [40, 41], etc features can be achieved by microstrip antennas.

Over the years, a variety of circularly polarized antennas have been designed for use in the UHF RFID field. A dual-polarized antenna was proposed by Kruekaew *et al*, [42], in which PIN diodes that were used as electronic switches allowed the RF current flowing through the antenna to be modified. Even though this allowed for an improvement in the polarization control, the beam width decreased and also the bandwidth. In 2014, Duraj *et al*, [43], introduced a paper on a high gain patch antenna. It utilized an air-substrate to achieve a broader bandwidth. The polarization was controlled by using two different

excitation ports. This antenna operates in the 865- 870 MHz range. In this paper it was found that the use of two separate connectors did provide the best results; however, it involves manually connecting these feed cables to one of the antenna connectors. A sequentially fed stacked circularly polarized patch antenna was proposed by Chen *et al*, [44]. The design covers the entire UHF spectrum from 840 to 960 MHz. It comprises of two suspended microstrip lines. It was also successively fed by using four probes that are joined to the microstrip line. Even though this type of antenna does cover the entire UHF spectrum, the high manufacturing cost will be its Achilles heel. The antenna presented by Sim *et al*, [45], overcame this shortfall in [44] by slot-loading a semi-circular slot into the circular radiating patch. The antenna is fed by a SubMiniature version A (SMA) connector, using the L-shaped probe fed technique. This technique showed that the antenna achieved a good circular polarized bandwidth and impedance bandwidth. The overall size was 150 mm × 150 mm with a thickness of 34 mm . However, the depth of this antenna does not meet the requirements for the UHF RFID inventory management application.

A more recent paper by Sarkar *et al*, [46], designed a dual-frequency circular polarized patch antenna. The antenna designed operates at the UHF RFID band of 915MHz and the wireless local area network (WLAN) band of 2.45 GHz. This dual-frequency design was achieved by utilizing a circular patch that included slots on the patch and slits in the ground plane. It also comprised of a single layer design. The antenna achieved a 3.47% axial ratio percentage bandwidth for the UHF band and a 1.5% axial ratio percentage bandwidth for the WLAN band. Also, the measured reflection coefficient bandwidth achieved was 43 MHz from 903 MHz to 946 MHz and 47 MHz from 2425 MHz to 2472 MHz. Unfortunately, the gain for the UHF band was 0.58 dBi and 6.48 dBi for the WLAN band. The low gain for the UHF band was associated with the use of the FR-4 material as the substrate. The main idea behind the design was to design an antenna that can be connected to a UHF RFID reader to scan RFID tags and then to send the information to data centers using the WLAN band.

In this chapter, a low-cost high performance circular polarized patch antenna with a low axial ratio and broad AR beam width was designed and fabricated. This chapter aims to develop an antenna that is low-cost and also has a lower axial ratio while still offering a respectable amount of gain, directivity and bandwidth. Previous papers [46], [53-60] showed that there was always a notably trade-off between having a low axial ratio and a high gain, directivity or bandwidth. In order to achieve this, a combination of design elements, such as the use of slots and truncated corners along with a larger ground plane,

was used. These design elements allowed for a lower-axial ratio while still maintaining an acceptable amount of gain and bandwidth.

4.1.1. Metallic patch

As discussed before the patch of the antenna is a thin piece of copper that is attached to the dielectric substrate. This patch can exist in a number of different shapes such as, a dipole, square, elliptical, triangle, etc. As shown in Figure 10. The most common shapes used are the square, rectangular, dipole and circular. The microstrip dipole also has a larger bandwidth and due to the shape, it occupies less space [26].

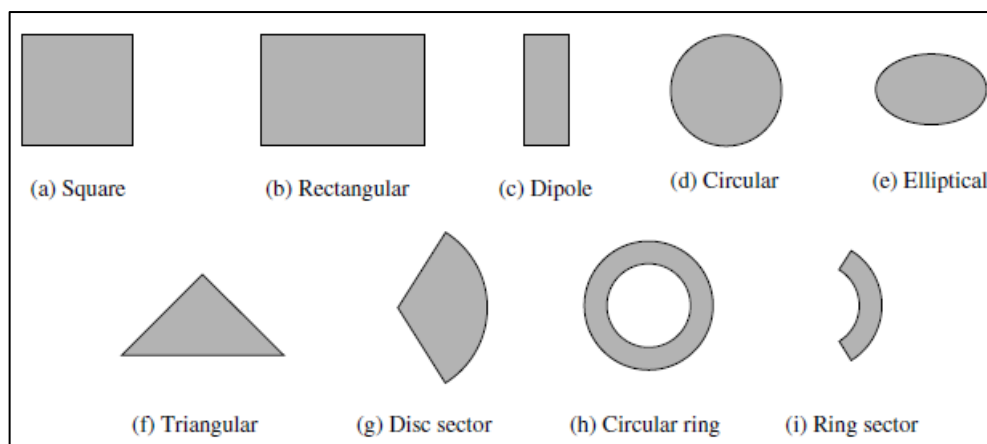


Figure 10: Geometries for patches [26].

4.1.2. Dielectric substrate

A number of dielectric substrates can be utilized to design a microstrip antenna, with their dielectric constants ranging from 2.2 up to 12. The two types of dielectric substrates used are either thin (1.6 mm) or thick (greater than 1.6 mm). The thicker substrate does offer a larger bandwidth and efficiency. Unfortunately, the drawback of using a thicker substrate is the large element size. A thinner substrate with a high dielectric constant is more suitable for microwave circuitry. This is due to it requiring tightly bound fields which minimize the unwanted radiation and coupling. However, this causes greater losses and less efficiency [47].

4.1.3. Ground plane

The ground plane serves two purposes. Firstly, the transmitter's ground wire is attached to it and secondly it serves as a reflective surface for the electro-magnetic radio waves. The ground plane is usually located on the other side of the substrate. In addition, further performance issues associated with microstrip patch antenna can be resolved by inserting cut-outs of varying shapes in the ground plane [48].

4.1.4. Feeding techniques

The four most common feeding methods are the microstrip line, aperture, coaxial probe, coupling and the proximity coupling [26]. The microstrip line and the coaxial probe are regarded as contacting feed techniques while the aperture and proximity coupling are regarded as non-contact feed techniques. Table 3 summarises the different feeding techniques with their respective characteristics.

The microstrip feed line forms a single structure with the patch. In addition, it is easy to fabricate, simple to match and also model. There exist three types of microstrip feeding techniques: direct feeding, inset feeding and gap coupled. The main disadvantage of using a microstrip feed is it offers a narrow bandwidth because as the substrate gets thicker the surface waves and the spurious feed radiation increases [49]. The microstrip feeding technique was chosen for this design. The bandwidth stipulated by the Independent Communications Authority of South Africa (ICASA) for this antenna is 4 MHz (915 MHz – 919 MHz) , as such the disadvantage associated with this antenna will not be an issue. In addition, it also offers other benefits such as easy fabrication and matching and also simple modelling which the other feeding techniques do not offer.

Table 3: Comparison of the different feeding techniques and their characteristics [50].

Characteristics	Co-axial Probe Feed	Radiating Edge Coupled	Non radiating Edge Coupled	Gap Coupled	Insert Feed	Proximity Coupled	Aperture Coupled
Configuration	Non-Planar	Coplanar	Coplanar	Coplanar	Coplanar	Planar	Planar
Spurious Feed Radiation	More	Less	Less	More	More	More	More
Polarization Purity	Poor	Good	Poor	Poor	Poor	Poor	excellent
Ease of fabrication	Soldering and drilling needed	Easy	Easy	Easy	Easy	Alignment required	Alignment required
Reliability	Poor due to soldering	Better	Better	Better	Better	Good	good
Impedance Matching	Easy	Poor	Easy	Easy	Easy	Easy	Easy
Bandwidth	2-5%	9-12%	2-5%	2-5%	2-5%	12%	21%

4.2. Antenna design and geometry

Figure 11 shows the geometry of the proposed antenna. A microstrip patch antenna was used because of its relatively small size, low cost, low profile and easy implementation [33]. These types of antennas are also used in the UHF, and higher frequencies range since the size of the antenna is reliant on the resonant frequency and the wavelength. A square microstrip patch antenna is chosen for this design. The required specifications for this UHF RFID antenna are as follows; the frequency range is from 915 MHz – 919 MHz; the impedance of the antenna is 50 ohms. This impedance was required to match the impedance of the cable used. Lastly, the radiated field of the antenna must be circularly polarized because the orientation of the RFID tags is not known.

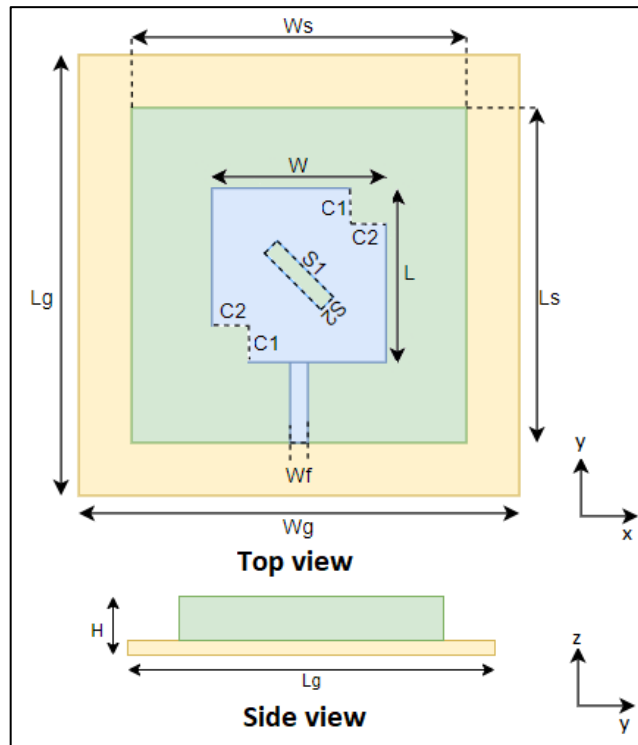


Figure 11: Geometry of the proposed square patch antenna.

The initial design of the circularly polarized microstrip patch antenna begins with the calculation of the width and length [26]. The size of the rectangular patch antenna for the resonant frequency 915 MHz and for a substrate with dielectric constant of 4.3 and thickness of 6.4 mm is calculated using the following equations [26]:

$$W = \frac{c}{2f_0 \sqrt{\frac{\epsilon_r + 1}{2}}} \quad (1)$$

$$L = L_{eff} - 2\Delta L \quad (2)$$

where,

$$L_{eff} = \frac{c}{2f_o\sqrt{\epsilon_{reff}}} \quad (3)$$

$$\epsilon_{reff} = \frac{\epsilon_r + 1}{2} + \frac{\epsilon_r - 1}{2} \left(1 + 12\frac{h}{W}\right)^{-\frac{1}{2}} \quad (4)$$

$$\Delta L = 0.412h \left[\frac{(\epsilon_{reff} + 0.3)\left(\frac{W}{h} + 0.264\right)}{(\epsilon_{reff} - 0.258)\left(\frac{W}{h} - 0.8\right)} \right] \quad (5)$$

where,

W – width of the patch (cm)

L – length of the patch (cm)

c – speed of light (3×10^8 m/s)

f_o – resonant frequency (Hz)

ϵ_r – dielectric constant of substrate (4.3)

L_{eff} – effective length (cm)

ΔL – fringing length (cm)

L_{eff} – effective length (cm)

ϵ_{reff} – effective dielectric constant

h – thickness of substrate (cm)

In order to obtain an input impedance of 50 ohm (to match the cable) the following formulae was used [26]:

When,

$$\left(\frac{W_f}{h} < 1\right)$$

$$Z_0 = \frac{60}{\sqrt{\epsilon_{reff}}} \ln \left(8 \frac{h}{W_f} + 0.25 \frac{W_f}{h} \right) \quad (6)$$

When,

$$\left(\frac{W_f}{h} \geq 1 \right)$$

$$Z_0 = \frac{120\pi}{\sqrt{\epsilon_{reff}} \times \left[\frac{W_f}{h} + 1.393 + \frac{2}{3} \ln \left(\frac{W_f}{h} + 1.444 \right) \right]} \quad (7)$$

Where,

Z_0 – characteristic impedance (*ohms*)

W_f – width of microstrip feed line (*cm*)

ϵ_{reff} – effective dielectric constant

Using Equations 1 to 7, the values for the width of the patch, length of the patch and microstrip line width was calculated and found to be 100.6 *mm*, 77.15 *mm* and 11.6 *mm*, respectively. However, for the initial design, the width and length were equal to 77.15 *mm*.

In order to obtain the length and width of the slot the following formula was used [26]:

$$S_1 = \frac{L}{2.72} = \frac{W}{2.72} \quad (8)$$

$$S_2 = \frac{S_1}{10} = \frac{L}{27.2} = \frac{W}{27.2} \quad (9)$$

Where,

S_1 – length of the slot (*cm*)

S_2 – width of the slot (*cm*)

W – width of the patch (*cm*)

L – length of the patch (*cm*)

From experimental work noted in [30, 32, 26], it was shown that the application of a slot was one of the methods used to produce a circularly polarized antenna. Using Equations 8 and 9, the values for the width and length of the slot was calculated and found to be 28.36 *mm* and 2.84 *mm*, respectively. After a number of repetitions, the following

dimensions of the patch antenna are shown in Table 4. These dimensions showed to optimize the performance of the antenna. The proposed antenna design utilizes the corner truncated technology along with a thicker substrate and large ground plane to achieve circular polarization and a low axial ratio. The equivalent circuit of the proposed structure is given in Figure 12. The equivalent circuit for a rectangular patch antenna is a combination of a resistor (R_p), capacitor (C_p) and an inductor (L_p) in parallel. Using the equivalent circuit of the rectangular patch antenna as the starting point, the equivalent circuit for this design will therefore add two additional steps. First, the truncated corners produce a capacitance effect which can be modelled by C_{tc} . Secondly, since the current must travel around the slot and the current path length increases on the edges, the effect can thus be modelled by adding a parallel combination of a radiation resistance and reactive component R_s and X_s [51] as shown in Figure 12.

Table 4: Dimensions of patch antenna.

Parameters	Symbol	Value (mm)
Width of ground plane	Wg	200
Length of ground plane	Lg	200
Width of substrate	Ws	160
Length of substrate	Ls	160
Height of substrate	H	6.4
Width of patch	W	76
Length of patch	L	76
Length of corner cut-out	C1	11
Length of corner cut-out	C2	11
Width of slot	S2	0.7
Length of slot	S1	22
Width of microstrip	Wf	11.6

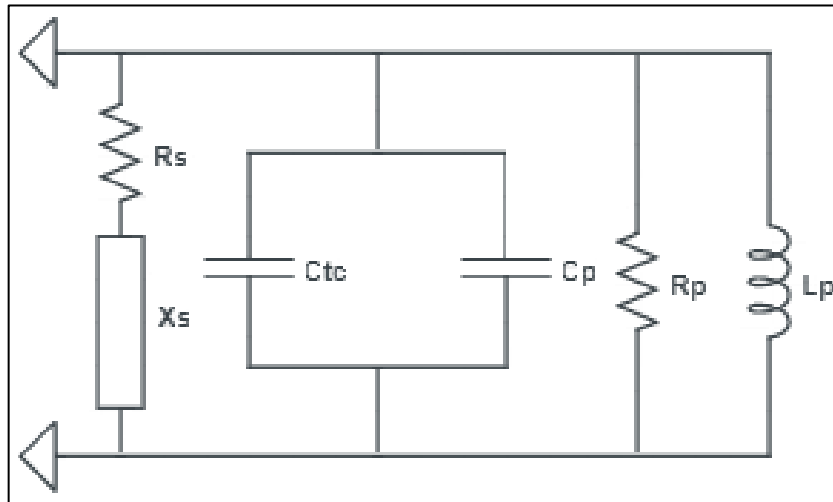


Figure 12: Equivalent circuit.

Figures 13 and 14 shows the fabricated antenna. The maximum thickness of a single FR-4 PCB is 1.6 mm . Hence in order to achieve the desired thickness of 6.4 mm , a total of 3 blank FR-4 PCBs are required to be fabricated. A bare PCB has no copper layer on the top and bottom sides. The antenna was fabricated using an FR-4 substrate, which has a dielectric constant of 4.3, referred design steps discussed above.

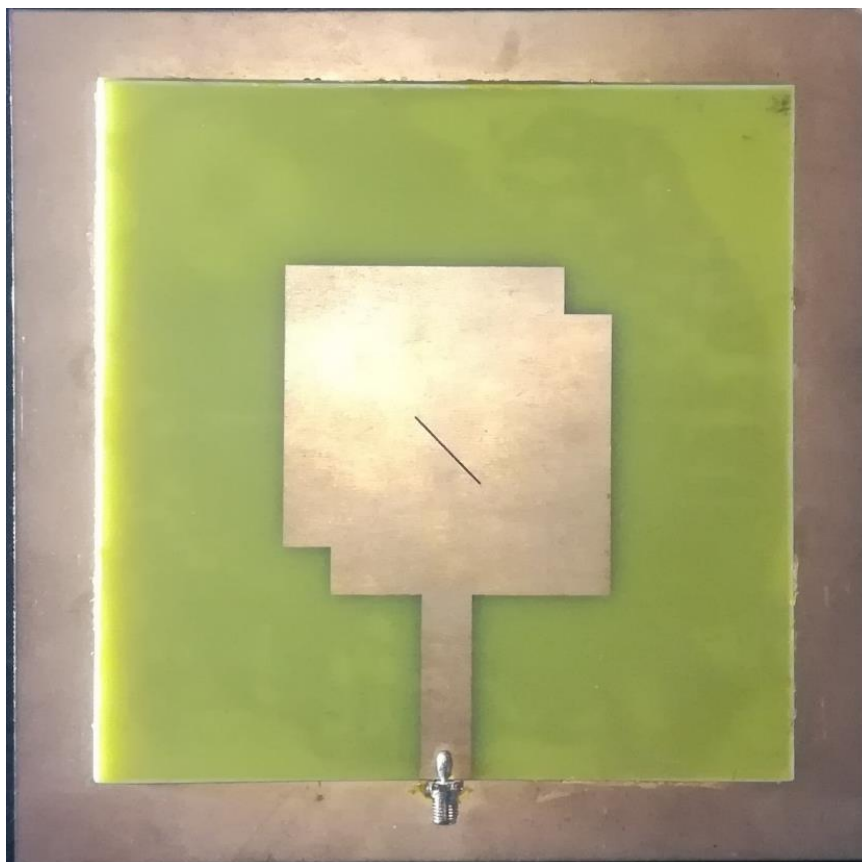


Figure 13: Fabricated antenna top view.



Figure 14: Fabricated antenna side view.

4.3. Results

The simulated and measured results are presented in this section. The simulated and measured reflection coefficient of the antenna is depicted in Figure 15. The measured reflection coefficient results show good agreement with simulated reflection coefficient results. The simulated antenna has a bandwidth of 38.73 MHz (4.28%). In addition, the minimum value of the return loss occurs at 903.20 MHz with a value of -15.33 dB . The fabricated antenna tested has a bandwidth of 57.53 MHz . The minimum value of the return loss occurs at 914 MHz with a value of -27.97 dB as shown in Figure 15. This implies that this antenna has almost perfect impedance matching at the input. Since minimal power is reflected in the source. The difference in results could be due to the cable used. In addition, in the simulation there was no air gap present in the substrate. However, in the fabricated antenna the layers of the substrate had to be combined with adhesive glue. Hence air gaps would have been present.

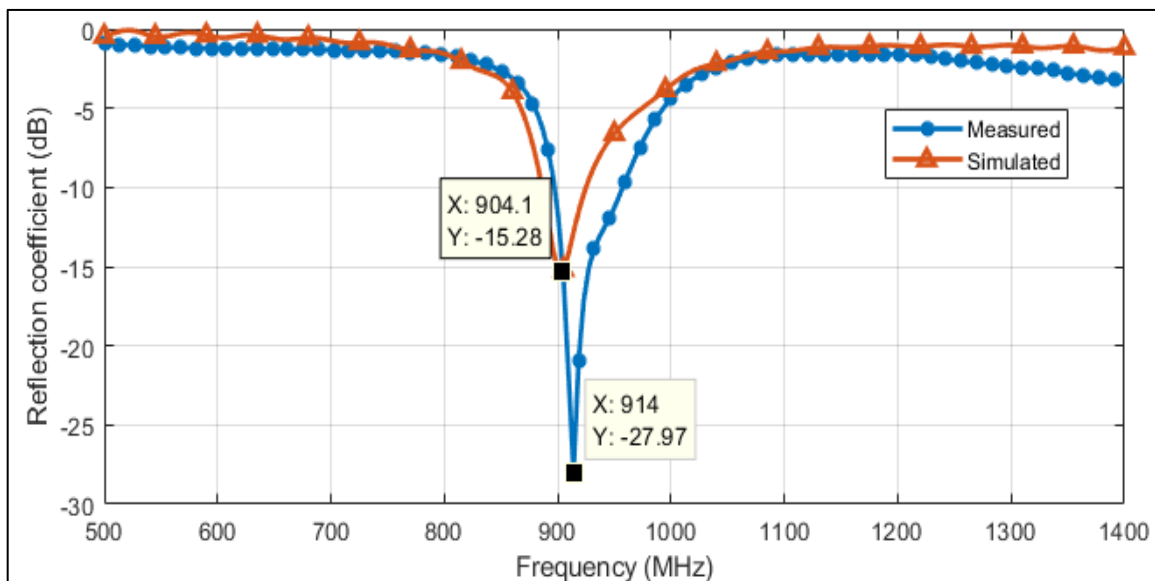


Figure 15: S11 parameter of the antenna.

Figure 16 shows the Voltage Standing Wave Ratio (VSWR) versus frequency. The VSWR is a measurement used to check the impedance matching between the antenna and the transmission line connected to it. The VSWR for the frequency range of 915 MHz – 919 MHz ranges from 1.62 to 1.74.

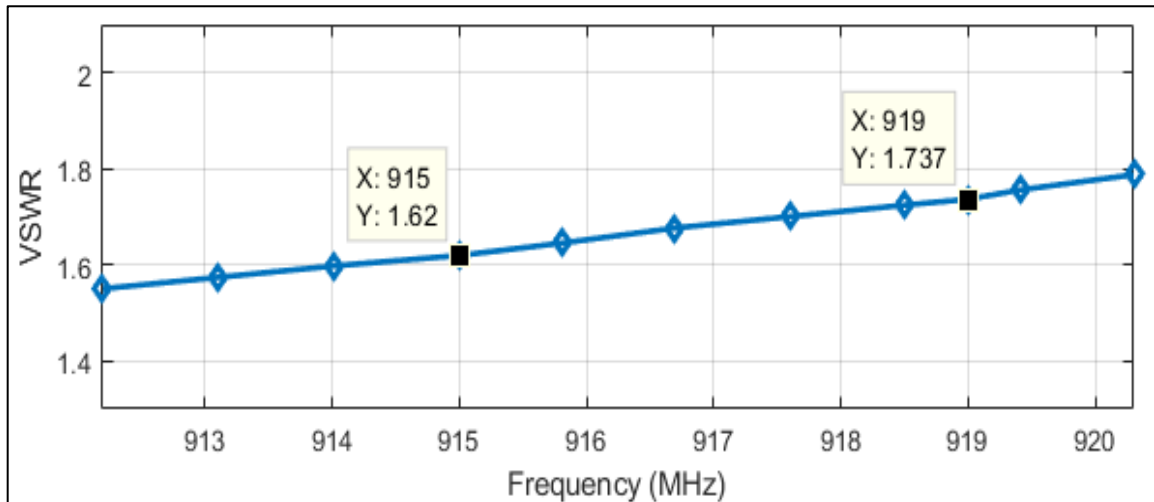


Figure 16: VSWR of the antenna.

Figure 17 shows the simulated normalized radiation patterns of the antenna for the antenna at 886 MHz, 891 MHz, 903 MHz and 924 MHz. In addition, the normalized 3 dB beam-width, together with its main lobe direction, is shown in Table 5 for the above-mentioned frequencies. From Figure 17, it can be observed that the shape of the radiation pattern remains relatively constant for all frequencies. In addition, from the results shown in Table 5, it can be determined that in both the electric ($\phi = 90$) x-z plane and magnetic ($\phi = 0$) y-z plane the 3 dB angular beam-width is high and the main lobe direction is more or less the same in both the electric and magnetic plane for all frequencies with the x-y plane of the antenna centred at 0° .

Figure 18 shows the directivity and gain of the simulated antenna for varying frequencies. From Figure 18, it is demonstrated that the directivity and gain reach its maximum of 6.56 dBi at 914 MHz and 2.68 dB at 924 MHz, respectively. Figure 19 shows the radiation efficiency and total efficiency versus frequency. The radiation efficiency is a ratio that is calculated using the power delivered to the antenna with respect to the power radiated from the antenna. Having a low efficiency means there is an impedance mismatch and having a high efficiency means most of the power received at the terminals of the antenna is radiated into free space [52]. The radiation efficiency achieved in the simulated antenna ranges from -3.94 dB to -3.91 dB for the frequency range of 915 MHz – 919 MHz,

respectively. Whereas the total efficiency varies from -4.19 dB to -4.23 dB for the frequency range of $915\text{ MHz} - 919\text{ MHz}$, respectively.

Table 5: Main lobe and angular width for varying frequencies.

Frequency (MHz)	Phi = 90		Phi = 0	
	Main lobe direction (degrees)	Angular width (3dB) (degrees)	Main lobe direction (degrees)	Angular width (3dB) (degrees)
886	7	94.9	5	90.9
891	8	93.5	4	90.7
903	8	91.1	2	90.3
924	8	91.0	356	88.5

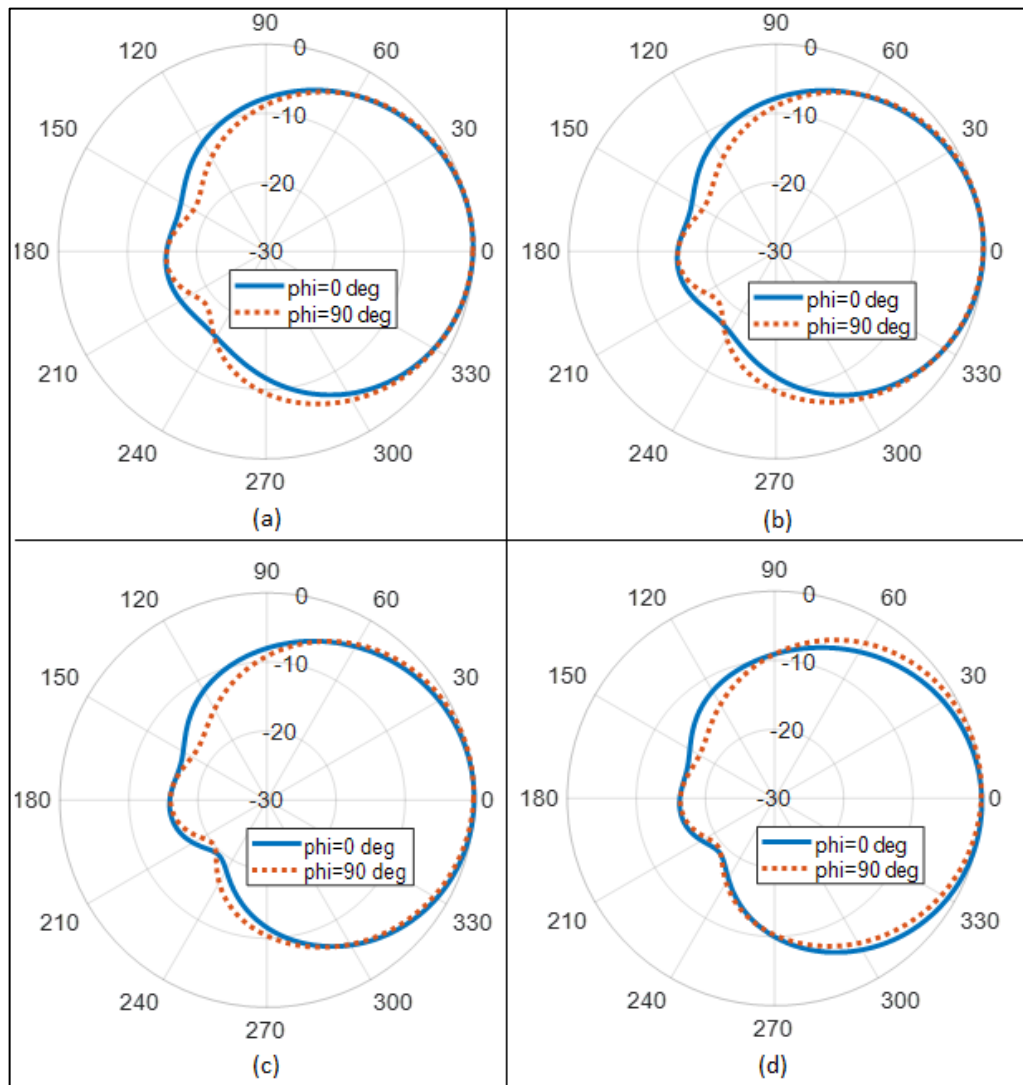


Figure 17: Radiation patterns at (a) 886MHz (b) 891 MHz (c) 903MHz (d) 924 MHz.

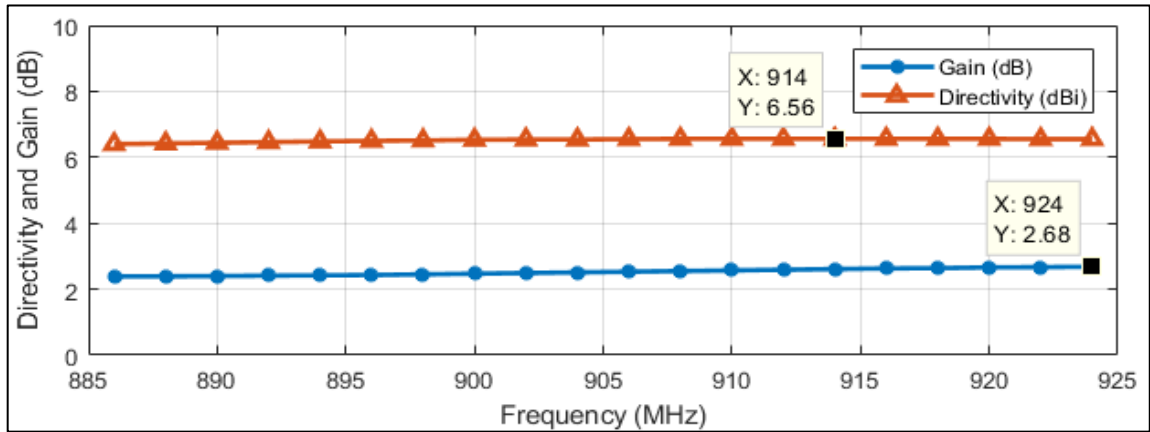


Figure 18: Directivity and gain versus frequency.

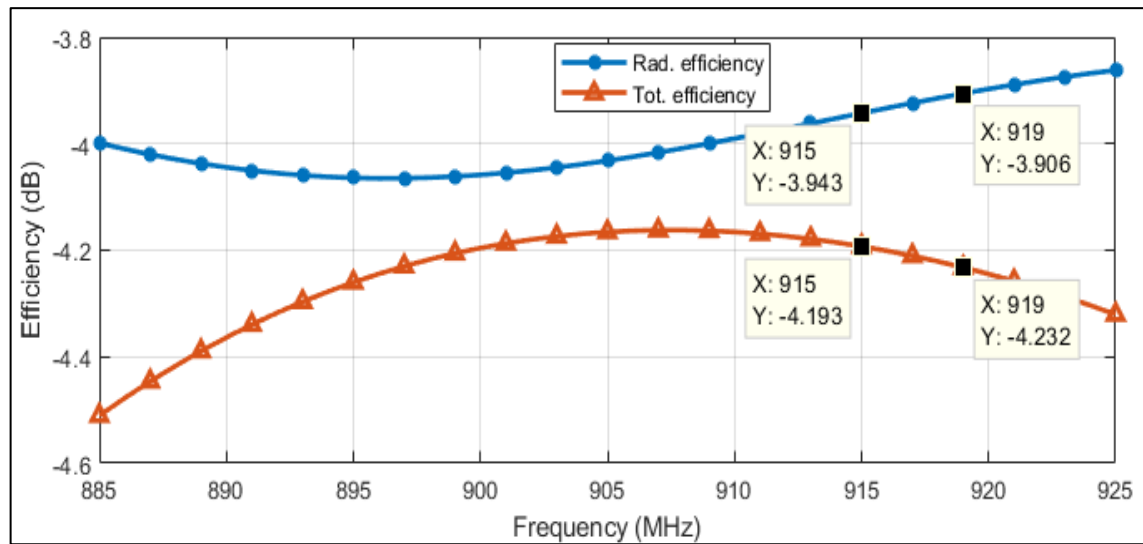


Figure 19: Radiation efficiency versus frequency.

In order to confirm that the proposed antenna is circularly polarized, the axial ratio of the antenna is given in Figure 20. From Figure 20, it can be observed that the minimum axial ratio occurs at 914 MHz with a value of 0.39 dB. The 3 dB AR frequency range is from 906 MHz – 921 MHz (1.59%). Figure 21 plots the AR against theta for varying frequencies. From Figure 21, it is shown that at 914 MHz, the polarization angular width is from 74° to 142° and at 918 MHz the polarization angular width is from 74° to 145°.

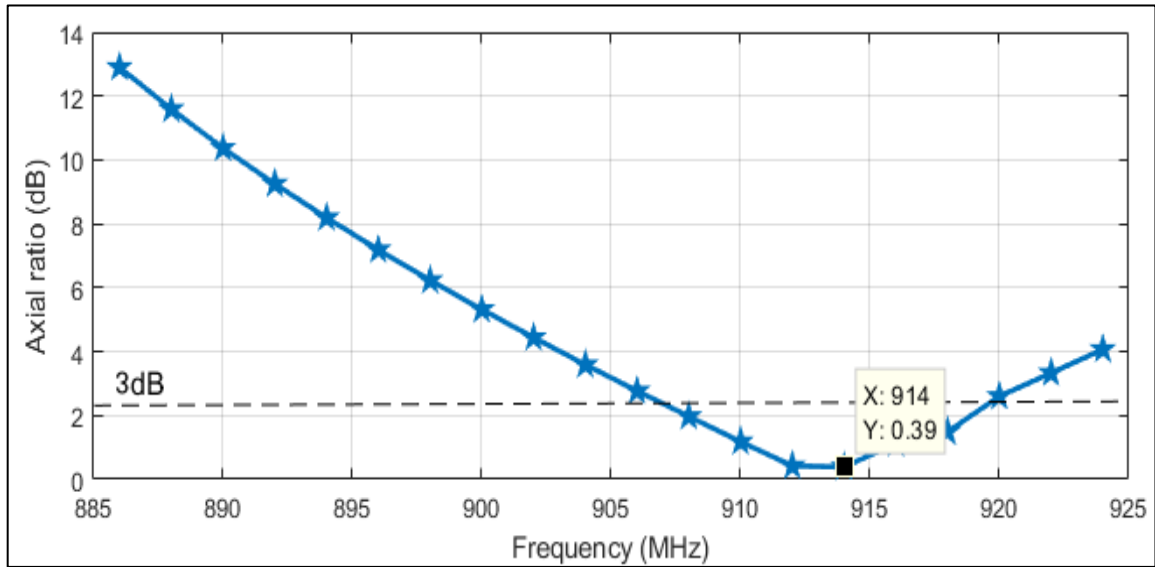


Figure 20: Axial ratio of the antenna.

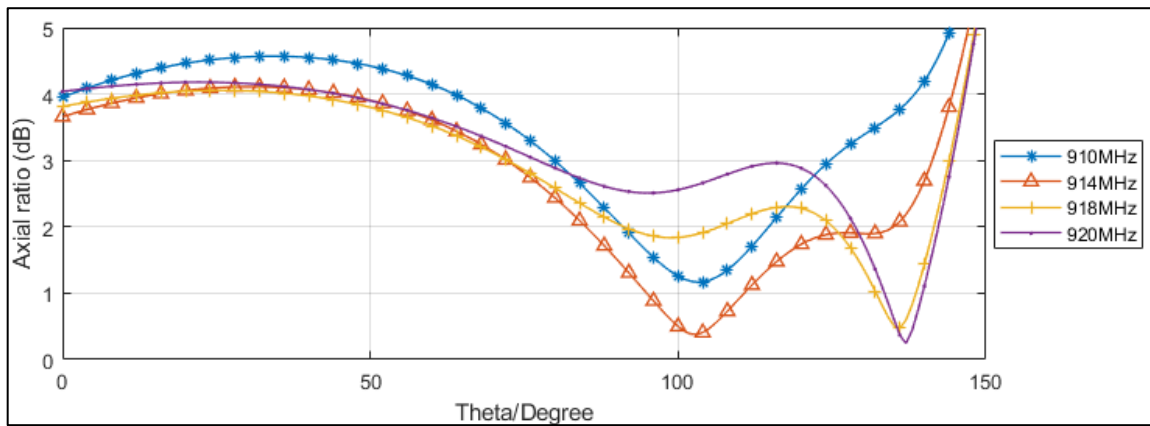


Figure 21: Axial ratio vs. theta for varying frequencies.

Table 6 compares the proposed antenna against reference values from literature, which shows the designed antennas for various performance parameters. The values in italics are approximate values recorded.

Table 6: Comparison of antennas.

Antenna	Bandwidth (BW)	Axial ratio BW %	Axial ratio	Polarization angular width (degrees)	Directivity	Gain
[46]	43MHz	3.47%	1.26dB	70	-	0.62dB
[53]	16MHz	0.65%	0.97dB	-	-	-
[54]	187MHz	4.3%	0.65dB	-	-	7.2dB
[55]	37MHz	0.54%	1.03dB	-	-	8.49dB
[56]	-	0.6%	1.11dB	-	-	-
[57]	23MHz	0.99%	0.20dB	-	-	10.8dB
[58]	66MHz	-	0.64dB	56	-	8.22dB
[59]	89MHz	6.5%	0.96dB	-	-	6.2dB
[60]	116MHz	10.5%	0.95dB	-	-	8.05dB
Proposed antenna	38MHz	1.59%	0.39dB	71	6.56dBi	2.68dB

By observing [54], [58, 59, 60], even though their bandwidth and gain are higher than that of the proposed antenna of 38 MHz and 2.68 dB respectively, their axial ratio exceeds the proposed antenna's axial ratio of 0.39 dB and their polarization angular width are smaller than the proposed antenna. Antenna [46], offers a higher bandwidth and axial ratio bandwidth of 43 MHz and 3.47% respectively, but it is achieved at the expense of its gain and axial ratio. Antenna [55] achieves a gain of 8.49 dB as compared to 2.68 dB for the proposed antenna, however it achieves this at the expense of its bandwidth, axial ratio bandwidth and axial ratio. Notably [57], produces the lowest axial ratio of 0.20 dB, which is lower than the proposed antenna, in addition it also has the highest gain of 10.8 dB. However, the bandwidth and axial ratio bandwidth is much lower than the proposed antenna. This was achieved by using two square cut-outs on the patch as well as a slit. In addition, a thicker substrate was used in conjunction with a larger ground plane. Table 7 shows the approximate total cost of the proposed antenna. The cost includes material and labor. Hence, it can be seen from Table 6 and Table 7 that the proposed antenna is low cost antenna with low AR and broad polarization angular width.

Table 7: Cost analysis.

Antenna designed Cost		Commercial antenna [61]
Materials	R 84.00	-
Labor (2 hours) [62]	R 356.00	-
Casing [63]	R 168.11	-
Total	R 608.11	R 1 130.22

4.4. Discussion

A low-cost UHF circularly polarized RFID antenna was designed. An overall size of $200\text{ mm} \times 200\text{ mm} \times 6.4\text{ mm}$ was achieved using the FR-4 material as the substrate. The antenna was fed using a 50 ohm PCB mount SMA connector. Practical testing of the antenna showed this antenna has a bandwidth of 57.53 MHz and achieved a return loss of -26.78 dB at a frequency of 914.05 MHz . In addition, the return loss at 915 MHz was approximately -21.65 dB . This shows the antenna has minimal power reflected to the source. In addition, it can be concluded that this antenna is circularly polarized, as demonstrated by the axial ratio. The antenna designed was also made using low-cost materials hence the overall cost to produce this antenna is low as compared to the commercial antenna. The fabricated antenna will be used to detect UHF RFID tags. Due to the low axial ratio achieved, it will allow the antenna to detect RFID tags in almost any orientation.

5. SIMULATION FOR MONITORING CONTAINARIZED CARGO IN AN UHF-RFID SYSTEM

5.1. Introduction

This chapter explores how EM waves behave inside a steel container by using a simulator. Two antennas were placed inside the steel container. One of the antennas was the transmitting antenna and the other antenna was the receiver antenna. The purpose of the simulation was to determine the behaviour of the EM waves inside the steel container when different materials were placed in front of the transmitting antenna. In reality the performance of an UHF RFID system will degrade when real world factors are introduced. According to Dobkin *et al*, [22], these factors include the placement of a RFID tag on various materials, such as metal surfaces, cement and the RF noise. Hence it is imperative that these factors are included together with the simulated results. This allows us to get a better understanding of how the system will behave in real world conditions. In addition, by understanding the behaviour of the EM waves inside the steel container, the power received by the receiver can also be calculated. The three materials that will be investigated are metal, plastic and wood.

5.2. Finite Difference Time Domain method

The FDTD method also known as Yee's method is commonly used for modelling computational electrodynamics by utilizing numerical analysis techniques. This method solves electromagnetic problems by simply discretizing Maxwell's equations in both space and time with central difference approximations [64]. The electric field vector components are solved in a given volume for a given time, once the electric field vector has been calculated the magnetic field vector components in the same volume are solved at the next time instant. This process then continues in a loop until the required transient electromagnetic field is reached.

5.2.1. Maxwell's equations in three dimensions

As mentioned before the FDTD method relies on Maxwell's equations [65], the time-dependent Maxwell's equations are given in differential and integral form by

Faraday's Law:

$$\frac{\partial \vec{B}}{\partial t} = -\nabla \times \vec{E} - \vec{M} \quad (10a)$$

$$\frac{\partial}{\partial t} \iint_A \vec{B} \cdot d\vec{A} = - \oint_l \vec{E} \cdot d\vec{l} - \iint_A \vec{M} \cdot d\vec{A} \quad (10b)$$

Ampere's Law:

$$\frac{\partial \vec{D}}{\partial t} = \nabla \times \vec{H} - \vec{J} \quad (11a)$$

$$\frac{\partial}{\partial t} \iint_A \vec{D} \cdot d\vec{A} = \oint_l \vec{H} \cdot d\vec{l} - \iint_A \vec{J} \cdot d\vec{A} \quad (11b)$$

Gauss' Law for the electric field:

$$\nabla \cdot \vec{D} = 0 \quad (12a)$$

$$\oiint_A \vec{D} \cdot d\vec{A} = 0 \quad (12b)$$

Gauss' Law for the magnetic field:

$$\nabla \cdot \vec{B} = 0 \quad (13a)$$

$$\oiint_A \vec{B} \cdot d\vec{A} = 0 \quad (13b)$$

Where,

\vec{E} – electric field (Volts/meter)

\vec{D} – electric flux density (Coulombs/meter²)

\vec{H} – magnetic field (Amperes/meter)

\vec{B} – magnetic flux density (Webers/meter²)

A – arbitrary three-dimensional surface

$d\vec{A}$ – differential normal vector that characterizes surface A (meter²)

l – closed contour that bounds surface A

$d\vec{l}$ – differential length vector that characterizes contour l (meters)

\vec{J} – electric current density (Amperes/meter²)

\vec{M} – equivalent magnetic current density (Volts/meter²)

The vectors \vec{D} and \vec{E} are related, assuming the material is linear, isotropic and nondispersive:

$$\vec{D} = \varepsilon \vec{E} = \varepsilon_r \varepsilon_0 \vec{E} \quad (14a)$$

The vectors \vec{B} and \vec{H} are related, assuming the material is linear, isotropic and nondispersive:

$$\vec{B} = \mu \vec{H} = \mu_r \mu_0 \vec{H} \quad (14b)$$

Where,

ε – electrical permittivity (Farads/meter)

ε_r – relative permittivity

ε_0 – free-space permittivity (8.854×10^{-12} Farads/meter)

μ – magnetic permeability (Henrys/meter)

μ_r – relative permeability

μ_0 – free-space permeability ($4\pi \times 10^{-7}$ Henrys/meter)

Since \vec{J} and \vec{M} can act as independent sources of the e-field and h-field we get \vec{J}_{source} and \vec{M}_{source} . In addition, since materials with isotropic, nondispersive and magnetic losses are allowed which attenuates the e-field and h-field by the conversion to heat energy. This therefore yields the following:

$$\vec{J} = \vec{J}_{source} + \sigma \vec{E} \quad (15a)$$

$$\vec{M} = \vec{M}_{source} + \sigma^* \vec{H} \quad (15b)$$

Where,

σ – electric conductivity (Siemens/meter)

σ^* – equivalent magnetic loss (Ohms/meter)

Substituting (14a), (14b) and (15a), (15b) into (10a) and (11a), will produce Maxwell's curl equations in a linear, isotropic, nondispersive, lossy material:

$$\frac{\delta \vec{H}}{\delta t} = -\frac{1}{\mu} \nabla \times \vec{E} - \frac{1}{\mu} (\vec{M}_{source} + \sigma^* \vec{H}) \quad (16)$$

$$\frac{\delta \vec{E}}{\delta t} = \frac{1}{\epsilon} \nabla \times \vec{H} - \frac{1}{\epsilon} (\vec{J}_{source} + \sigma \vec{E}) \quad (17)$$

This therefore means that Maxwell's equation in 3D as six coupled partial differential equations, which are shown below [66].

$$\frac{\delta E_x}{\delta t} = \frac{1}{\epsilon} \left[\frac{\delta H_z}{\delta y} - \frac{\delta H_y}{\delta z} - (J_{source_x} + \sigma E_x) \right] \quad (18a)$$

$$\frac{\delta E_y}{\delta t} = \frac{1}{\epsilon} \left[\frac{\delta H_x}{\delta z} - \frac{\delta H_z}{\delta x} - (J_{source_y} + \sigma E_y) \right] \quad (18b)$$

$$\frac{\delta E_z}{\delta t} = \frac{1}{\epsilon} \left[\frac{\delta H_y}{\delta x} - \frac{\delta H_x}{\delta y} - (J_{source_z} + \sigma E_z) \right] \quad (18c)$$

$$\frac{\delta H_x}{\delta t} = \frac{1}{\mu} \left[\frac{\delta E_y}{\delta z} - \frac{\delta E_z}{\delta y} - (M_{source_x} + \sigma^* H_x) \right] \quad (19a)$$

$$\frac{\delta H_y}{\delta t} = \frac{1}{\mu} \left[\frac{\delta E_z}{\delta x} - \frac{\delta E_x}{\delta z} - (M_{source_y} + \sigma^* H_y) \right] \quad (19b)$$

$$\frac{\delta H_z}{\delta t} = \frac{1}{\mu} \left[\frac{\delta E_x}{\delta y} - \frac{\delta E_y}{\delta x} - (M_{source_z} + \sigma^* H_z) \right] \quad (19c)$$

It is also important to consider the simplified two-dimensional and one-dimensional cases. As these cases also shows the importance of the electromagnetic phenomena, in addition it also yields insight into the analytical and algorithmic features of the above three-dimensional case.

5.2.2. Maxwell's equations in two dimensions

If it is assumed that these following conditions are true below:

- The model goes to infinity in the z-direction without any change in the position of its transverse cross section or shape.
- The incident wave in the z- direction is uniform, therefore all the fields with respect to z of the partial derivatives must be equal to zero.

Then the Maxwell's equations reduce to:

$$\frac{\delta E_x}{\delta t} = \frac{1}{\epsilon} \left[\frac{\delta H_z}{\delta y} - (J_{source_x} + \sigma E_x) \right] \quad (20a)$$

$$\frac{\delta E_y}{\delta t} = \frac{1}{\epsilon} \left[-\frac{\delta H_z}{\delta x} - (J_{source_y} + \sigma E_y) \right] \quad (20b)$$

$$\frac{\delta E_z}{\delta t} = \frac{1}{\epsilon} \left[\frac{\delta H_y}{\delta x} - \frac{\delta H_x}{\delta y} - (J_{source_z} + \sigma E_z) \right] \quad (20c)$$

$$\frac{\delta H_x}{\delta t} = \frac{1}{\mu} \left[-\frac{\delta E_z}{\delta y} - (M_{source_x} + \sigma^* H_x) \right] \quad (21a)$$

$$\frac{\delta H_y}{\delta t} = \frac{1}{\mu} \left[\frac{\delta E_z}{\delta x} - (M_{source_y} + \sigma^* H_y) \right] \quad (21b)$$

$$\frac{\delta H_z}{\delta t} = \frac{1}{\mu} \left[\frac{\delta E_x}{\delta y} - \frac{\delta E_y}{\delta x} - (M_{source_z} + \sigma^* H_z) \right] \quad (21c)$$

The transvers-magnetic mode with respect to z (TM_z) in two dimensions is therefore:

$$\frac{\delta E_z}{\delta t} = \frac{1}{\epsilon} \left[\frac{\delta H_y}{\delta x} - \frac{\delta H_x}{\delta y} - (J_{source_z} + \sigma E_z) \right] \quad (22a)$$

$$\frac{\delta H_x}{\delta t} = \frac{1}{\mu} \left[-\frac{\delta E_z}{\delta y} - (M_{source_x} + \sigma^* H_x) \right] \quad (22b)$$

$$\frac{\delta H_y}{\delta t} = \frac{1}{\mu} \left[\frac{\delta E_z}{\delta x} - (M_{source_y} + \sigma^* H_y) \right] \quad (22c)$$

The transvers-electric mode with respect to z (TE_z) in two dimensions is therefore:

$$\frac{\delta E_x}{\delta t} = \frac{1}{\epsilon} \left[\frac{\delta H_z}{\delta y} - (J_{source_x} + \sigma E_x) \right] \quad (23a)$$

$$\frac{\delta E_y}{\delta t} = \frac{1}{\epsilon} \left[-\frac{\delta H_z}{\delta x} - (J_{source_y} + \sigma E_y) \right] \quad (23b)$$

$$\frac{\delta H_z}{\delta t} = \frac{1}{\mu} \left[\frac{\delta E_x}{\delta y} - \frac{\delta E_y}{\delta x} - (M_{source_z} + \sigma^* H_z) \right] \quad (23c)$$

5.2.3. Maxwell's equations in one dimension

If it is assumed that these following conditions are true below:

- The EM field excitation and the modelled geometry must not have any differences in the y-direction.
- All field partial derivatives with respect to both y and z equal to zero.
- The contact structure contains an infinite space with possible material layering in the x-direction

Then the two-dimensional (TM_z) mode will reduce to:

$$\frac{\delta H_x}{\delta t} = -\frac{1}{\mu} [M_{source_x} + \sigma^* H_x] \quad (24a)$$

$$\frac{\delta H_y}{\delta t} = \frac{1}{\mu} \left[\frac{\delta E_z}{\delta x} - (M_{source_y} + \sigma^* H_y) \right] \quad (24b)$$

$$\frac{\delta E_z}{\delta t} = \frac{1}{\epsilon} \left[\frac{\delta H_y}{\delta x} - (J_{source_z} + \sigma E_z) \right] \quad (24c)$$

Assuming that $M_{source_x} = 0$ for all time and $H_x = 0$ at $t = 0$, then this implies that at $t = 0$, $\frac{\delta H_x}{\delta t} = 0$. By using simple inductive argument, it can also be seen that $H_x = 0$ for the entire time period.

Then we call this mode a z-polarized transverse electromagnetic (TEM) wave in the x direction in one dimension:

$$\frac{\delta H_y}{\delta t} = \frac{1}{\mu} \left[\frac{\delta E_z}{\delta x} - (M_{source_y} + \sigma^* H_y) \right] \quad (25a)$$

$$\frac{\delta E_z}{\delta t} = \frac{1}{\epsilon} \left[\frac{\delta H_y}{\delta x} - (J_{source_z} + \sigma E_z) \right] \quad (25b)$$

If it is assumed that these following conditions are true below:

- All field partial derivatives with respect to y equal to zero.

Then the two-dimensional (TE_z) mode reduce to:

$$\frac{\delta E_x}{\delta t} = -\frac{1}{\epsilon} [J_{source_x} + \sigma E_x] \quad (26a)$$

$$\frac{\delta E_y}{\delta t} = \frac{1}{\epsilon} \left[-\frac{\delta H_z}{\delta x} - (J_{source_y} + \sigma E_y) \right] \quad (26b)$$

$$\frac{\delta H_z}{\delta t} = \frac{1}{\mu} \left[\frac{\delta E_x}{\delta y} - \frac{\delta E_y}{\delta x} - (M_{source_z} + \sigma^* H_z) \right] \quad (26c)$$

Assuming that $J_{source_x} = 0$ for all time and $E_x = 0$ at $t = 0$, then this implies that at $t = 0$, $\frac{\delta E_x}{\delta t} = 0$. By using simple inductive argument, it can also be seen that $E_x = 0$ for the entire time period.

Then we call this mode a y-polarized TEM wave in the x direction in one dimension:

$$\frac{\delta E_y}{\delta t} = \frac{1}{\epsilon} \left[-\frac{\delta H_z}{\delta x} - (J_{source_y} + \sigma E_y) \right] \quad (27a)$$

$$\frac{\delta H_z}{\delta t} = \frac{1}{\mu} \left[\frac{\delta E_x}{\delta y} - \frac{\delta E_y}{\delta x} - (M_{source_z} + \sigma^* H_z) \right] \quad (27b)$$

5.2.4. Yee's algorithm

The Yee's algorithm which was introduced in 1966, is a set of finite-difference equations for the time-dependent Maxwell's curl equations. These equations have been proven to be robust because:

- Unlike previous solutions that solved the electric and magnetic fields one after the other, Yee's algorithm rather makes use of the coupled Maxwell's curl equation in order to solve both the electric and magnetic field in time and space.
- Figure 22 illustrates Yee space lattice using a cubic unit cell. It is shown that the Yee algorithm centres the electric and magnetic field components in the three-dimensional space. Therefore, every electric field component is surrounded by four magnetic field components and vice-versa.
- Lastly the Yee algorithm also centres the electric and magnetic field components in time. This is known as the leapfrog arrangement. All the electric field components computed in the sample space are kept in memory at a specific time instant and it uses previously stored data of the magnetic field components. This process is then repeated for the magnetic field component and it steps until the time-stepping is finished.

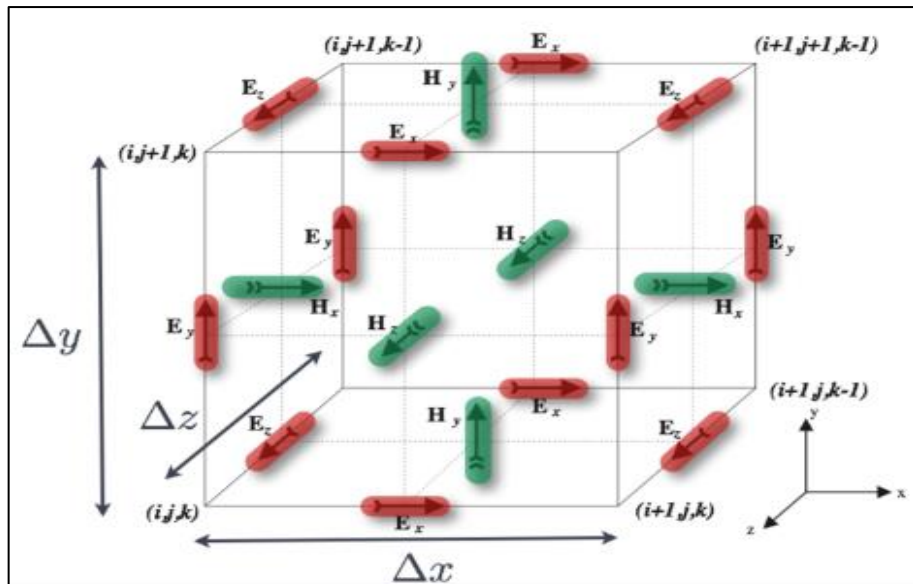


Figure 22: FDTD Yee cell displaying the electric (red) and magnetic (green) fields [67].

5.2.4.1. Finite difference expressions for Maxwell's equation

From the Yee algorithm above, the finite-difference expression using Maxwell's equations is as follows:

Firstly, the notation introduced by Yee for space points in a uniform rectangular lattice was:

$$(i, j, k) = (i\Delta x, j\Delta y, k\Delta z) \quad (28)$$

Where,

i, j, k – are integers.

$\Delta x, \Delta y, \Delta z$ – represents the lattice space increments in the x, y and z coordinate directions.

Secondly, Yee also introduced functions of space and time that are evaluated at a particular point in the grid and a particular point in time as:

$$u(i\Delta x, j\Delta y, k\Delta z, n\Delta t) \quad (29)$$

where,

n – is an integer.

Δt – is a time increment that is assumed to be uniform over the simulation interval.

And finally, the first partial space derivative of u in the x, y and z-direction at time $t_n = n\Delta t$ are:

$$\frac{\partial u}{\partial x}(i\Delta x, j\Delta y, k\Delta z, n\Delta t) = \frac{u_{i+\frac{1}{2},j,k}^n - u_{i-\frac{1}{2},j,k}^n}{\Delta x} + O[(\Delta x)^2] \quad (30a)$$

$$\frac{\partial u}{\partial y}(i\Delta x, j\Delta y, k\Delta z, n\Delta t) = \frac{u_{i,j+\frac{1}{2},k}^n - u_{i,j-\frac{1}{2},k}^n}{\Delta y} + O[(\Delta y)^2] \quad (30b)$$

$$\frac{\partial u}{\partial z}(i\Delta x, j\Delta y, k\Delta z, n\Delta t) = \frac{u_{i,j,k+\frac{1}{2}}^n - u_{i,j,k-\frac{1}{2}}^n}{\Delta z} + O[(\Delta z)^2] \quad (30c)$$

It can be shown that Yee used the central difference to obtain the finite difference approximation. Furthermore, the first-time partial derivative of u at a fixed point in space (i, j, k) is:

$$\frac{\partial u}{\partial t}(i\Delta x, j\Delta y, k\Delta z, n\Delta t) = \frac{u_{i,j,k}^{n+\frac{1}{2}} - u_{i,j,k}^{n-\frac{1}{2}}}{\Delta t} + O[(\Delta t)^2] \quad (31)$$

Therefore, using the above background the central difference substitution for the time and space derivative in Equation 18a (repeated below) at $E_x(i, j + \frac{1}{2}, k + \frac{1}{2}, n)$ is:

$$\frac{\delta E_x}{\delta t} = \frac{1}{\epsilon} \left[\frac{\delta H_z}{\delta y} - \frac{\delta H_y}{\delta z} - (J_{source_x} + \sigma E_x) \right] \quad (18a)$$

$$\begin{aligned} & \frac{E_x|_{i,j+\frac{1}{2},k+\frac{1}{2}}^{n+\frac{1}{2}} - E_x|_{i,j+\frac{1}{2},k+\frac{1}{2}}^{n-\frac{1}{2}}}{\Delta t} \\ &= \frac{1}{\epsilon_{i,j+\frac{1}{2},k+\frac{1}{2}}} \cdot \left(\frac{H_z|_{i,j+1,k+\frac{1}{2}}^n - H_z|_{i,j,k+\frac{1}{2}}^n}{\Delta y} - \frac{H_y|_{i,j+\frac{1}{2},k+1}^n - H_y|_{i,j+\frac{1}{2},k}^n}{\Delta z} \right. \\ & \quad \left. - J_{source_x}|_{i,j+\frac{1}{2},k+\frac{1}{2}}^n - \sigma_{i,j+\frac{1}{2},k+\frac{1}{2}} E_x|_{i,j+\frac{1}{2},k+\frac{1}{2}}^n \right) \end{aligned} \quad (32)$$

Using the semi-implicit approximation yields

$$E_x|_{i,j+\frac{1}{2},k+\frac{1}{2}}^n = \frac{E_x|_{i,j+\frac{1}{2},k+\frac{1}{2}}^{n+\frac{1}{2}} + E_x|_{i,j+\frac{1}{2},k+\frac{1}{2}}^{n-\frac{1}{2}}}{2} \quad (33)$$

Therefore, multiplying both sides by Δt and then substituting Equation 33 into Equation 32 will yield:

$$\begin{aligned}
& E_x \Big|_{i,j+\frac{1}{2},k+\frac{1}{2}}^{n+\frac{1}{2}} - E_x \Big|_{i,j+\frac{1}{2},k+\frac{1}{2}}^{n-\frac{1}{2}} \\
&= \frac{\Delta t}{\varepsilon_{i,j+\frac{1}{2},k+\frac{1}{2}}} \\
& \cdot \left(\begin{array}{c} \frac{H_z \Big|_{i,j+1,k+\frac{1}{2}}^n - H_z \Big|_{i,j,k+\frac{1}{2}}^n}{\Delta y} - \frac{H_y \Big|_{i,j+\frac{1}{2},k+1}^n - H_y \Big|_{i,j+\frac{1}{2},k}^n}{\Delta z} \\ -J_{source_x} \Big|_{i,j+\frac{1}{2},k+\frac{1}{2}}^n - \sigma_{i,j+\frac{1}{2},k+\frac{1}{2}} \left(\frac{E_x \Big|_{i,j+\frac{1}{2},k+\frac{1}{2}}^{n+\frac{1}{2}} + E_x \Big|_{i,j+\frac{1}{2},k+\frac{1}{2}}^{n-\frac{1}{2}}}{2} \right) \end{array} \right) \quad (34)
\end{aligned}$$

From Equation 34 the terms $E_x \Big|_{i,j+\frac{1}{2},k+\frac{1}{2}}^{n+\frac{1}{2}}$ and $E_x \Big|_{i,j+\frac{1}{2},k+\frac{1}{2}}^{n-\frac{1}{2}}$ appear on both sides. Therefore, collecting these terms and then isolating $E_x \Big|_{i,j+\frac{1}{2},k+\frac{1}{2}}^{n+\frac{1}{2}}$ on the left-hand side will yield:

$$\begin{aligned}
& \left(1 + \frac{\sigma_{i,j+\frac{1}{2},k+\frac{1}{2}} \Delta t}{2\varepsilon_{i,j+\frac{1}{2},k+\frac{1}{2}}} \right) E_x \Big|_{i,j+\frac{1}{2},k+\frac{1}{2}}^{n+\frac{1}{2}} \\
&= \left(1 - \frac{\sigma_{i,j+\frac{1}{2},k+\frac{1}{2}} \Delta t}{2\varepsilon_{i,j+\frac{1}{2},k+\frac{1}{2}}} \right) E_x \Big|_{i,j+\frac{1}{2},k+\frac{1}{2}}^{n-\frac{1}{2}} + \frac{\Delta t}{\varepsilon_{i,j+\frac{1}{2},k+\frac{1}{2}}} \\
& \cdot \left(\begin{array}{c} \frac{H_z \Big|_{i,j+1,k+\frac{1}{2}}^n - H_z \Big|_{i,j,k+\frac{1}{2}}^n}{\Delta y} - \frac{H_y \Big|_{i,j+\frac{1}{2},k+1}^n - H_y \Big|_{i,j+\frac{1}{2},k}^n}{\Delta z} \\ -J_{source_x} \Big|_{i,j+\frac{1}{2},k+\frac{1}{2}}^n \end{array} \right) \quad (35)
\end{aligned}$$

Finally dividing both sides by $\left(1 + \sigma_{i,j+\frac{1}{2},k+\frac{1}{2}} \Delta t / 2\varepsilon_{i,j+\frac{1}{2},k+\frac{1}{2}} \right)$ will yield the explicit time-stepping relation for $E_x \Big|_{i,j+\frac{1}{2},k+\frac{1}{2}}^{n+\frac{1}{2}}$:

$$\begin{aligned}
E_x \Big|_{i,j+\frac{1}{2},k+\frac{1}{2}}^{n+\frac{1}{2}} &= \left(\frac{1 - \frac{\sigma_{i,j+\frac{1}{2},k+\frac{1}{2}} \Delta t}{2\varepsilon_{i,j+\frac{1}{2},k+\frac{1}{2}}}}{1 + \frac{\sigma_{i,j+\frac{1}{2},k+\frac{1}{2}} \Delta t}{2\varepsilon_{i,j+\frac{1}{2},k+\frac{1}{2}}}} \right) E_x \Big|_{i,j+\frac{1}{2},k+\frac{1}{2}}^{n-\frac{1}{2}} \\
&+ \left(\frac{\frac{\Delta t}{\varepsilon_{i,j+\frac{1}{2},k+\frac{1}{2}}}}{1 + \frac{\sigma_{i,j+\frac{1}{2},k+\frac{1}{2}} \Delta t}{2\varepsilon_{i,j+\frac{1}{2},k+\frac{1}{2}}}} \right) \cdot \left(\frac{\frac{H_z \Big|_{i,j+1,k+\frac{1}{2}}^n - H_z \Big|_{i,j,k+\frac{1}{2}}^n}{\Delta y}}{H_y \Big|_{i,j+\frac{1}{2},k+1}^n - H_y \Big|_{i,j+\frac{1}{2},k}^n} \right. \\
&\quad \left. \frac{\Delta z}{-J_{source_x} \Big|_{i,j+\frac{1}{2},k+\frac{1}{2}}^n} \right) \quad (36a)
\end{aligned}$$

Using the above method to derive the finite difference expression for E_x , the finite difference expressions for E_y and E_z will be:

$$\begin{aligned}
E_y \Big|_{i-\frac{1}{2},j+1,k+\frac{1}{2}}^{n+\frac{1}{2}} &= \left(\frac{1 - \frac{\sigma_{i-\frac{1}{2},j+1,k+\frac{1}{2}} \Delta t}{2\varepsilon_{i-\frac{1}{2},j+1,k+\frac{1}{2}}}}{1 + \frac{\sigma_{i-\frac{1}{2},j+1,k+\frac{1}{2}} \Delta t}{2\varepsilon_{i-\frac{1}{2},j+1,k+\frac{1}{2}}}} \right) E_y \Big|_{i-\frac{1}{2},j+1,k+\frac{1}{2}}^{n-\frac{1}{2}} \\
&+ \left(\frac{\frac{\Delta t}{\varepsilon_{i-\frac{1}{2},j+1,k+\frac{1}{2}}}}{1 + \frac{\sigma_{i-\frac{1}{2},j+1,k+\frac{1}{2}} \Delta t}{2\varepsilon_{i-\frac{1}{2},j+1,k+\frac{1}{2}}}} \right) \cdot \left(\frac{\frac{H_x \Big|_{i-\frac{1}{2},j+1,k+1}^n - H_x \Big|_{i-\frac{1}{2},j+1,k}^n}{\Delta z}}{H_z \Big|_{i,j+1,k+\frac{1}{2}}^n - H_z \Big|_{i-1,j+1,k+\frac{1}{2}}^n} \right. \\
&\quad \left. \frac{\Delta x}{-J_{source_y} \Big|_{i-\frac{1}{2},j+1,k+\frac{1}{2}}^n} \right) \quad (36b)
\end{aligned}$$

$$E_z \Big|_{i-\frac{1}{2},j+\frac{1}{2},k+1}^{n+\frac{1}{2}} = \left(\frac{1 - \frac{\sigma_{i-\frac{1}{2},j+\frac{1}{2},k+1} \Delta t}{2\varepsilon_{i-\frac{1}{2},j+\frac{1}{2},k+1}}}{1 + \frac{\sigma_{i-\frac{1}{2},j+\frac{1}{2},k+1} \Delta t}{2\varepsilon_{i-\frac{1}{2},j+\frac{1}{2},k+1}}} \right) E_z \Big|_{i-\frac{1}{2},j+\frac{1}{2},k+1}^{n-\frac{1}{2}}$$

$$+ \left(\frac{\frac{\Delta t}{\varepsilon_{i-\frac{1}{2},j+\frac{1}{2},k+1}}}{1 + \frac{\sigma_{i-\frac{1}{2},j+\frac{1}{2},k+1} \Delta t}{2\varepsilon_{i-\frac{1}{2},j+\frac{1}{2},k+1}}} \right) \cdot \begin{pmatrix} \frac{H_y|_{i,j+\frac{1}{2},k+1}^n - H_y|_{i-1,j+\frac{1}{2},k+1}^n}{\Delta z} \\ \frac{H_x|_{i-\frac{1}{2},j+1,k+1}^n - H_x|_{i-\frac{1}{2},j,k+1}^n}{\Delta y} \\ -J_{sourcez}|_{i-\frac{1}{2},j+\frac{1}{2},k+1}^n \end{pmatrix} \quad (36c)$$

Now by analogy the derivation of the finite difference equations for the magnetic field components will follow the same procedure. In addition, the magnetic loss term $\sigma^* H$ was also estimated by using the semi-implicit approximation as done in Equation 33. Therefore, the finite difference equations for H_x , H_y and H_z is:

$$H_x|_{i-\frac{1}{2},j+1,k+1}^{n+1} = \left(\frac{1 - \frac{\sigma^*_{i-\frac{1}{2},j+1,k+1} \Delta t}{2\mu_{i-\frac{1}{2},j+1,k+1}}}{1 + \frac{\sigma^*_{i-\frac{1}{2},j+1,k+1} \Delta t}{2\mu_{i-\frac{1}{2},j+1,k+1}}} \right) H_x|_{i-\frac{1}{2},j+1,k+1}^n$$

$$+ \left(\frac{\frac{\Delta t}{\mu_{i-\frac{1}{2},j+1,k+1}}}{1 + \frac{\sigma^*_{i-\frac{1}{2},j+1,k+1} \Delta t}{2\mu_{i-\frac{1}{2},j+1,k+1}}} \right) \cdot \begin{pmatrix} \frac{E_y|_{i-\frac{1}{2},j+1,k+\frac{3}{2}}^{n+\frac{1}{2}} - E_y|_{i-\frac{1}{2},j+1,k+\frac{1}{2}}^{n+\frac{1}{2}}}{\Delta z} \\ -E_z|_{i-\frac{1}{2},j+\frac{3}{2},k+1}^{n+\frac{1}{2}} - E_z|_{i-\frac{1}{2},j+\frac{1}{2},k+1}^{n+\frac{1}{2}} \\ \Delta y \\ -M_{sourcex}|_{i-\frac{1}{2},j+1,k+1}^{n+\frac{1}{2}} \end{pmatrix} \quad (37a)$$

$$H_y|_{i,j+\frac{1}{2},k+1}^{n+1} = \left(\frac{1 - \frac{\sigma^*_{i,j+\frac{1}{2},k+1} \Delta t}{2\mu_{i,j+\frac{1}{2},k+1}}}{1 + \frac{\sigma^*_{i,j+\frac{1}{2},k+1} \Delta t}{2\mu_{i,j+\frac{1}{2},k+1}}} \right) H_y|_{i,j+\frac{1}{2},k+1}^n$$

$$+ \left(\frac{\frac{\Delta t}{\mu_{i,j+\frac{1}{2},k+1}}}{1 + \frac{\sigma_{i,j+\frac{1}{2},k+1}^* \Delta t}{2\mu_{i,j+\frac{1}{2},k+1}}} \right) \cdot \begin{pmatrix} \frac{E_z|_{i+\frac{1}{2},j+\frac{1}{2},k+1}^{n+\frac{1}{2}} - E_z|_{i-\frac{1}{2},j+\frac{1}{2},k+1}^{n+\frac{1}{2}}}{\Delta x} \\ - \frac{E_x|_{i,j+\frac{1}{2},k+\frac{3}{2}}^{n+\frac{1}{2}} - E_x|_{i,j+\frac{1}{2},k+\frac{1}{2}}^{n+\frac{1}{2}}}{\Delta z} \\ -M_{source_x}|_{i,j+\frac{1}{2},k+1}^{n+\frac{1}{2}} \end{pmatrix} \quad (37b)$$

$$H_z|_{i,j+1,k+\frac{1}{2}}^{n+1} = \left(\frac{1 - \frac{\sigma_{i,j+1,k+\frac{1}{2}}^* \Delta t}{2\mu_{i,j+1,k+\frac{1}{2}}}}{1 + \frac{\sigma_{i,j+1,k+\frac{1}{2}}^* \Delta t}{2\mu_{i,j+1,k+\frac{1}{2}}}} \right) H_z|_{i,j+1,k+\frac{1}{2}}^n$$

$$+ \left(\frac{\frac{\Delta t}{\mu_{i,j+1,k+\frac{1}{2}}}}{1 + \frac{\sigma_{i,j+1,k+\frac{1}{2}}^* \Delta t}{2\mu_{i,j+1,k+\frac{1}{2}}}} \right) \cdot \begin{pmatrix} \frac{E_x|_{i,j+\frac{3}{2},k+\frac{1}{2}}^{n+\frac{1}{2}} - E_x|_{i,j+\frac{1}{2},k+\frac{1}{2}}^{n+\frac{1}{2}}}{\Delta y} \\ - \frac{E_y|_{i+\frac{1}{2},j+1,k+\frac{1}{2}}^{n+\frac{1}{2}} - E_y|_{i-\frac{1}{2},j+1,k+\frac{1}{2}}^{n+\frac{1}{2}}}{\Delta x} \\ -M_{source_z}|_{i,j+1,k+\frac{1}{2}}^{n+\frac{1}{2}} \end{pmatrix} \quad (37c)$$

Using these finite difference expressions, the new values of the electromagnetic field vector components located anywhere on the lattice only depends on three things; the previous value, the previous values of the other field vector which must be at next to each other and lastly the electric and magnetic current sources must be known.

5.2.4.2. Update Coefficients

Update coefficients are necessary because they allow a region of space to have a continuous variation in the material properties. Therefore, before the time-stepping starts, it is imperative that these coefficients are defined and stored for each field vector component.

Updating coefficients at general E-field component location (i, j, k) :

$$C_a|_{i,j,k} = \frac{\left(1 - \frac{\sigma_{i,j,k}\Delta t}{2\varepsilon_{i,j,k}}\right)}{\left(1 + \frac{\sigma_{i,j,k}\Delta t}{2\varepsilon_{i,j,k}}\right)} \quad (38a)$$

$$C_{b_1}|_{i,j,k} = \frac{\left(\frac{\Delta t}{2\varepsilon_{i,j,k}\Delta_1}\right)}{\left(1 + \frac{\sigma_{i,j,k}\Delta t}{2\varepsilon_{i,j,k}}\right)} \quad (38b)$$

$$C_{b_2}|_{i,j,k} = \frac{\left(\frac{\Delta t}{2\varepsilon_{i,j,k}\Delta_2}\right)}{\left(1 + \frac{\sigma_{i,j,k}\Delta t}{2\varepsilon_{i,j,k}}\right)} \quad (38c)$$

Updating coefficients at general H-field component location (i, j, k) :

$$D_a|_{i,j,k} = \frac{\left(1 - \frac{\sigma^*_{i,j,k}\Delta t}{2\mu_{i,j,k}}\right)}{\left(1 - \frac{\sigma^*_{i,j,k}\Delta t}{2\mu_{i,j,k}}\right)} \quad (39a)$$

$$D_{b_1}|_{i,j,k} = \frac{\left(\frac{\Delta t}{2\mu_{i,j,k}\Delta_1}\right)}{\left(1 + \frac{\sigma^*_{i,j,k}\Delta t}{2\mu_{i,j,k}}\right)} \quad (39b)$$

$$D_{b_2}|_{i,j,k} = \frac{\left(\frac{\Delta t}{2\mu_{i,j,k}\Delta_1}\right)}{\left(1 + \frac{\sigma^*_{i,j,k}\Delta t}{2\mu_{i,j,k}}\right)} \quad (39c)$$

where,

Δ_1 and Δ_2 – denotes the two possible lattice space increments used for the finite differences in each field component calculation.

Since for a cubic lattice $\Delta_x = \Delta_y = \Delta_z = \Delta$, therefore $\Delta_1 = \Delta_2 = \Delta$. Hence it can then be concluded that $C_{b_1} = C_{b_2}$ and $D_{b_1} = D_{b_2}$, thus this reduces the memory needed to store this two updating coefficients per field vector component. The finite difference expression in Equations 36 and 37 can be rewritten as follows:

$$E_x \Big|_{i,j+\frac{1}{2},k+\frac{1}{2}}^{n+\frac{1}{2}} = C_{a,E_x} \Big|_{i,j+\frac{1}{2},k+\frac{1}{2}} E_x \Big|_{i,j+\frac{1}{2},k+\frac{1}{2}}^{n-\frac{1}{2}} \\ + C_{b,E_x} \Big|_{i,j+\frac{1}{2},k+\frac{1}{2}} \cdot \left(\begin{array}{c} H_z \Big|_{i,j+1,k+\frac{1}{2}}^n - H_z \Big|_{i,j,k+\frac{1}{2}}^n + H_y \Big|_{i,j+\frac{1}{2},k}^n - H_y \Big|_{i,j+\frac{1}{2},k+1}^n \\ - J_{source_x} \Big|_{i,j+\frac{1}{2},k+\frac{1}{2}}^n \Delta \end{array} \right) \quad (40a)$$

$$E_y \Big|_{i-\frac{1}{2},j+1,k+\frac{1}{2}}^{n+\frac{1}{2}} = C_{a,E_y} \Big|_{i-\frac{1}{2},j+1,k+\frac{1}{2}} E_y \Big|_{i-\frac{1}{2},j+1,k+\frac{1}{2}}^{n-\frac{1}{2}} \\ + C_{b,E_y} \Big|_{i-\frac{1}{2},j+1,k+\frac{1}{2}} \cdot \left(\begin{array}{c} H_x \Big|_{i-\frac{1}{2},j+1,k+1}^n - H_x \Big|_{i-\frac{1}{2},j+1,k}^n + H_z \Big|_{i-1,j+1,k+\frac{1}{2}}^n - H_z \Big|_{i,j+1,k+\frac{1}{2}}^n \\ - J_{source_y} \Big|_{i-\frac{1}{2},j+1,k+\frac{1}{2}}^n \Delta \end{array} \right) \quad (40b)$$

$$E_z \Big|_{i-\frac{1}{2},j+\frac{1}{2},k+1}^{n+\frac{1}{2}} = C_{a,E_z} \Big|_{i-\frac{1}{2},j+\frac{1}{2},k+1} E_z \Big|_{i-\frac{1}{2},j+\frac{1}{2},k+1}^{n-\frac{1}{2}} \\ + C_{b,E_z} \Big|_{i-\frac{1}{2},j+\frac{1}{2},k+1} \cdot \left(\begin{array}{c} H_y \Big|_{i,j+\frac{1}{2},k+1}^n - H_y \Big|_{i-1,j+\frac{1}{2},k+1}^n + H_x \Big|_{i-\frac{1}{2},j,k+1}^n - H_x \Big|_{i-\frac{1}{2},j+1,k+1}^n \\ - J_{source_z} \Big|_{i-\frac{1}{2},j+\frac{1}{2},k+1}^n \Delta \end{array} \right) \quad (40c)$$

And,

$$H_x \Big|_{i-\frac{1}{2},j+1,k+1}^{n+1} = D_{a,H_x} \Big|_{i-\frac{1}{2},j+1,k+1} H_x \Big|_{i-\frac{1}{2},j+1,k+1}^n \\ + D_{b,H_x} \Big|_{i-\frac{1}{2},j+1,k+1} \cdot \left(\begin{array}{c} E_y \Big|_{i-\frac{1}{2},j+1,k+\frac{3}{2}}^{n+\frac{1}{2}} - E_y \Big|_{i-\frac{1}{2},j+1,k+\frac{1}{2}}^{n+\frac{1}{2}} + E_z \Big|_{i-\frac{1}{2},j+\frac{1}{2},k+1}^{n+\frac{1}{2}} - E_z \Big|_{i-\frac{1}{2},j+\frac{3}{2},k+1}^{n+\frac{1}{2}} \\ - M_{source_x} \Big|_{i-\frac{1}{2},j+1,k+1}^{n+\frac{1}{2}} \Delta \end{array} \right) \quad (41a)$$

$$H_y \Big|_{i,j+\frac{1}{2},k+1}^{n+1} = D_{a,H_y} \Big|_{i,j+\frac{1}{2},k+1} H_y \Big|_{i,j+\frac{1}{2},k+1}^n$$

$$+ D_{b,H_y} \Big|_{i,j+\frac{1}{2},k+1} \cdot \left(\begin{array}{c} E_z \Big|_{i+\frac{1}{2},j+\frac{1}{2},k+1}^{n+\frac{1}{2}} - E_z \Big|_{i-\frac{1}{2},j+\frac{1}{2},k+1}^{n+\frac{1}{2}} + E_x \Big|_{i,j+\frac{1}{2},k+\frac{1}{2}}^{n+\frac{1}{2}} - E_x \Big|_{i,j+\frac{1}{2},k+\frac{3}{2}}^{n+\frac{1}{2}} \\ - M_{source_y} \Big|_{i,j+\frac{1}{2},k+1}^{n+\frac{1}{2}} \Delta \end{array} \right) \quad (41b)$$

$$H_z \Big|_{i,j+1,k+\frac{1}{2}}^{n+1} = D_{a,H_z} \Big|_{i,j+1,k+\frac{1}{2}} H_z \Big|_{i,j+1,k+\frac{1}{2}}^n$$

$$+ D_{b,H_z} \Big|_{i,j+1,k+\frac{1}{2}} \cdot \left(\begin{array}{c} E_x \Big|_{i,j+\frac{3}{2},k+\frac{1}{2}}^{n+\frac{1}{2}} - E_x \Big|_{i,j+\frac{1}{2},k+\frac{1}{2}}^{n+\frac{1}{2}} + E_y \Big|_{i-\frac{1}{2},j+1,k+\frac{1}{2}}^{n+\frac{1}{2}} - E_y \Big|_{i+\frac{1}{2},j+1,k+\frac{1}{2}}^{n+\frac{1}{2}} \\ - M_{source_z} \Big|_{i,j+1,k+\frac{1}{2}}^{n+\frac{1}{2}} \Delta \end{array} \right) \quad (41c)$$

5.2.4.3. Sample space with distinct media

The Equations 40 and 41 can be further simplified by using an integer array called MEDIA (i, j, k) . This array will store the data for a limited number of media which have unique electrical properties. The simplified equations are therefore:

$$m = MEDIA_{E_x} \Big|_{i,j+\frac{1}{2},k+\frac{1}{2}} \quad (42a)$$

$$E_x \Big|_{i,j+\frac{1}{2},k+\frac{1}{2}}^{n+\frac{1}{2}} = C_a(m) E_x \Big|_{i,j+\frac{1}{2},k+\frac{1}{2}}^{n-\frac{1}{2}} + C_b(m) \cdot \left(\begin{array}{c} H_z \Big|_{i,j+1,k+\frac{1}{2}}^n - H_z \Big|_{i,j,k+\frac{1}{2}}^n + H_y \Big|_{i,j+\frac{1}{2},k}^n - H_y \Big|_{i,j+\frac{1}{2},k+1}^n - J_{source_x} \Big|_{i,j+\frac{1}{2},k+\frac{1}{2}}^n \Delta \end{array} \right)$$

$$m = MEDIA_{E_y} \Big|_{i-\frac{1}{2},j+1,k+\frac{1}{2}} \quad (42b)$$

$$E_y \Big|_{i-\frac{1}{2},j+1,k+\frac{1}{2}}^{n+\frac{1}{2}} = C_a(m) E_y \Big|_{i-\frac{1}{2},j+1,k+\frac{1}{2}}^{n-\frac{1}{2}} + C_b(m) \cdot \left(\begin{array}{c} H_x \Big|_{i-\frac{1}{2},j+1,k+1}^n - H_x \Big|_{i-\frac{1}{2},j+1,k}^n + H_z \Big|_{i-1,j+1,k+\frac{1}{2}}^n - H_z \Big|_{i,j+1,k+\frac{1}{2}}^n \\ - J_{source_y} \Big|_{i-\frac{1}{2},j+1,k+\frac{1}{2}}^n \Delta \end{array} \right)$$

$$m = MEDIA_{E_z} \Big|_{i-\frac{1}{2},j+\frac{1}{2},k+1} \quad (42c)$$

$$E_z \Big|_{i-\frac{1}{2}, j+\frac{1}{2}, k+1}^{n+\frac{1}{2}} = C_a(m) E_z \Big|_{i-\frac{1}{2}, j+\frac{1}{2}, k+1}^{n-\frac{1}{2}} + C_b(m) \cdot \left(\begin{array}{c} H_y \Big|_{i, j+\frac{1}{2}, k+1}^n - H_y \Big|_{i-1, j+\frac{1}{2}, k+1}^n + H_x \Big|_{i-\frac{1}{2}, j, k+1}^n - H_x \Big|_{i-\frac{1}{2}, j+1, k+1}^n \\ - J_{source_z} \Big|_{i-\frac{1}{2}, j+\frac{1}{2}, k+1}^n \Delta \end{array} \right)$$

And,

$$m = MEDIA_{H_x} \Big|_{i-\frac{1}{2}, j+1, k+1} \quad (43a)$$

$$H_x \Big|_{i-\frac{1}{2}, j+1, k+1}^{n+1} = D_a(m) H_x \Big|_{i-\frac{1}{2}, j+1, k+1}^n + D_a(m) \cdot \left(\begin{array}{c} E_y \Big|_{i-\frac{1}{2}, j+1, k+\frac{3}{2}}^{n+\frac{1}{2}} - E_y \Big|_{i-\frac{1}{2}, j+1, k+\frac{1}{2}}^{n+\frac{1}{2}} + E_z \Big|_{i-\frac{1}{2}, j+\frac{1}{2}, k+1}^{n+\frac{1}{2}} - E_z \Big|_{i-\frac{1}{2}, j+\frac{3}{2}, k+1}^{n+\frac{1}{2}} \\ - M_{source_x} \Big|_{i-\frac{1}{2}, j+1, k+1}^{n+\frac{1}{2}} \Delta \end{array} \right)$$

$$m = MEDIA_{H_y} \Big|_{i, j+\frac{1}{2}, k+1} \quad (43b)$$

$$H_y \Big|_{i, j+\frac{1}{2}, k+1}^{n+1} = D_a(m) H_y \Big|_{i, j+\frac{1}{2}, k+1}^n + D_b(m) \cdot \left(\begin{array}{c} E_z \Big|_{i+\frac{1}{2}, j+\frac{1}{2}, k+1}^{n+\frac{1}{2}} - E_z \Big|_{i-\frac{1}{2}, j+\frac{1}{2}, k+1}^{n+\frac{1}{2}} + E_x \Big|_{i, j+\frac{1}{2}, k+\frac{1}{2}}^{n+\frac{1}{2}} - E_x \Big|_{i, j+\frac{1}{2}, k+\frac{3}{2}}^{n+\frac{1}{2}} \\ - M_{source_y} \Big|_{i, j+\frac{1}{2}, k+1}^{n+\frac{1}{2}} \Delta \end{array} \right)$$

$$m = MEDIA_{H_z} \Big|_{i, j+1, k+\frac{1}{2}} \quad (43c)$$

$$H_z \Big|_{i, j+1, k+\frac{1}{2}}^{n+1} = D_a(m) H_z \Big|_{i, j+1, k+\frac{1}{2}}^n + D_b(m) \cdot \left(\begin{array}{c} E_x \Big|_{i, j+\frac{3}{2}, k+\frac{1}{2}}^{n+\frac{1}{2}} - E_x \Big|_{i, j+\frac{1}{2}, k+\frac{1}{2}}^{n+\frac{1}{2}} + E_y \Big|_{i-\frac{1}{2}, j+1, k+\frac{1}{2}}^{n+\frac{1}{2}} - E_y \Big|_{i+\frac{1}{2}, j+1, k+\frac{1}{2}}^{n+\frac{1}{2}} \\ - M_{source_z} \Big|_{i, j+1, k+\frac{1}{2}}^{n+\frac{1}{2}} \Delta \end{array} \right)$$

- Nonpermeable media

In the event nonpermeable media is used the finite difference equations in Equations 42 and 43 can be reduced by using the proportional \vec{E} and \vec{M} vectors:

$$\hat{\vec{E}} = \left(\frac{\Delta t}{\mu_0 \Delta} \right) \vec{E} \quad (44)$$

$$\hat{\vec{M}} = \left(\frac{\Delta t}{\mu_0} \right) \vec{M} \quad (45)$$

The scaled E-field updating coefficient $\widehat{C}_b(m)$ is defined as:

$$\widehat{C}_b(m) = \left(\frac{\Delta t}{\mu_0 \Delta} \right) C_b(m) \quad (46)$$

Therefore, the reduced finite-difference equations now become:

$$m = MEDIA_{E_x} \Big|_{i,j+\frac{1}{2},k+\frac{1}{2}} \quad (47a)$$

$$\begin{aligned} \widehat{E}_x \Big|_{i,j+\frac{1}{2},k+\frac{1}{2}}^{n+\frac{1}{2}} &= C_a(m) \widehat{E}_x \Big|_{i,j+\frac{1}{2},k+\frac{1}{2}}^{n-\frac{1}{2}} + \widehat{C}_b(m) \\ &\cdot \left(H_z \Big|_{i,j+1,k+\frac{1}{2}}^n - H_z \Big|_{i,j,k+\frac{1}{2}}^n + H_y \Big|_{i,j+\frac{1}{2},k}^n - H_y \Big|_{i,j+\frac{1}{2},k+1}^n - J_{source_x} \Big|_{i,j+\frac{1}{2},k+\frac{1}{2}}^n \Delta \right) \end{aligned}$$

$$m = MEDIA_{E_y} \Big|_{i-\frac{1}{2},j+1,k+\frac{1}{2}} \quad (47b)$$

$$\begin{aligned} \widehat{E}_y \Big|_{i-\frac{1}{2},j+1,k+\frac{1}{2}}^{n+\frac{1}{2}} &= C_a(m) \widehat{E}_y \Big|_{i-\frac{1}{2},j+1,k+\frac{1}{2}}^{n-\frac{1}{2}} + \widehat{C}_b(m) \\ &\cdot \left(H_x \Big|_{i-\frac{1}{2},j+1,k+1}^n - H_x \Big|_{i-\frac{1}{2},j+1,k}^n + H_z \Big|_{i-1,j+1,k+\frac{1}{2}}^n - H_z \Big|_{i,j+1,k+\frac{1}{2}}^n \right. \\ &\quad \left. - J_{source_y} \Big|_{i-\frac{1}{2},j+1,k+\frac{1}{2}}^n \Delta \right) \end{aligned}$$

$$m = MEDIA_{E_z} \Big|_{i-\frac{1}{2},j+\frac{1}{2},k+1} \quad (47c)$$

$$\widehat{E}_z \Big|_{i-\frac{1}{2},j+\frac{1}{2},k+1}^{n+\frac{1}{2}} = C_a(m)\widehat{E}_z \Big|_{i-\frac{1}{2},j+\frac{1}{2},k+1}^{n-\frac{1}{2}} + \widehat{C}_b(m) \cdot \left(\begin{array}{c} H_y \Big|_{i,j+\frac{1}{2},k+1}^n - H_y \Big|_{i-1,j+\frac{1}{2},k+1}^n + H_x \Big|_{i-\frac{1}{2},j,k+1}^n - H_x \Big|_{i-\frac{1}{2},j+1,k+1}^n \\ - J_{source_z} \Big|_{i-\frac{1}{2},j+\frac{1}{2},k+1}^n \Delta \end{array} \right)$$

And,

$$\begin{aligned} H_x \Big|_{i-\frac{1}{2},j+1,k+1}^{n+1} &= H_x \Big|_{i-\frac{1}{2},j+1,k+1}^n + \widehat{E}_y \Big|_{i-\frac{1}{2},j+1,k+\frac{3}{2}}^{n+\frac{1}{2}} - \widehat{E}_y \Big|_{i-\frac{1}{2},j+1,k+\frac{1}{2}}^{n+\frac{1}{2}} + \widehat{E}_z \Big|_{i-\frac{1}{2},j+\frac{1}{2},k+1}^{n+\frac{1}{2}} \\ &\quad - \widehat{E}_z \Big|_{i-\frac{1}{2},j+\frac{3}{2},k+1}^{n+\frac{1}{2}} - M_{source_x} \Big|_{i-\frac{1}{2},j+1,k+1}^{n+\frac{1}{2}} \end{aligned} \quad (48a)$$

$$\begin{aligned} H_y \Big|_{i,j+\frac{1}{2},k+1}^{n+1} &= H_y \Big|_{i,j+\frac{1}{2},k+1}^n + \widehat{E}_z \Big|_{i+\frac{1}{2},j+\frac{1}{2},k+1}^{n+\frac{1}{2}} - \widehat{E}_z \Big|_{i-\frac{1}{2},j+\frac{1}{2},k+1}^{n+\frac{1}{2}} + \widehat{E}_x \Big|_{i,j+\frac{1}{2},k+\frac{1}{2}}^{n+\frac{1}{2}} - \widehat{E}_x \Big|_{i,j+\frac{1}{2},k+\frac{3}{2}}^{n+\frac{1}{2}} \\ &\quad - M_{source_y} \Big|_{i,j+\frac{1}{2},k+1}^{n+\frac{1}{2}} \end{aligned} \quad (48b)$$

$$\begin{aligned} H_z \Big|_{i,j+1,k+\frac{1}{2}}^{n+1} &= H_z \Big|_{i,j+1,k+\frac{1}{2}}^n + \widehat{E}_x \Big|_{i,j+\frac{3}{2},k+\frac{1}{2}}^{n+\frac{1}{2}} - \widehat{E}_x \Big|_{i,j+\frac{1}{2},k+\frac{1}{2}}^{n+\frac{1}{2}} + \widehat{E}_y \Big|_{i-\frac{1}{2},j+1,k+\frac{1}{2}}^{n+\frac{1}{2}} - \widehat{E}_y \Big|_{i+\frac{1}{2},j+1,k+\frac{1}{2}}^{n+\frac{1}{2}} \\ &\quad - M_{source_z} \Big|_{i,j+1,k+\frac{1}{2}}^{n+\frac{1}{2}} \end{aligned} \quad (48c)$$

This reduced finite difference equations take away the multiplications that was previously required to update the H-field vector components and only now requires that the MEDIA arrays are stored for the E-field components only. Thus, reducing the storage space required.

5.2.5. gprMax software

gprMax is an open source software package that solves Maxwell's equations in 3D and 2D domains by means of the FDTD method. This software achieves this by specifying a single cell slice of the domain. Once this is done the electric and magnetic field components on the two faces of the single cell in the invariant direction are set to zero. This is illustrated in Figure 23.

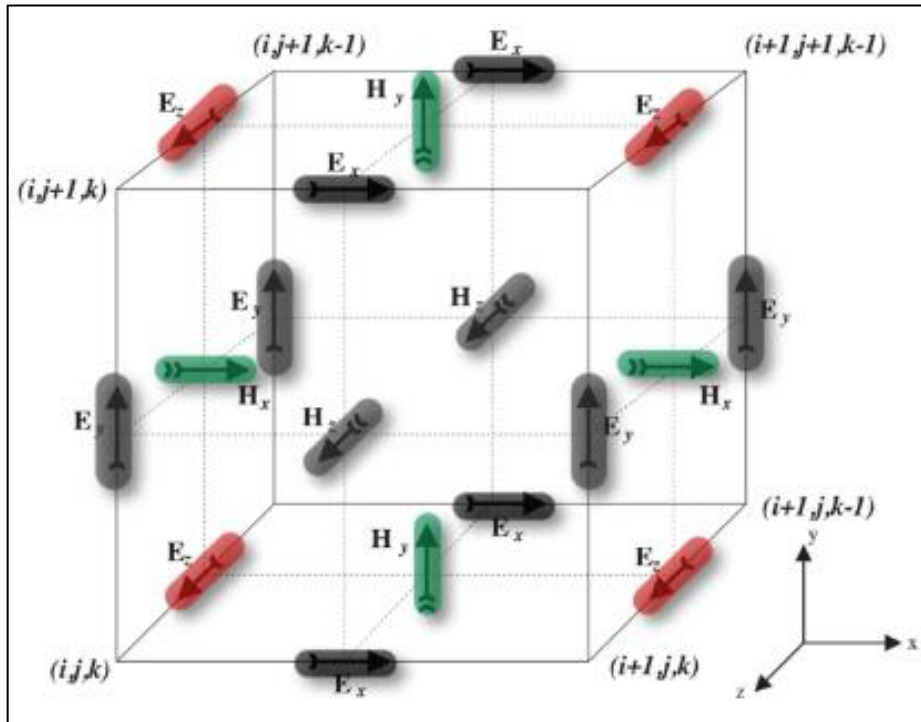


Figure 23: FDTD Yee cell displaying the electric (red), magnetic (green) and zeroed out fields (grey) [67].

As mentioned before these equations are then discretized in space and time and applied in each FDTD cell. The solution is then obtained in the time domain in an iterative manner. With each repetition the electromagnetic waves travel in the FDTD grid. Each propagation agrees to an elapsed simulation time.

5.3. Simulation

5.3.1. Modelling

As mentioned before the open source software gprMax was used to simulate how the EM waves propagate inside a steel container. Figure 24 shows the geometry of the scenario. The boundary is made of steel and the inside of the steel container is free space. The transmitting antenna (RFID tag) is sandwiched in between a plastic RFID tag mount and the material that will be investigated i.e. wood, plastic, or steel. From Figure 25, two RFID tag positions inside the steel container will be investigated. These positions are shown as position 1 and position 2. Position 1 is considered to be the worse-case scenario because it is located the furthest away from the RFID reader's antenna. Position 2 is the best-case scenario because it is located directly in line with the RFID reader's antenna. The simulation was carried out in a two-dimensional space. A three-dimensional space was not used because of memory constraints. A total of 228 GB of random-access memory

(RAM) was needed for a three-dimensional simulation. However, the results from the simulation were comparable to the practical testing in Section 5.4.

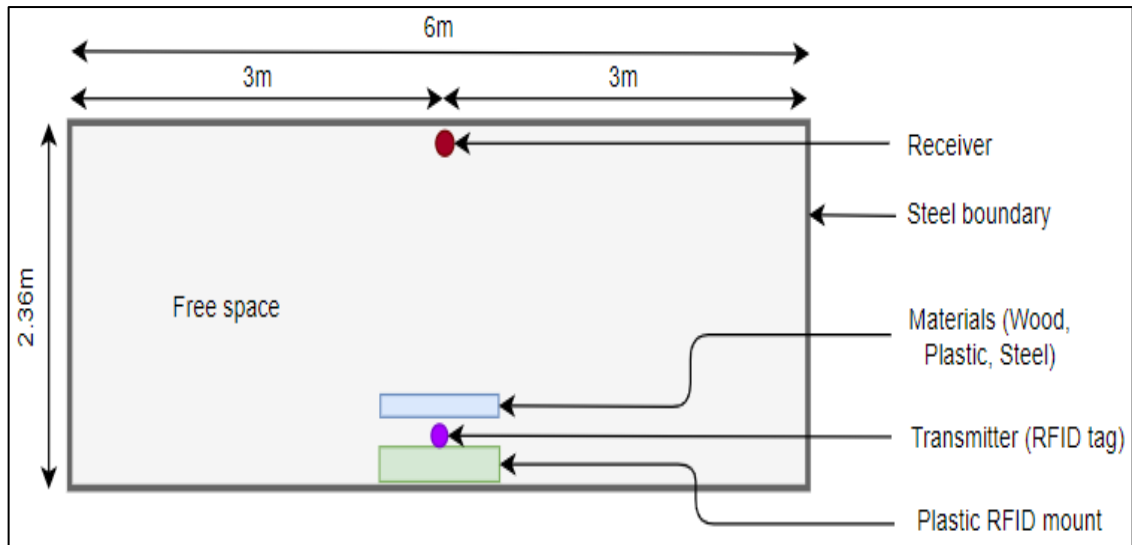


Figure 24: Geometry of the scenario to be investigated.

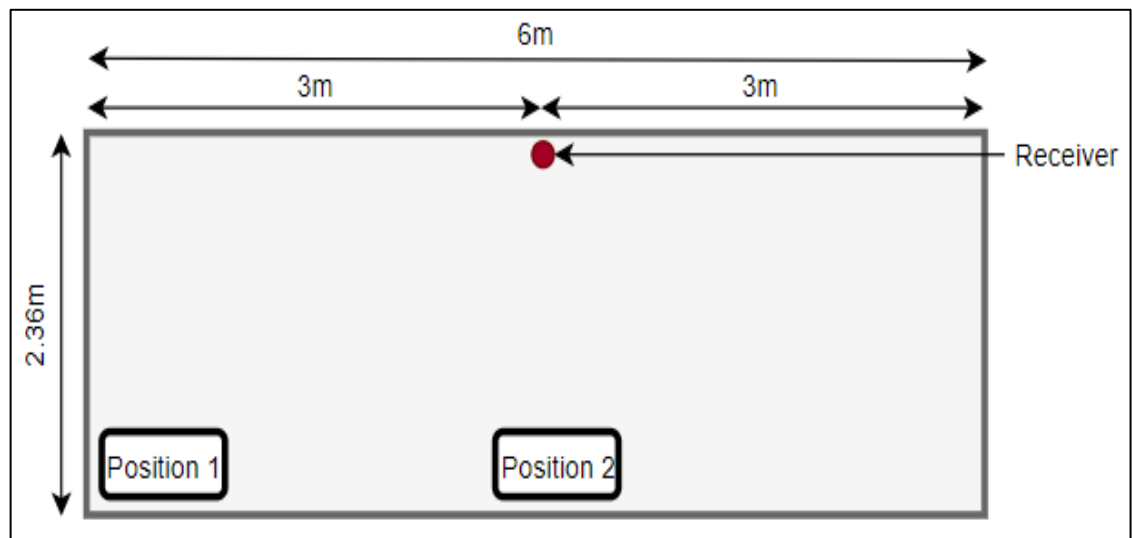


Figure 25: Location of position 1 and position 2 within the container.

Once the geometry was setup it was then implemented in gprMax. The spacing between the material and the RFID tag was 2mm. This was chosen because it allows the RFID to be affixed to the cargo as close as possible. The reason for this was to prevent the RFID tag from getting damaged and being removed when different types of cargo are placed in the container. The implementation of the procedure to simulate this scenario can be broken down into six categories; determining the domain and spatial resolution, determining the time domain, determining the constitutive parameters for the materials,

determining the source type and excitation frequency, receiver and creating the objects. These five categories will be elaborated on further.

1. Determining the domain and spatial resolution

The domain size is determined by the volume that needs to be investigated. The syntax for this is `#domain: f1 f2 f3`, f_1 is the size of the domain in the x direction (length), f_2 is the size of the domain in the y direction (width) and f_3 is the size of the domain in the z direction (height) in meters. In this case f_1 is 6m, f_2 is 2.36m and f_3 is 0.002m.

The syntax for the spatial discretization is `#dx_dy_dz: f1 f2 f3`. f_1 corresponds to a spatial step directed in the x direction, f_2 corresponds to a step directed in the y direction, f_3 corresponds to a step directed in the z direction. A good rule-of-thumb in gprMax for determining the spatial resolution should be one tenth of the smallest wavelength present in the model. Since there are three materials used; steel, wood and plastic. The smallest wavelength is calculated as follows:

$$\lambda = \frac{c}{f\sqrt{\epsilon_r}} \quad (49)$$

where,

$$c = 3 \times 10^8 \text{ m/s}$$

$$f = 915 \times 10^6 \text{ Hz}$$

$$\epsilon_{r_{steel}} = 1$$

$$\epsilon_{r_{plastic}} = 2.4$$

$$\epsilon_{r_{wood}} = 5$$

Therefore,

$$\lambda_{steel} = \frac{3 \times 10^8}{915 \times 10^6 \sqrt{1}} \approx 330 \text{ mm}$$

$$\lambda_{plastic} = \frac{3 \times 10^8}{915 \times 10^6 \sqrt{2.4}} \approx 212 \text{ mm}$$

$$\lambda_{wood} = \frac{3 \times 10^8}{915 \times 10^6 \sqrt{5}} \approx 140 \text{ mm}$$

Hence this would give a minimum spatial resolution of 140 mm. Since the length of the plastic mount is 200 mm, this would be resolved to 14 cells. However, a more accurate resolution would be 2 mm, which resolves the plastic mount to 100 cells. As such $f_1 = f_2 = f_3 = 0.002$.

2. Determining the time domain

The time domain command as the syntax *#time_window: f₁*, where f_1 determines the required simulation time in seconds. For this case f_1 is 31ns. This simulation time was used because it allows enough time for the signal to be transmitted from the source (RFID tag) to the receiver (RFID reader's antenna). In addition, this time was sufficient to see the reflection of the EM waves as it makes contact with the steel walls of the container. A fixed worst-case scenario signal amplitude was used, which is discussed below.

3. Determining the constitutive parameters for the materials

Materials can be added by using the following syntax *#material: f₁ f₂ f₃ f₄ str₁*, where f_1 corresponds to the relative permittivity, f_2 corresponds to the conductivity, f_3 corresponds to the relative permeability, f_4 corresponds to the magnetic loss and str_1 corresponds to an identifier for the material. The four materials used in this model are air, steel, plastic and wood.

4. Determining the source type and excitation frequency

The source of excitation is selected using two commands. The first is the waveform command which has the following syntax *#waveform: str₁ f₁ f₂ str₂* where str_1 corresponds to the sort of waveform, in this case it was a single cycle sine waveform, f_1 corresponds to the scaling of the maximum amplitude. Since a Hertzian dipole will be used, the worst-case amplitude is 400 μ A [68], f_2 corresponds to the center frequency of the waveform which is 915MHz. Finally, str_2 corresponds to an identifier for the waveform that was assigns it to a source. The command is the source. The syntax for the source is *#hertzian_dipole: c₁ f₁ f₂ f₃ str₁*, where c_1 is the polarization of the source. f_1 , f_2 and f_3 are the coordinates (x, y, z) of the source. If the source is at position 1 the coordinates are (0.14, 0.091, 0) and the coordinates at position 2 is (3, 0.097, 0). Lastly, str_1 corresponds to the identifier of the particular waveform which should be utilized for that source.

5. Receiver

The syntax for the receiver command is $\#rx: f_1 f_2 f_3$, where f_1 , f_2 and f_3 corresponds to the coordinates (x, y, z) of the receiver. The coordinates of the receiver are $(3, 2.32, 0)$.

6. Creating the objects

The only object used in the model was the box. The syntax for this command is $\#box: f_1 f_2 f_3 f_4 f_5 f_6 str_1$. f_1 , f_2 and f_3 corresponds to the (x, y, z) coordinates that are located at the lower left part of the parallelepiped and f_4 , f_5 and f_6 corresponds to the (x, y, z) coordinates that are located at the upper right part of the parallelepiped. str_1 is the material identifier, that must agree to the material that has previously been defined.

5.3.2. Testing procedure

The testing procedure involved varying the thickness of each material which was placed in front of the RFID tag. In addition, the entire simulation procedure was done inside a steel container, see Figure 24. Different material thicknesses were investigated in order to simulate different types of cargo in terms of their thicknesses. Table 8 shows the thicknesses of each material that was used. The materials are first placed at position 1, shown in Figure 25 and at each material thickness the electric and magnetic field is recorded at the receiver. Once all the electric and magnetic fields for each materials thickness are recorded the materials and the transmitter are then moved to position 2. The entire process of acquiring the electric and magnetic fields are done again at the receiver.

Table 8: Thickness values of the materials used.

Thickness	Metal (mm)	Plastic (mm)	Wood (mm)
1	2	5	20
2	4	10	40
3	6	15	60
4	8	20	80
5	10	25	100
6	12	30	120
7	14	35	140
8	16	40	160
9	18	45	180
10	20	50	200

The power received at the receiver is calculated by using the electric and magnetic fields recorded. The power in dBm is calculated as follows:

$$\vec{S} = \vec{E} \times \vec{H} \quad (50)$$

$$P = |\vec{S}|A_e \cos \theta \quad (51)$$

$$P(\text{dBm}) = 10\log_{10}(P) + 30 \quad (52)$$

where,

\vec{S} – Poynting vector

\vec{E} – electric field vector

\vec{H} – magnetic field vector

A_e – aperture area

θ – angle between the normal of the antenna and the incoming EM waves

P – power in Watts

$P(\text{dBm})$ – power in dBm

The simulations are performed on the assumption that the RFID tag acquires enough power to be activated. The simulator software used only provided a model of a dipole antenna (RFID tag) and not a patch antenna (RFID reader's antenna). Hence it was assumed that the transmitter was the RFID tag and the receiver was the RFID reader's antenna.

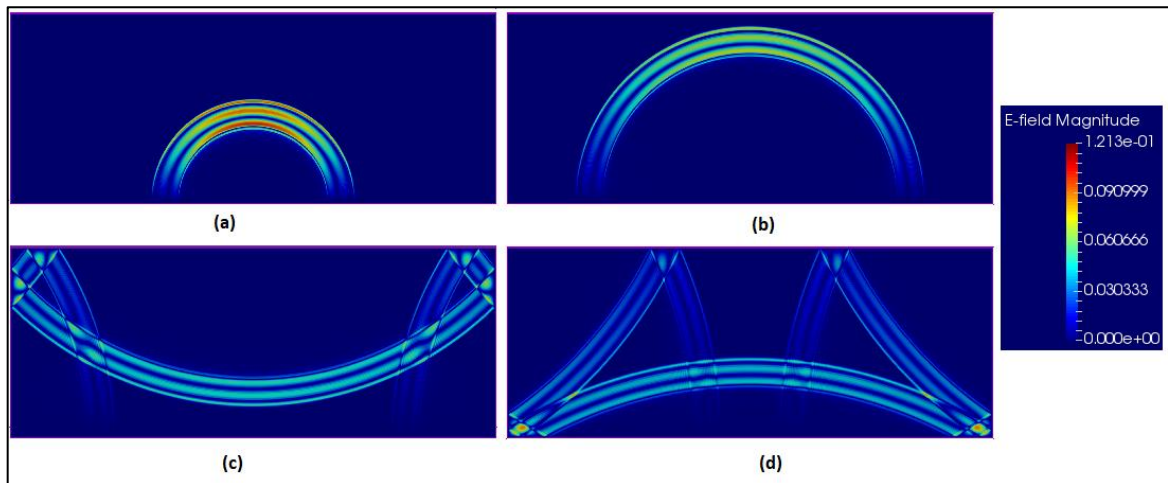


Figure 26: Propagation of EM waves inside a steel, (a) time step = 1, (b) time step = 2, (c) time step = 3, (d) time step = 4.

Figure 26 shows the propagation of the EM wave inside the steel container. From Figure 26, two properties of the propagation of the EM wave was noted. Firstly, as the EM waves

propagates the EM strength decreases. This was expected according to the inverse square law. Secondly, When the EM waves comes into contact with the steel boundary, Figure 26b, it was shown that the EM waves is reflected from the steel boundary, Figure 26c. Both Figures 26c and 26d further shows that when the reflected wave combines with another EM wave, constructive and destructive interference occurs. In addition, when the EM waves strikes the steel boundary some of its strength was absorbed by the steel container resulting in the further degradation the EM wave strength. This was also expected whenever an EM wave strikes a conductive material.

5.3.2.1. Steel

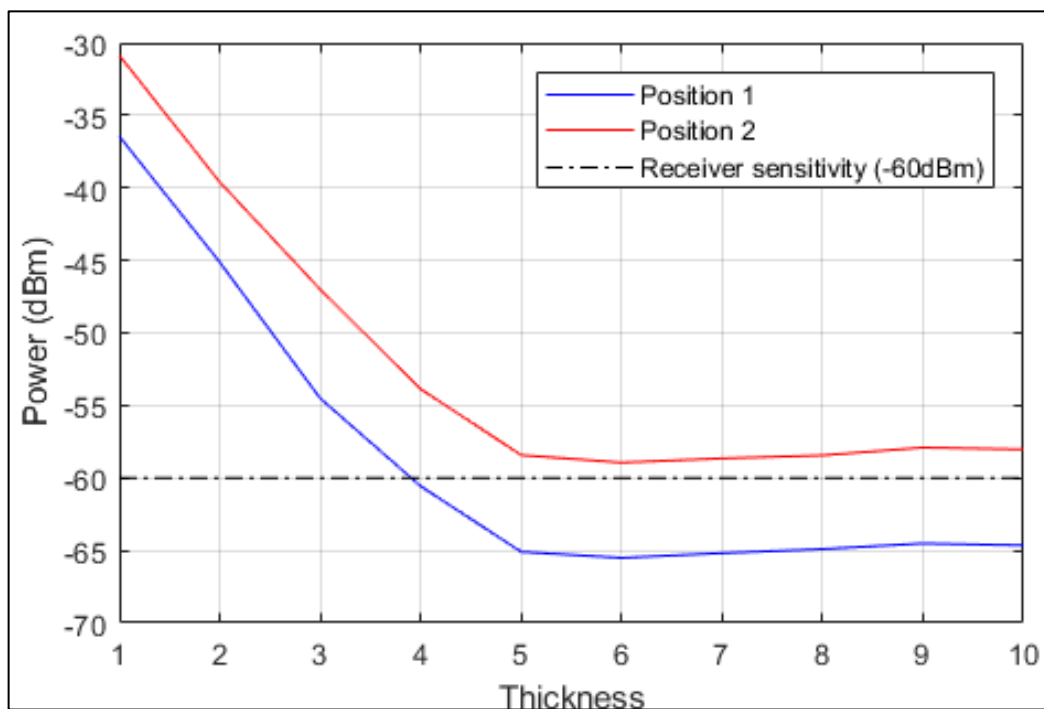


Figure 27: Graph of thickness vs power (dBm) for steel.

The first material investigated was steel. The power that was received at the receiver was plotted against the thickness. This is shown in Figure 27. According to commercial readers the receiver's sensitivity was set at -60dBm [69]. From Table 8 the thickness of a sheet of steel was 2mm.

From Figure 27 it can be shown that the RFID tag (transmitter) performs better at position 2 than at position 1. The power received at the receiver decreases when the thickness of the steel sheets increases. This occurs at position 1 and position 2. At position 1 and position 2 a thickness of one steel sheet achieves the most power received of -36.42dBm and -30.86dBm respectively. When the RFID tag was placed at position 2, it is shown that the receiver will receive enough power from the RFID tag in order for it to be detected.

The worst-case power received is -58.94dBm and it occurs at a thickness of six steel sheets. At position 1 the receiver stops detecting the RFID tag when the steel thickness is greater than four or 8mm. This is due to the power received falling below -60dBm threshold. From Figure 28, it can be shown that minimal amount of the EM wave penetrates the steel at a thickness of 2mm. The maximum E field that travels towards the receiver (reader's antenna) was approximately 0.09 V/m. Figure 29, shows that as the thickness of the steel increases the amount of EM waves that can penetrate the steel reduces. In addition, it can be shown that the EM waves actually escapes through the sides of the steel and then travels through the steel container. The maximum E field that travels towards the receiver (reader's antenna) was approximately 0.06 V/m.

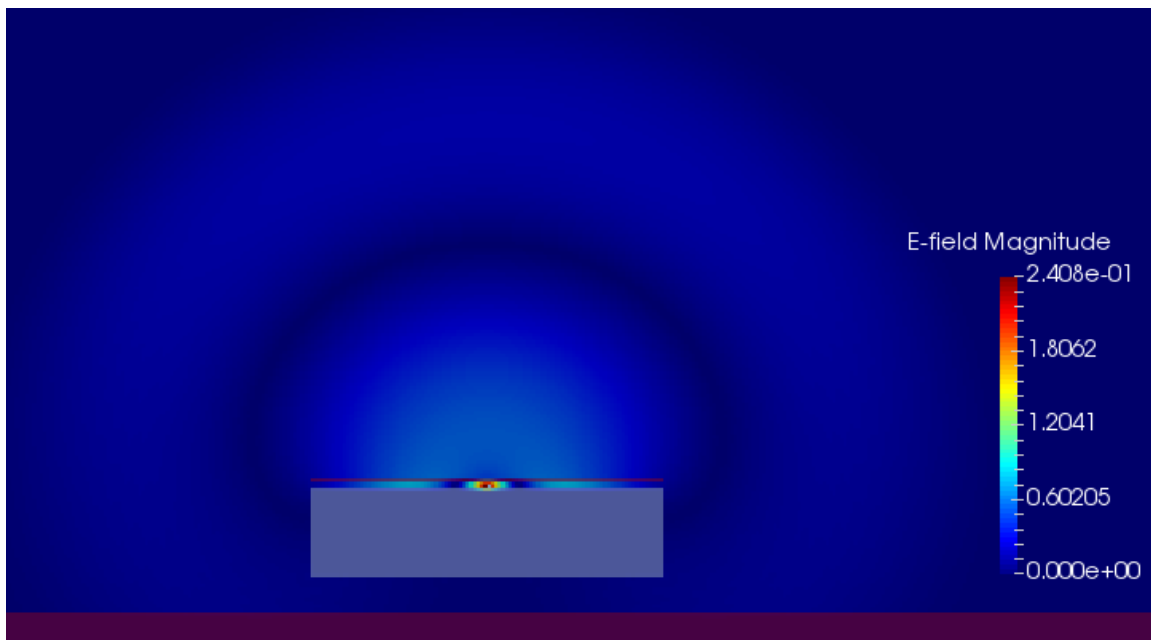


Figure 28: E-field pattern for a thickness value of 1 (2 mm) for steel.

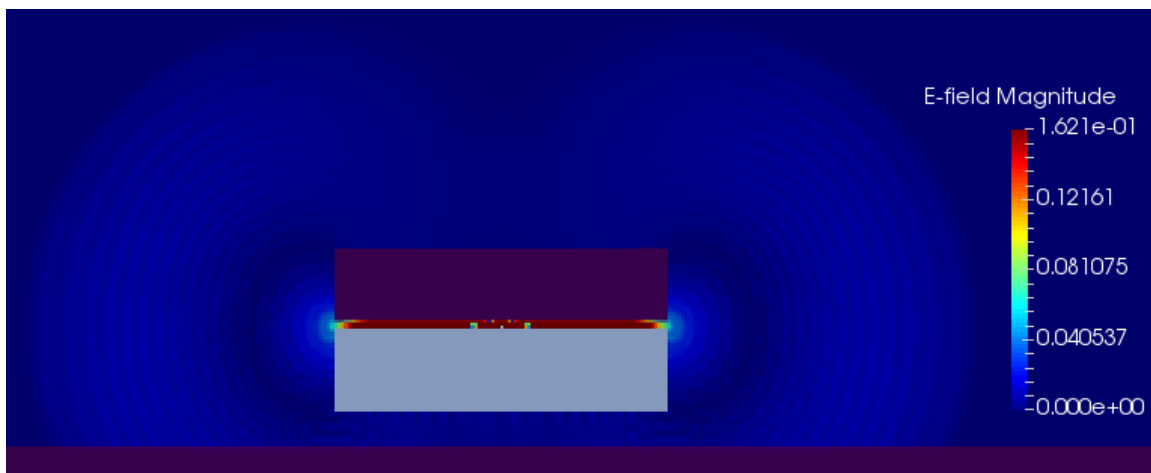


Figure 29: E-field pattern for a thickness value of 10 (20 mm) for steel.

5.3.2.2. Plastic

The second material investigated was plastic. Once again, the power that was received at the receiver was plotted against the thickness. This is shown in Figure 30. From Table 8 the thickness of the plastic was 5mm.

From Figure 30 it can be shown that the RFID tag (transmitter) performs better at position 2 than at position 1. The power received at the receiver increases at position 1, while the power received at position 2 decreases from a thickness of 1. At position 1 the power received at the receiver is greatest at a thickness of 10 at -27.76dBm while at position 2 the power received at the receiver is greatest at a thickness of 1 at -20.98dBm. The worse-case power received at position 1 is -31.49dBm at a thickness of 1 while the worse-case power received at position 2 is -22.59dBm at a thickness of 10. In addition, since the worse-case received power at position 1 and position 2 are greater than -60dBm, the RFID tag will be detected at the maximum thickness.

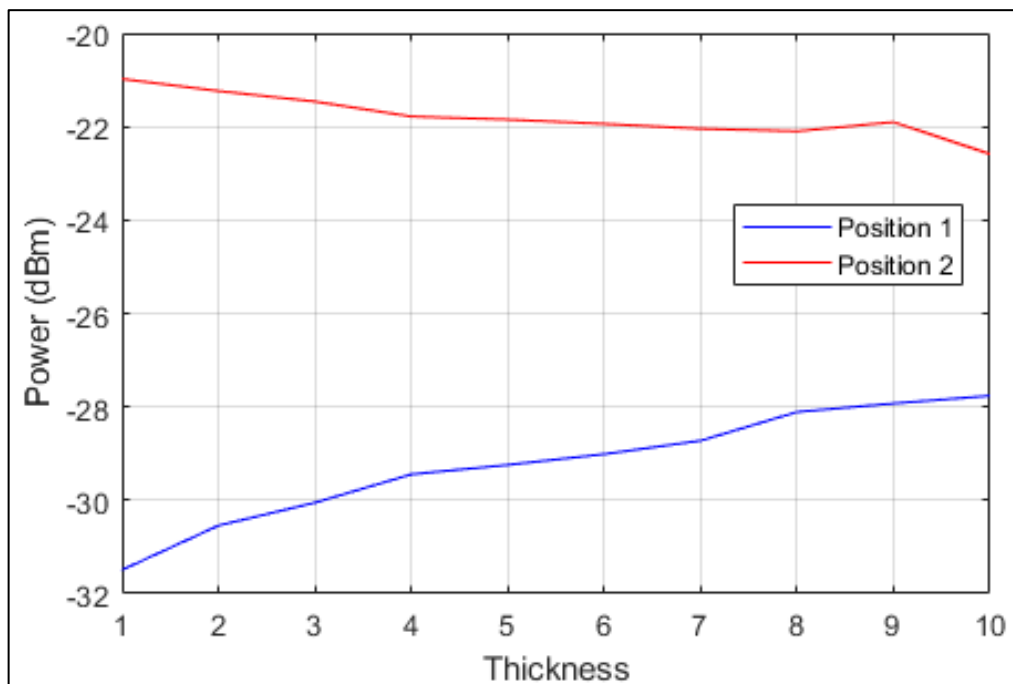


Figure 30: Graph of thickness vs power (dBm) for plastic.

The reason why the power at position 1 increases when the thickness of the material increases is due to the plastic material behaving like a dielectric lens. A dielectric lens dates to 1888, where a man by the name of Oliver Lodge used a dielectric lens for his experiments. These lenses were used to alter the radiation pattern emitted from the source in order to improve its gain, either for fixed or scanning beam applications [70]. From Figure 31, it can be shown that once the electromagnetic wave propagates out of the plastic the E-field splits along the centre into two separate E-field lobes. In addition,

from Figure 32, it can also be shown that the E-field does increase as the thickness of the material increases and the splitting of the E-field becomes more pronounced. The E-field increases from 0.4917 V/m to 0.5148 V/m. However, the E-field in the center of the radiation does decrease. Therefore, this dielectric material does tend to split the E-field in the center, when an electromagnetic wave enters it. Hence since position 1 is located to the side of the receiver and the E-field is directed towards the receiver, the power will increase at the receiver as the thickness increases. On the other hand, when the RFID tag is at position 2, it is expected that the power received at the receiver will decrease because the two main E-field lobes travel away from the receiver. The reason why position 2 still receives more power than position 1 is due to the distance travelled for the electromagnetic wave is greater at position 1 than at position 2.

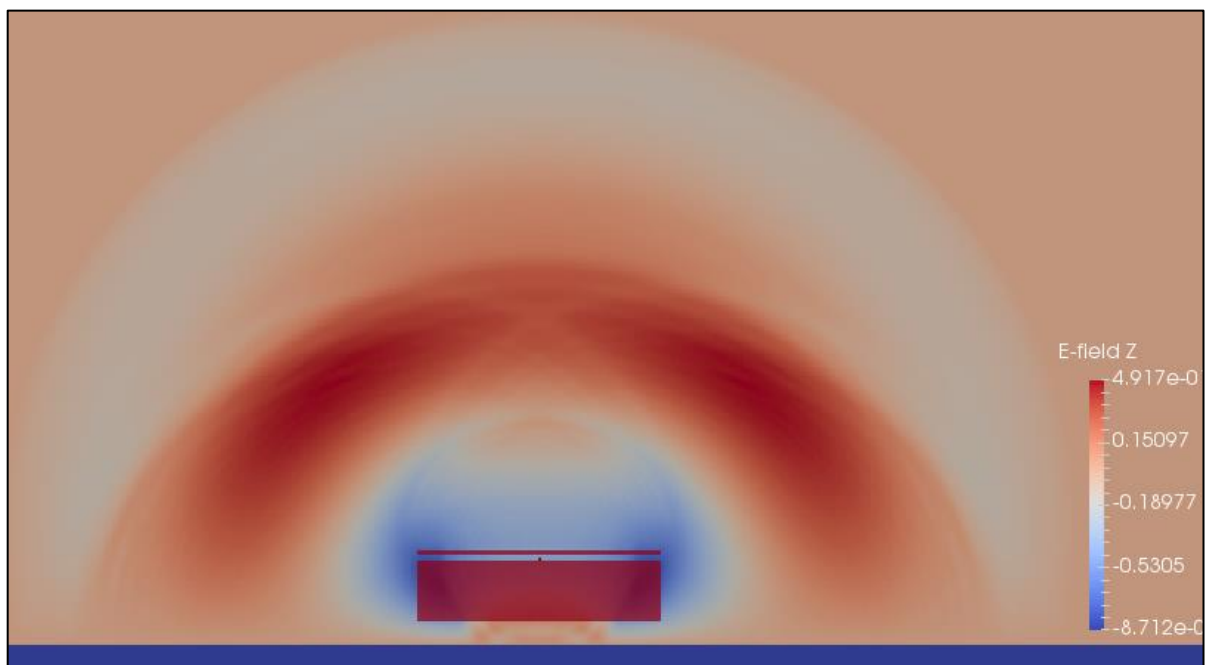


Figure 31: E-field pattern for a thickness value of 1 (5 mm) for plastic.

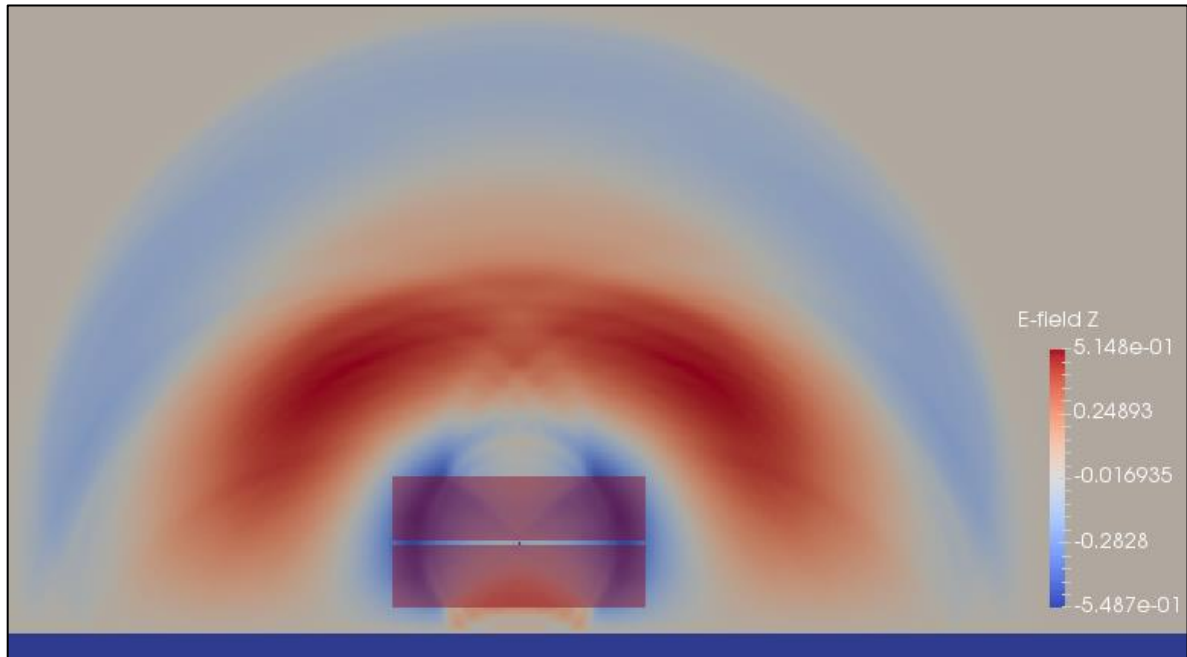


Figure 32: E-field pattern for a thickness of 10 (50 mm) for plastic.

5.3.2.3. Wood

The third and final material to be investigated was wood. The power that is received at the receiver was plotted against the thickness. This is shown in Figure 33. From Table 8 the thickness of the wood was 2cm. From Figure 33 it can be shown that the RFID tag (transmitter) performs better at position 2 than at position 1, just like when plastic was used. The power received at the receiver increases at position 2, while the power received at position 1 decreases as the thickness increases. At position 1 the power received at the receiver is greatest at a thickness of 4 at -28.40dBm, while at position 2 the power received at the receiver is greatest at a thickness of 10 at -20.35dBm. The worst-case power received at position 1 is -38.34dBm at a thickness of 10, while the worse-case power received at position 2 is -27.89dBm at a thickness of 1. From the results for wood, it can be shown that wood behaves inversely to plastic. For plastic at position 1 the power at the receiver increases as the thickness increases while for wood the power at the receiver decreases as the thickness increases. At position 2 the power decreases as the thickness increases for the plastic material while for wood the power at the receiver increases as the thickness increases. In addition, since the worse-case received power at position 1 and position 2 are greater than -60dBm, the RFID tag will therefore be detected at the maximum thickness.

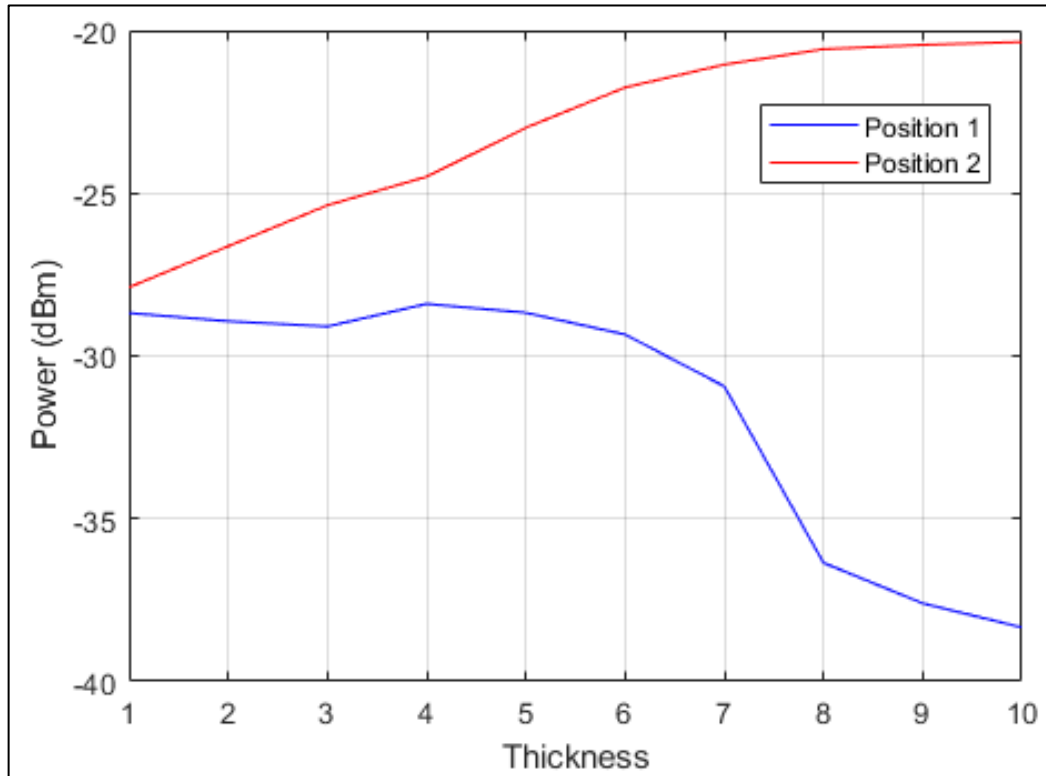


Figure 33: Graph of thickness vs power (dBm) for wood.

The reason why the power at position 2 increases as the thickness of the material increases is due to the wood behaving like a dielectric lens. From Figure 34, it can be shown that at a thickness of 1, the E-field is minimally affected. However, when the thickness is increased, Figure 35 shows that the E-field converges at the top of the wood as time increases, as if the E-field is being focused as it propagates through the material. In addition, from Figure 35, it can also be shown that the E-field does increase as the thickness of the material increases. The E-field increases from 0.757 V/m at a thickness of 1 to 1.232 V/m at a thickness of 10. Hence this dielectric lens tends to increase the E-field by focusing the E-field at a particular focal-point as it propagates through the material. Therefore, since position 2 is located directly below the receiver and the E-field is directed straight towards the receiver, the power will therefore increase as the material thickness increases. On the other hand, when the RFID tag is at position 1 it is expected that the power received at the receiver will decrease because the “amplified” E-field does not travel straight towards the receiver. In addition, due to the distance travelled for the electromagnetic wave is greater at position 1 than position 2, position 2 will receive more power.

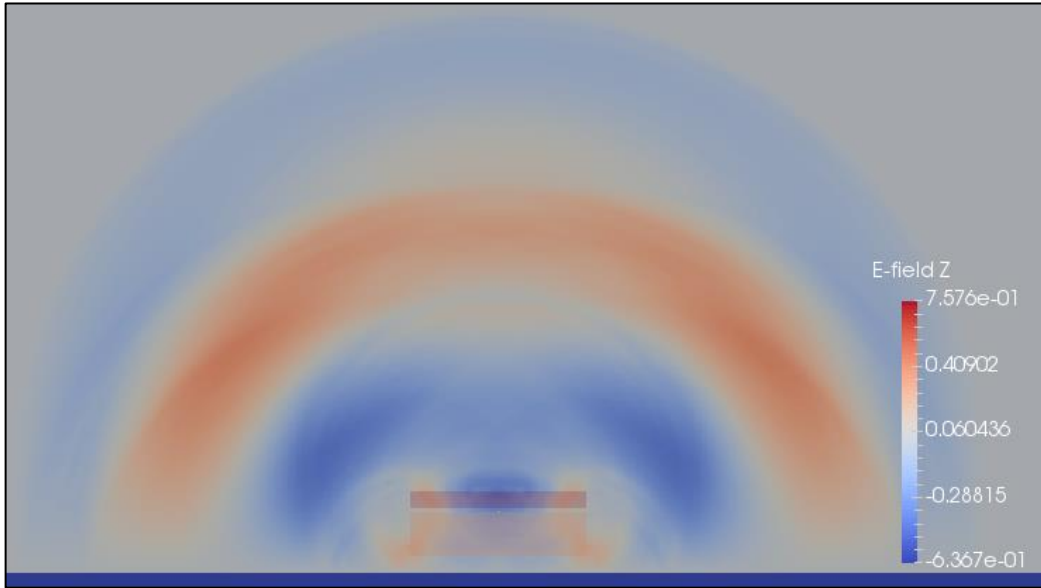


Figure 34: E-field pattern for a thickness of 1 (20 mm) for wood.

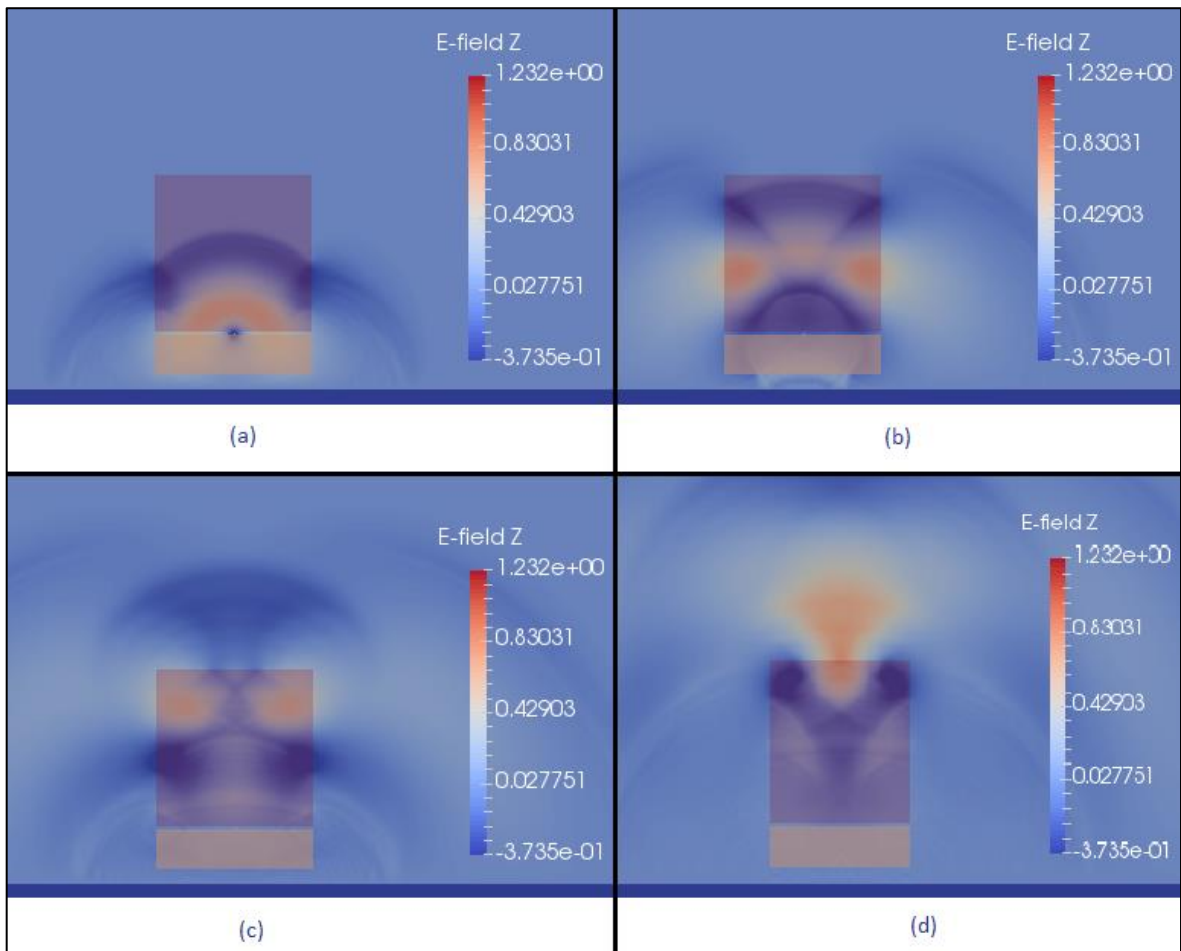


Figure 35: E-field pattern for a thickness of 10 (200 mm) for wood, (a) time step = 1, (b) time step = 2, (c) time step = 3, (d) time step = 4.

5.3.3. Validation

The results obtained in the above experiments was compared to the results from Bleda *et al*, [71], and Arora *et al*, [23], in order to validate the work presented in this thesis. The paper by [71] investigated the effects of the different materials on a RFID system. Their goal was to study the behavior of the EM radiation with an extended set of materials. Their experimental framework included the following equipment, RFID antenna, RFID reader, metal box, support for RFID tags, RFID tags and finally the materials. The materials investigated was wood, plastic and metal. Their investigational setup is shown in Figure 36. After performing the experiments, the following which was relevant to the findings of this thesis was concluded, wood presented the best performance, followed by plastic and then metal. The reason for this was that for wood the EM radiation can penetrate this material with few losses. In addition, the use of metal does not allow the EM radiation to go through easily. However, it was also noted in the discussion that placing the RFID tag closer to the material greatly improved the results, since RFID reader only required 1% of its power to detect the RFID tag. They also concluded that the metal box used in the experiments influences the behavior of the RFID tag in a positive manner. This was also proven in the practical results performed as a part of this research.

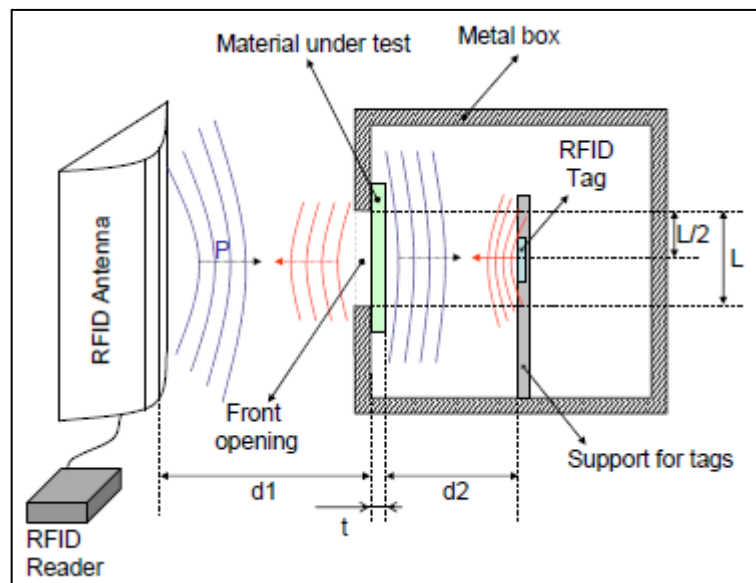


Figure 36: Experimental setup [71].

The paper by [23] investigated the effects of placing different types of metals in front of a RFID tag. The experimental setup and the findings were discussed in detail in Chapter 2 of this thesis. The findings that are relevant to the validation of the work carried out in this chapter was related to the experiment conducted when different thicknesses of metal were used. The experiment used mild steel of two thicknesses. One was 1.5mm thick

while the other was 1mm thick. The results from their experiment is shown in Figure 37. Figure 37a is the result from the 1mm thick mild steel and Figure 37b is result from the 1.5mm thick mild steel. The light spot in Figure 37 represents places where the RFID tag could be read. Lighter spots correspond to the RFID tag could be read at a higher attenuation. Therefore, it can be shown the effect of the thicker mild steel negatively affects the performance of the RFID system. Figure 37a shows that the RFID tag could be read at 77% of total 3780 data points while Figure 37b could shows only 45% of the total data points been read.

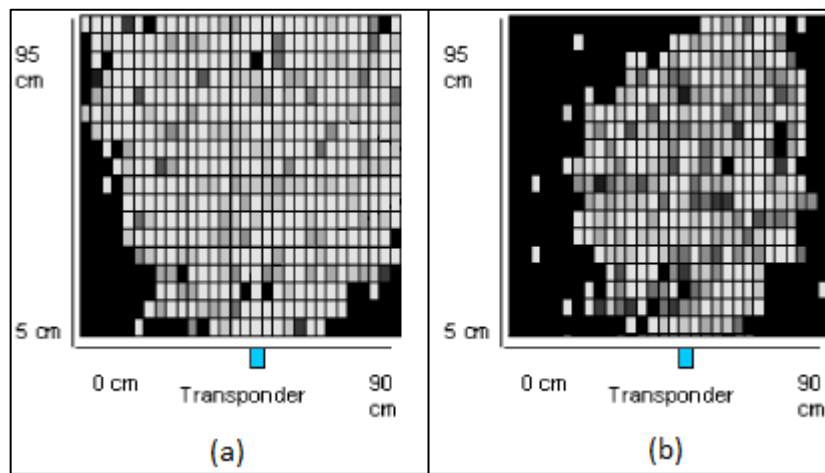


Figure 37: Readability of the RFID tag at different thicknesses of mild steel (a) 1mm thick mild steel, (b) 1.5mm thick mild steel [23].

5.3.4. Discussion

When a single RFID reader's antenna was used the following was concluded, steel performs the worst followed by plastic and then wood. The use of steel is best used when it is placed directly in line with the receiver. However, a greater range can be achieved by reducing the thickness to 6 mm. When using plastics, placing them directly inline of the receiver does not offer the best performance. However, if the plastic material is to be placed away from the receiver it is best to use thicker material as this does cause a slight increase in the power received at the receiver as compared to using a thinner plastic. Lastly as mentioned earlier, wood shows the best performance when compared to the other two materials been investigated. The system's performance exponentially increases when the RFID tag is in line with the receiver and the thickness increases, see chapter 5.3.2.3. This was due to the material acting like a dielectric lens. However, when the RFID tag is placed away from the receiver i.e. not in line, the system's performance decreases as the thickness is increased. The performance of the system can still be optimized by employing a multiple antenna design in order to achieve a 100% coverage. This will reduce the restriction of where certain materials must be placed in relation to the RFID

reader's antenna to achieve optimal performance. It can also be concluded that a UHF RFID system can operate inside a metal structure.

As mentioned before a multiple antenna design is required to obtain the 100% coverage. Implementation of such a system will no doubt incur great cost, hence utilizing techniques that can reduce this cost is of great importance. This will also produce a system that is more feasible to design in terms of the cost. Implementing various single UHF RFID readers with their own antennas i.e. mobile UHF RFID readers will incur substantial cost from the onset. In addition, having multiple mobile UHF RFID readers scanning the sample space at the same time will result in an increase of the RF interferences within the sample space. This is due to the dense UHF RFID environment R. Pous *et al*, [72]. Another solution would be to introduce antenna multiplexing. A RFID reader multiplexer consists of multiplexers and de-multiplexers. The multiplexer's (mux) role is to select one of the several input signals and transfer the data to an output. The de-multiplexer (de-mux) on the other hand transfers an input signal to one of the several outputs. The setup of a RFID reader multiplexer usually allows for a single port of the mux/de-mux to be connected to a RFID reader and the multiple ports are dedicated to the antennas. Some of the key advantages of using a RFID reader multiplexer are, firstly the RF power is switched between all the antennas via control signals. Hence only one connected antenna will be on at a specific time. Secondly very high isolation is achieved. This is necessary to avoid cross-tag reads between the antennas. Finally, this system has a minimal impact in antenna cancellation, which creates null zones within the sample space that reduces the coverage [73].

5.4. Practical results

5.4.1. Component selection

5.4.1.1. RFID tag

From the criteria used to distinguish passive RFID tags from active RFID tags in Table 1, a passive RFID tag will be used. The reason for using this tag is for the following reasons:

1. The environment that this tag is going to be used does not require a long-range tag. This is due to the size of a truck container.
2. The passive RFID tag is robust and hard-wearing. Having a RFID tag that is robust is essential because the cargo, which is affixed with a RFID tag, is going to be loaded and unloaded from a truck container. In order to maximise the amount of cargo placed inside a container, they need to be packed close to each other. This means certain goods in the container might rub against each other and in turn also on the RFID tag

during the loading process. Also, if the containers are not air conditioned the conditions within the container might not be favourable for active tags, due to the heat within the container.

3. The passive RFID tag is also inexpensive.

One of the disadvantages of using passive RFID tags is the complexity of designing such a system is more difficult.

5.4.1.2. RFID reader

The following parts, namely; power options, interconnectivity, antenna ports, General Purpose Input/output (GPIO) ports, additional utilities, onboard processing and application program interface (API) options aids us in narrowing the field for selecting a suitable UHF RFID reader. The parts discussed below was taken from [74].

1. Power options

1a. Battery

Using a battery to power the RFID reader system is a convenient solution. In order to extend the battery life, the RFID system can be activated at predetermined intervals.

1b. In-vehicle

This option allows the RFID reader system to be powered through the vehicle. The biggest drawback is having a universal power lead, since not many RFID readers are designed specifically for such use.

Antenna ports

2a. Fixed reader

These types of readers usually come in two ports, four ports or eight ports. A fixed reader can therefore be configured to occupy one read zone or a few different ones.

2b. Multiplexors

Multiplexors or antenna hubs are used to increase the number of the antennas that can be used with a single RFID reader. As an example, a single eight port fixed RFID reader can connect up to 256 antennas.

2. GPIO ports

3a. Input

This option is useful when motion detectors or light-break sensors are used in conjunction with a RFID reader. When these sensors are activated an electrical signal will then be sent to the RFID reader to perform a specific function.

3b. Output

Having an auxiliary device connected to an RFID reader can be useful. For example, if the RFID reader scans a particular tag. The RFID reader will then send an electrical signal to the auxiliary device to perform a specific function.

For the purpose of testing the Alien ALR-9680 commercial 4-port RFID reader was chosen.

5.4.2. Testing procedure in a container

Practical testing was done in a 650 x 236 x 220 cm ($z \times x \times y$) steel container. The apparatus used during the practical testing was:

- Alien ALR-9680 commercial 4-port RFID reader, see Figure 39
- A 50-ohm antenna cable connector, see Figure 41
- A circular polarized UHF microstrip patch antenna, see Figure 41
- An anti-metal RFID tag and paper RFID tag.
- 8 sheets of steel, 10 sheets of plastic and 10 blocks of wood, see Figures 46 and 47
- A laptop with the Alien GUI, see Figure 40
- A plastic RFID tag mount, see Figure 44

As discussed in Section 5.3.2 the testing procedure will follow the same steps and the thickness of the materials will be the same as in Table 8. However, the difference in the practical testing is as follows, in the simulation only two positions are investigated, however in the practical testing six positions are investigated. The reason why these four additional position was not investigated was firstly because of symmetry there was not need to investigate the other far side of the container and secondly if the height of the container was introduced into the simulations to investigate the other positions a total of 228 GB of RAM was needed.

The recording of the results was done by using the Alien software GUI. This interface displays the RFID tag's information when the RFID tag is detected. Unfortunately, this software does not show the power that was received from the RFID tag. Therefore, the results will only check if the RFID tag is detected or not detected. A detected RFID tag will have yes assigned to the readability column while a no will assigned to the readability column if the RFID tag is not detected at a particular position within the steel container.

Table 9 shows the positions of the RFID tag inside the steel container. The circular dots represent the positions of the RFID tag to be investigated.

Table 9: Locations of the positions to be investigated inside the steel container.

Position index	RFID tag color description	Position		
		X	Y	Z
1	Red	225	137	-310
2	Green	225	213	-310
3	Orange	225	137	0
4	Yellow	225	213	0
5	Purple	225	137	333
6	Blue	225	213	333

It must also be noted that the truck's container contained additional materials in it, such as in Figure 45. These additional materials found in the steel container will have a negative effect on the performance of the system. Hence, the simulated results would first differ from the practical results.

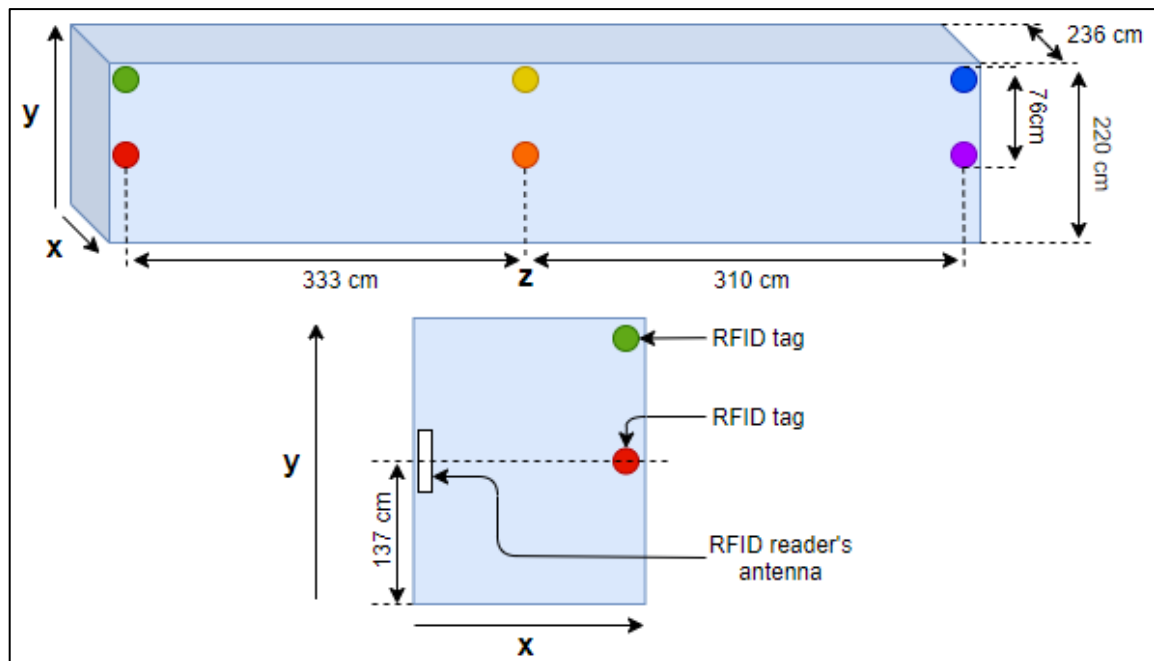


Figure 38: Practical testing setup inside the steel container.



Figure 39: Alien ALR-9680 commercial 4-port RFID reader [61].

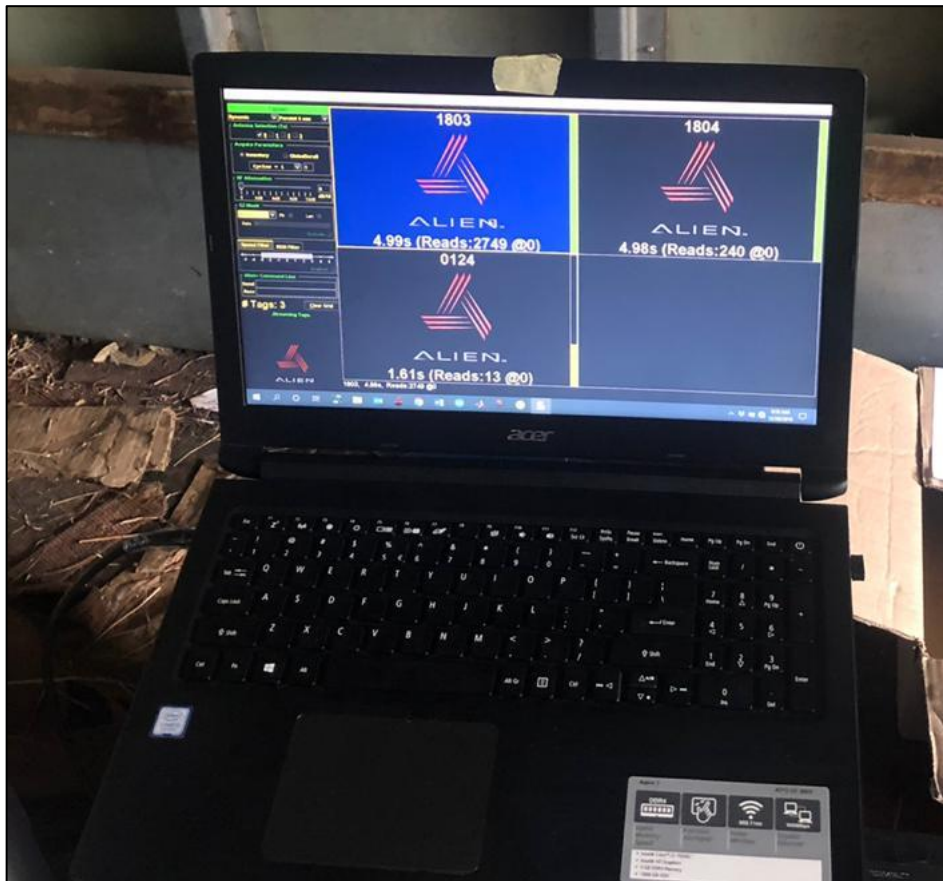


Figure 40: Alien RFID graphical user interface.



Figure 41: Placing of the UHF RFID antenna connected to a 50-ohm cable.

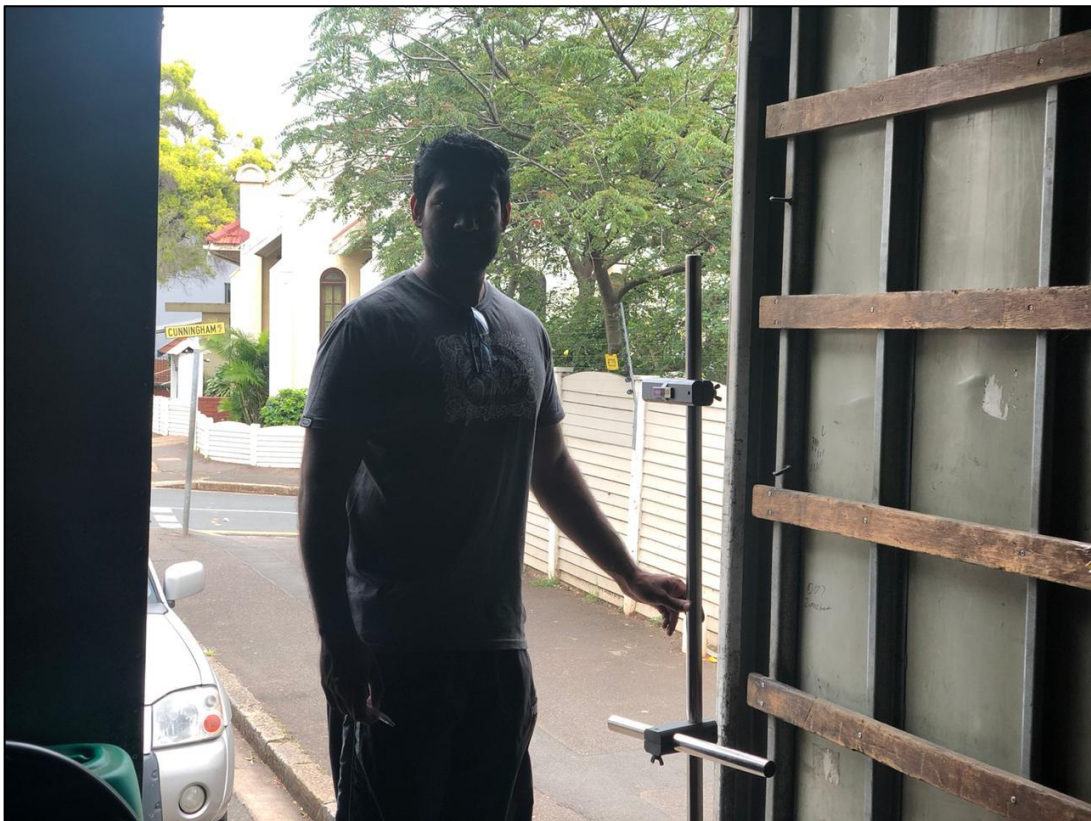


Figure 42: Master's student (Mr S.J Naidoo) placing the RFID tag mount.



Figure 43: Master's student supervisor (Adv. Dr. E. Bhero) placing the RFID tag mount.



Figure 44: Plastic RFID tag mount with a RFID tag affixed to it.



Figure 45: Plastic container located inside the truck's container during testing.

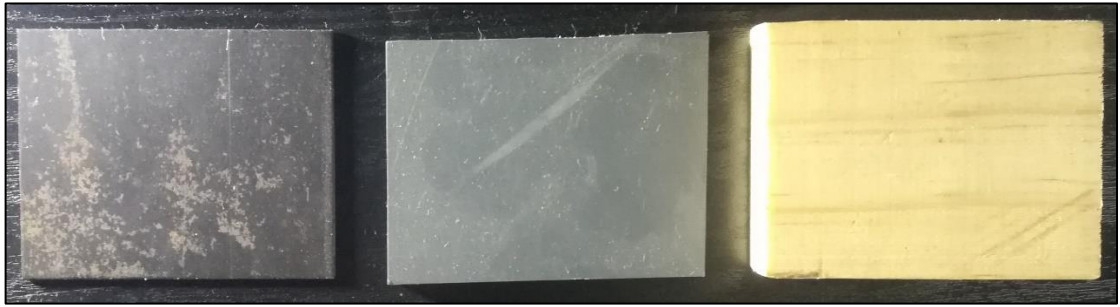


Figure 46: Materials used, steel (left), plastic (middle), wood (right).

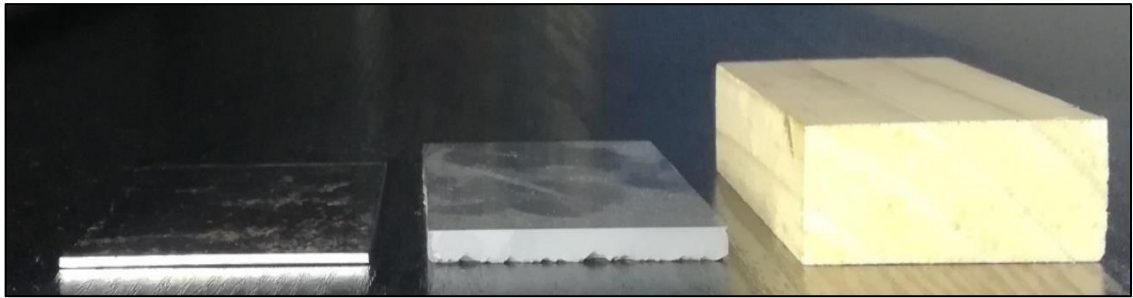


Figure 47: Side view of thickness for each material.

5.4.3. Results in shipping container

5.4.3.1. Steel

From Table 10, it can be shown that when the maximum number of sheets (eight) of steel was placed on metal RFID tag the RFID reader did detect the RFID tag successfully, in both the horizontal and vertical orientation at positions 3 and 4.

Table 10: Readability of a metal RFID tag using steel inside steel container.

Material: Steel									
Tag used: Metal RFID tag									
Horizontal Orientated Tag					Vertical Orientated Tag				
Thickness	x	y	z	Readability	Thickness	x	y	z	Readability
8	225	137	0	Yes	8	225	137	0	Yes
8	225	213	0	Yes	8	225	213	0	Yes
8	225	137	333	No	8	225	137	333	No
8	225	213	333	No	8	225	213	333	No
4	225	137	333	No	3	225	137	333	No
4	225	213	333	No	3	225	213	333	No
4	225	137	180	Yes	3	225	137	160	Yes
4	225	213	180	Yes	3	225	213	160	Yes
8	225	137	-310	No	8	225	137	-310	No
8	225	213	-310	No	8	225	213	-310	No
4	225	137	-310	No	3	225	137	-310	No
4	225	213	-310	No	3	225	213	-310	No
4	225	137	-175	Yes	3	225	137	-150	Yes
4	225	213	-175	Yes	3	225	213	-150	Yes
8	98	137	180	Yes	4	93	137	182	Yes
8	98	213	180	Yes	4	93	213	182	Yes
8	73	137	-253	Yes	4	180	137	-224	Yes
8	73	213	-253	Yes	4	180	213	-224	Yes

However, when the RFID tag was placed at positions 1,2,4 and 5 the RFID reader did not detect the RFID tag. This was also proven in the simulations. The thickness of the steel sheets was then halved, and the RFID reader still unsuccessfully detected the RFID tag at the same positions. This was noted for both orientations of the RFID tag. The RFID tag was only detected when the RFID tag was moved closer to the RFID reader's antenna. For a horizontal orientated RFID tag and a thickness four the maximum distance is 298cm with its location at (225; 213; 180) on the positive z-plane and 295cm on the negative z-plane with its location at (225; 213; -175). While the vertically orientated RFID tag at a thickness of three achieved a maximum distance of 286cm with its location at (225; 213; 160) on the positive z-plane and 281cm on the negative z-plane with its location at (225; 213; -150). In addition, for a horizontally orientated RFID with a maximum thickness of

eight, a maximum range of 219cm with its location at (98; 213; 180) on the positive z-plane and 274cm along the negative z-plane with its location at (73; 213; -253).

Table 11: Readability of a paper RFID tag using steel inside steel container.

Material: Steel									
Tag used: Paper RFID tag									
Horizontal Orientated Tag					Vertical Orientated Tag				
Thickness	X	y	z	Readability	Thickness	x	y	z	Readability
8	225	137	0	No	8	225	137	0	No
8	225	213	0	No	8	225	213	0	No
8	112	137	0	Yes	8	62	137	0	Yes
8	112	213	0	Yes	8	62	213	0	Yes
8	225	137	333	No	8	225	137	333	No
8	225	213	333	No	8	225	213	333	No
1	225	137	333	No	1	225	137	333	No
1	225	213	333	No	1	225	213	333	No
1	91	137	39	Yes	8	225	137	-310	No
1	91	213	39	Yes	8	225	213	-310	No
8	225	137	-310	No	1	225	137	-310	No
8	225	213	-310	No	1	225	213	-310	No
1	225	137	-310	No					
1	225	213	-310	No					
1	89	137	-28	Yes					
1	89	213	-28	Yes					

From Table 11, it can be seen that when the maximum number of sheets (eight) of steel was placed on the paper RFID tag the RFID reader did not detect the RFID tag successfully, in both the horizontal and vertical orientation at positions 3 and 4. The horizontally orientated RFID tag was detected when it was 112cm away from the RFID reader's antenna, at a height of 137cm and 213cm. When the RFID tag was orientated vertically the RFID reader detected it when it was 62cm away from the RFID reader's, at a height of 137cm and 213cm. When the RFID tag was placed at positions 1,2,4 and 5 the RFID reader unsuccessfully detected the RFID tag. Even at a thickness of just one steel sheet the RFID reader still unsuccessfully detected the paper RFID tag. For a horizontal orientated RFID tag and a thickness of one sheet the maximum distance is 124cm with its location at (91; 213; 39) along the positive z-plane and 122cm on the negative z-plane with its location at (89 ;213; -28).

5.4.3.2. Plastic

From Table 12, it can be seen that when the maximum number of sheets (ten) of plastic was placed on metal RFID tag the RFID reader did detect the RFID tag successfully, in both the horizontal and vertical orientation at positions 3 and 4. In addition the RFID tag was successfully detected by the RFID reader at all positions in the steel container when the RFID tag was orientated horizontally. However, the performance of the RFID system did decrease when the RFID tag was orientated vertically for positions 1,2,5 and 6. The RFID tag was only detected when the RFID tag was moved closer to the RFID reader's antenna. For the maximum thickness the maximum distance achieved is 288 cm with its location at (225; 213; 163) on the positive z-plane and 286cm along the negative z-plane with its location at (225; 213; -160).

Table 12: Readability of a metal RFID tag using plastic inside steel container.

Material: Plastic									
Tag used: Metal RFID tag									
Horizontal Orientated Tag					Vertical Orientated Tag				
Thickness	x	y	z	Readability	Thickness	x	y	z	Readability
10	225	137	0	Yes	10	225	137	0	Yes
10	225	213	0	Yes	10	225	213	0	Yes
10	225	137	333	Yes	10	225	137	333	No
10	225	213	333	Yes	10	225	213	333	No
10	225	137	-310	Yes	10	225	137	163	Yes
10	225	213	-310	Yes	10	225	213	163	Yes
					10	128	137	-310	No
					10	128	213	-310	No
					10	120	137	-160	Yes
					10	120	213	-160	Yes
					10	45	137	333	Yes
					10	45	213	333	Yes
					10	45	137	-310	Yes
					10	45	213	-310	Yes

Table 13: Readability of a paper RFID tag using plastic inside steel container.

Material: Plastic									
Tag used: Paper RFID tag									
Horizontal Orientated Tag					Vertical Orientated Tag				
Thickness	x	y	z	Readability	Thickness	x	y	z	Readability
10	225	137	0	No	10	225	137	0	No
10	225	213	0	No	10	225	213	0	No
10	162	137	0	No	10	112	137	0	Yes
10	162	213	0	No	10	112	213	0	Yes
10	135	137	0	Yes	10	225	137	333	No
10	135	213	0	Yes	10	225	213	333	No
10	225	137	333	No	10	111	137	52	Yes
10	225	213	333	No	10	111	213	52	Yes
10	162	137	73	Yes	10	225	137	-310	No
10	162	213	73	Yes	10	225	213	-310	No
10	225	137	-310	No	10	102	137	-61	Yes
10	225	213	-310	No	10	102	213	-61	Yes
10	161	137	-71	Yes					
10	161	213	-71	Yes					

From Table 13, it can be seen that when the maximum number of sheets (ten) of plastic was placed on the paper RFID tag the RFID reader did not detect the RFID tag successfully, in both the horizontal and vertical orientation at positions 3 and 4. The horizontally orientated RFID tag was detected when it was 135 cm away from the RFID reader's antenna, at a height of 137 cm and 213 cm. While the vertically orientated was detected when it was 112 cm away from the RFID reader's antenna at a height of 137 cm and 213 cm. When the RFID tag was placed at positions 1,2,4 and 5 the RFID reader unsuccessfully detected the RFID tag. However, when the RFID tag was brought closer to the RFID reader's antenna the RFID reader did detect the RFID tag. For the maximum thickness a horizontally orientated RFID tag achieved a maximum distance of 193 cm with its location at (162; 213; 73) on the positive z-plane and 191 cm on the negative z-plane with its location at (161 ;213; -71). While the vertically orientated RFID tag at also at its maximum thickness achieved a maximum distance of 144 cm with its location at (111; 213; 52) on the positive z-plane and 141 cm on the negative z-plane with its location at (102; 213; -61).

5.4.3.3. Wood

Table 14: Readability of a metal RFID tag using wood inside steel container.

Material: Wood									
Tag used: Metal RFID tag									
Horizontal Orientated Tag					Vertical Orientated Tag				
Thickness	x	y	z	Readability	Thickness	x	y	z	Readability
10	225	137	0	Yes	10	225	137	0	Yes
10	225	213	0	Yes	10	225	213	0	Yes
10	225	137	333	Yes	10	225	137	333	Yes
10	225	213	333	Yes	10	225	213	333	Yes
10	225	137	-310	Yes	10	225	137	-310	Yes
10	225	213	-310	Yes	10	225	213	-310	Yes
					10	128	137	276	Yes
					10	128	213	276	Yes
					10	120	137	-198	Yes
					10	120	213	-198	Yes

Table 15: Readability of a paper RFID tag using wood inside steel container.

Material: Wood									
Tag used: Paper RFID tag									
Horizontal Orientated Tag					Vertical Orientated Tag				
Thickness	x	y	z	Readability	Thickness	x	y	z	Readability
10	225	137	0	Yes	10	225	137	0	No
10	225	213	0	Yes	10	225	213	0	No
10	225	137	333	No	10	141	137	0	Yes
10	225	213	333	No	10	141	213	0	Yes
10	225	137	120	Yes	10	225	137	333	No
10	225	213	120	Yes	10	225	213	333	No
10	225	137	-310	No	10	140	137	42	Yes
10	225	213	-310	No	10	140	213	42	Yes
10	225	137	-61	Yes	10	225	137	-310	No
10	225	213	-61	Yes	10	225	213	-310	No
					10	121	137	-72	Yes
					10	121	213	-72	Yes

As mentioned in the simulations wood performs the best and this was also true in the practical testing. From Table 14, it can be seen that when the maximum number of blocks (ten) of wood was placed on metal RFID tag the RFID reader did detect the RFID tag successfully, in both the horizontal and vertical orientation at positions 3 and 4 for all the positions within the steel container.

From Table 15, it can be seen that when the maximum number of blocks (ten) of wood was placed on the paper RFID tag the RFID reader did detect the RFID tag successfully, in both the horizontal and vertical orientation at positions 3 and 4. When the RFID tag was placed at positions 1,2,4 and 5 the RFID reader unsuccessfully detected the RFID tag. However, when the RFID tag was brought closer to the RFID reader's antenna the RFID reader did detect the RFID tag. For the maximum thickness a horizontally orientated RFID tag achieved a maximum distance of 266 cm with its location at (225; 213; 120) on the positive z-plane and 245 cm on the negative z-plane with its location at (225; 213; -61). While the vertically orientated RFID tag at also at its maximum thickness achieved a maximum distance of 165 cm with its location at (140; 213; 42) on the positive z-plane and 160 cm along the negative z-plane with its location at (121; 213; -72).

5.4.4. Testing procedure in free space

Testing of the RFID system was also carried out in free space. This was necessary in order to determine if placing a RFID system inside a steel container increases or decreases the performance of the system. In order to determine this, the results obtained in the free space testing was used as a benchmark. The apparatus remains the same as discussed before. The free space testing was conducted in a garage. The height and length of the garage was the same as the steel container. The width was however measured and marked off on the floor. Figures 48 to 51 shows the setup used and the environment where the test was conducted. From Figure 49, metal objects such as the metal railing existed in the garage. The surface area of these metal objects only contributed 0.82% towards the total surface area of the garage testing field. This was calculated by first calculating the total surface area of the metal objects and then dividing it by the total surface area of the garage. Therefore, the metal objects are negligible.



Figure 48: Hardware setup using an Alien RFID reader and a laptop.



Figure 49: Sample space used to perform the free space experiments.



Figure 50: Placement of UHF RFID antenna with a 50-ohm connector cable.



Figure 51: Investigate the effects of wood on the RFID system.

5.4.5. Results in free space

5.4.5.1. Steel

Table 16: Readability of a metal RFID tag using steel in free space.

Material: Steel									
Tag used: Metal RFID tag									
Horizontal Orientated Tag					Vertical Orientated Tag				
Thickness	x	y	z	Readability	Thickness	x	y	z	Readability
8	225	137	0	Yes	8	225	137	0	No
8	225	213	0	Yes	8	225	213	0	No
8	225	137	333	No	1	225	137	0	No
8	225	213	333	No	1	225	213	0	No
8	225	137	98	Yes	8	225	213	333	No
8	225	213	98	Yes	8	225	137	333	No
8	225	137	-310	No	1	225	213	333	No
8	225	213	-310	No	1	225	137	333	No
8	225	137	-69	Yes	8	225	213	-310	No
8	225	213	-69	Yes	8	225	137	-310	No
					1	225	213	-310	No
					1	225	137	-310	No

From Table 16, it can be seen that when the maximum number of sheets (eight) of steel was placed on metal RFID tag the RFID reader did not detect the RFID tag successfully, in the horizontal orientation only at positions 3 and 4. The RFID tag was not detected for all positions in the vertical orientated position even when one steel sheet was used.

When the RFID tag was placed at positions 1,2,5 and 6 the RFID reader unsuccessfully detected the RFID tag when it was orientated horizontally. The RFID tag was only detected when the RFID tag was moved closer to the RFID reader's antenna. For a horizontal orientated RFID tag and a thickness of eight the maximum distance is 257 cm with its location at (225; 213; 98) on the positive z-plane and 247cm on the negative z-plane with its location at (225; 213; -69).

From Table 17, it can be seen that when the maximum number of sheets (eight) of steel was placed on the paper RFID tag the RFID reader did not detect the RFID tag successfully, in both the horizontal and vertical orientation at positions 3 and 4. The horizontally orientated RFID tag was detected when it was 90cm away from the RFID reader's antenna for a thickness of eight steel sheets, at a height of 137 cm and 213 cm. When the RFID tag was orientated vertically the RFID reader detected it when it was 53 cm away from the RFID reader for a thickness of one steel sheet, at a height of 137 cm and 213 cm.

When the RFID tag was placed at positions 1,2,5 and 6 the RFID reader unsuccessfully detected the RFID tag. For a horizontal orientated RFID tag and a thickness of one sheet the maximum distance is 123 cm with its location at (89; 213; 38) on the positive z-plane and 119cm on the negative z-plane with its location at (87 ;213; -27). The RFID tag was not detected for positions 1,2,5 and 6 and in the vertical orientated position even when one steel sheet was used.

Table 17: Readability of a paper RFID tag using steel in free space.

Material: Steel									
Tag used: Paper RFID tag									
Horizontal Orientated Tag					Vertical Orientated Tag				
Thickness	x	y	z	Readability	Thickness	x	y	z	Readability
8	225	137	0	No	8	225	137	0	No
8	225	213	0	No	8	225	213	0	No
8	90	137	0	Yes	1	53	137	0	Yes
8	90	213	0	Yes	1	53	213	0	Yes
8	225	137	333	No	8	225	213	333	No
8	225	213	333	No	8	225	137	333	No
1	89	137	38	Yes	1	225	213	333	No
1	89	213	38	Yes	1	225	137	333	No
8	225	137	-310	No	8	225	213	-310	No
8	225	213	-310	No	8	225	137	-310	No
1	87	137	-27	Yes	1	225	213	-310	No
1	87	213	-27	Yes	1	225	137	-310	No

5.4.5.2. Plastic

Table 18: Readability of a metal RFID tag using plastic in free space.

Material: Plastic									
Tag used: Metal RFID tag									
Horizontal Orientated Tag					Vertical Orientated Tag				
Thickness	x	y	z	Readability	Thickness	x	y	z	Readability
10	225	137	0	Yes	10	225	137	0	No
10	225	213	0	Yes	10	225	213	0	No
10	225	137	333	No	10	190	137	0	Yes
10	225	213	333	No	10	190	213	0	Yes
10	225	137	173	Yes	10	225	137	333	No
10	225	213	173	Yes	10	225	213	333	No
10	225	137	-310	Yes	10	225	137	80	Yes
10	225	213	-310	No	10	225	213	80	Yes
10	225	137	-168	Yes	10	225	137	-310	No
10	225	213	-168	Yes	10	225	213	-310	No
					10	225	137	-106	Yes
					10	225	213	-106	Yes

From Table 18, it can be seen that when the maximum number of sheets (ten) of plastic was placed on metal RFID tag the RFID reader did detect the RFID tag successfully, in the horizontal orientation only at positions 3 and 4. However the RFID tag was not detected at positions 3 and 4 when it was orientated vertically. The vertically orientated was only detected when it was moved closer to the RFID reader's antenna. The RFID tag was orientated detected when it was 53 cm away from the RFID reader's antenna for a thickness of ten plastic sheets, at a height of 137 cm and 213 cm.

It was shown that when the RFID tag was placed at position 1 for a horizontally orientated RFID tag the RFID reader detected the RFID tag. However, when it was placed at positions 5 and 6, the RFID reader did not detect the RFID tag. The reason for this was the testing equipment was placed at position 1. This shows that the equipment is reflecting the EM waves towards the RFID tag. When the RFID tag was placed at positions 2,5 and 6 the RFID reader unsuccessfully detected the RFID tag when it was orientated horizontally. In addition, the RFID reader unsuccessfully detected a vertically orientated RFID tag at positions 1, 2, 5 and 6. The RFID tag was only detected when the RFID tag was moved closer to the RFID reader's antenna. For a horizontal orientated RFID tag and a thickness of ten the maximum distance is 294cm with its location at (225; 213; 173) on the positive z-plane and 291cm on the negative z-plane with its location at (225; 213; -168). While the vertically orientated RFID tag at a thickness of ten achieved a maximum

distance of 251 cm with its location at (225; 213; 80) on the positive z-plane and 286 cm on the negative z-plane with its location at (225; 213; -106).

Table 19: Readability of a paper RFID tag using plastic in free space.

Material: Plastic									
Tag used: Paper RFID tag									
Horizontal Orientated Tag					Vertical Orientated Tag				
Thickness	x	y	z	Readability	Thickness	x	y	z	Readability
10	225	137	0	Yes	10	225	137	0	No
10	225	213	0	Yes	10	225	213	0	No
10	114	137	0	Yes	10	104	137	0	Yes
10	114	213	0	Yes	10	104	213	0	Yes
10	225	137	333	No	10	225	137	333	No
10	225	213	333	No	10	225	213	333	No
10	225	137	68	Yes	10	225	137	40	Yes
10	225	213	68	Yes	10	225	213	40	Yes
10	225	137	-310	Yes	10	225	137	-310	No
10	225	213	-310	No	10	225	213	-310	No
10	225	137	-65	Yes	10	225	137	-42	Yes
10	225	213	-65	Yes	10	225	213	-42	Yes

From Table 19, it can be seen that when the maximum number of sheets (ten) of plastic was placed on metal RFID tag the RFID reader did detect the RFID tag successfully, in the horizontal orientation only at positions 3 and 4. However the RFID tag was not detected at positions 3 and 4 when it was orientated vertically. The vertically orientated was only detected when it was moved closer to the RFID reader's antenna. The RFID tag was orientated detected when it was 104cm away from the RFID reader's antenna for a thickness of ten plastic sheets, at a height of 137 cm and 213 cm.

Once again it was noted that when the RFID tag was placed at position 1 for a horizontally orientated RFID tag the RFID reader detected the RFID tag. However, when it was placed at positions 5 and 6, the RFID reader did not detect the RFID tag. The reason again for this was the testing equipment was placed at position 1. This shows that the equipment is reflecting the EM waves towards the RFID tag. When the RFID tag was placed at positions 2,5 and 6 the RFID reader unsuccessfully detected the RFID tag when it was orientated horizontally. In addition, the RFID reader unsuccessfully detected a vertically orientated RFID tag at positions 1, 2, 5 and 6. The RFID tag was only detected when the RFID tag was moved closer to the RFID reader's antenna. For a horizontal orientated RFID tag and a thickness of ten the maximum distance is 247 cm with its location at (225; 213; 68) on the positive z-plane and 246 cm on the negative z-plane with its location at

(225; 213; -65). While the vertically orientated RFID tag at a thickness of ten achieved a maximum distance of 241 cm with its location at (225; 213; 40) on the positive z-plane and 241 cm on the negative z-plane with its location at (225; 213; -42).

5.4.5.3. Wood

Table 20: Readability of a metal RFID tag using wood in free space.

Material: Wood									
Tag used: Metal RFID tag									
Horizontal Orientated Tag					Vertical Orientated Tag				
Thickness	x	y	z	Readability	Thickness	x	y	z	Readability
10	225	137	0	Yes	10	225	137	0	Yes
10	225	213	0	Yes	10	225	213	0	Yes
10	225	137	333	No	10	225	137	333	No
10	225	213	333	No	10	225	213	333	No
10	225	137	180	Yes	10	225	137	122	Yes
10	225	213	180	Yes	10	225	213	122	Yes
10	225	137	-310	Yes	10	225	137	-310	No
10	225	213	-310	No	10	225	213	-310	No
10	225	137	-165	Yes	10	225	137	-180	Yes
10	225	213	-165	Yes	10	225	213	-180	Yes

From Table 20, it can be seen that when the maximum number of blocks (ten) of wood was placed on metal RFID tag the RFID reader did detect the RFID tag successfully, in the horizontal and vertical orientation only at positions 3 and 4.

As explained before it was noted that when the RFID tag was placed at position 1 for a horizontally orientated RFID tag the RFID reader detected the RFID tag. However, when it was placed at positions 5 and 6, the RFID reader did not detect the RFID tag. When the RFID tag was placed at positions 2,5 and 6 the RFID reader unsuccessfully detected the RFID tag when it was orientated horizontally. In addition, the RFID reader unsuccessfully detected a vertically orientated RFID tag at positions 1, 2, 5 and 6. The RFID tag was only detected when the RFID tag was moved closer to the RFID reader's antenna. For a horizontal orientated RFID tag and a thickness of ten the maximum distance is 298 cm with its location at (225; 213; 180) on the positive z-plane and 289 cm on the negative z-plane with its location at (225; 213; -165). While the vertically orientated RFID tag at a thickness of ten achieved a maximum distance of 267 cm with its location at (225; 213; 122) on the positive z-plane and 298cm on the negative z-plane with its location at (225; 213; -180).

Table 21: Readability of a paper RFID tag using wood in free space.

Material: Wood									
Tag used: Paper RFID tag									
Horizontal Orientated Tag					Vertical Orientated Tag				
Thickness	x	y	z	Readability	Thickness	x	y	z	Readability
10	225	137	0	Yes	10	225	137	0	No
10	225	213	0	Yes	10	225	213	0	No
10	225	137	333	No	10	130	137	0	Yes
10	225	213	333	No	10	130	213	0	Yes
10	225	137	97	Yes	10	225	137	333	No
10	225	213	97	Yes	10	225	213	333	No
10	225	137	-310	Yes	10	225	137	31	Yes
10	225	213	-310	No	10	225	213	31	Yes
10	225	137	-40	Yes	10	225	137	-310	No
10	225	213	-40	Yes	10	225	213	-310	No
					10	225	137	-60	Yes
					10	225	213	-60	Yes

Lastly from Table 21, it can be seen that when the maximum number of blocks (ten) of wood was placed on paper RFID tag the RFID reader did detect the RFID tag successfully, in the horizontal orientation only at positions 3 and 4. However the RFID tag was not detected at positions 3 and 4 when it was orientated vertically. The vertically orientated was only detected when it was moved closer to the RFID reader's antenna. The RFID tag was detected when it was 130 cm away from the RFID reader's antenna for a thickness of ten wooden blocks, at a height of 137 cm and 213 cm.

As explained before it was noted that when the RFID tag was placed at position 1 for a horizontally orientated RFID tag the RFID reader detected the RFID tag. However, when it was placed at positions 5 and 6, the RFID reader did not detect the RFID tag. When the RFID tag was placed at positions 2,5 and 6 the RFID reader unsuccessfully detected the RFID tag when it was orientated horizontally. In addition, the RFID reader unsuccessfully detected a vertically orientated RFID tag at positions 1, 2, 5 and 6. The RFID tag was only detected when the RFID tag was moved closer to the RFID reader's antenna. For a horizontal orientated RFID tag and a thickness of ten the maximum distance is 257cm with its location at (225; 213; 97) on the positive z-plane and 241cm on the negative z-plane with its location at (225; 213; -40). While the vertically orientated RFID tag at a thickness of ten achieved a maximum distance of 240cm with its location at (225; 213; 31) on the positive z-plane and 245cm along the negative z-plane with its location at (225; 213; -60).

5.4.6. Discussion

From Table 13 and 15 it can be seen that a horizontally orientated paper RFID tag closely resembles the behaviour of the RFID tag obtained in the Section 5.3.2. The data from Table 13 and 15 is graphical shown in Figure 52 and 53 respectively. In Figure 52, it is shown that the probability for the RFID tag to be detected is low at the center of the container, however when the RFID tag was moved slowly across the container the probability for detection increases. This was expected because the plastic acts like a lens. This was discussed in detail in Section 5.3.2.2, it can be shown that once the EM wave propagates out of the plastic the E-field splits along the centre into two separate E-field lobes. In addition, it was also shown that this effect is more pronounced when the thickness of plastic increases and the E-field also increases as the thickness of the material increases. Hence the probability of detection will increase when the RFID tag moves away from the reader's antenna because the E-field is now been directed towards the reader's antenna. However, there comes a point when this effect produced by the plastic will reduce. This was due to the distance between the RFID tag and reader's antenna increasing to a point where by the loss of E-field due to the distance outweighs the benefits of the lens. This point was at 73 cm in the positive z direction and 71 cm in the negative z direction.

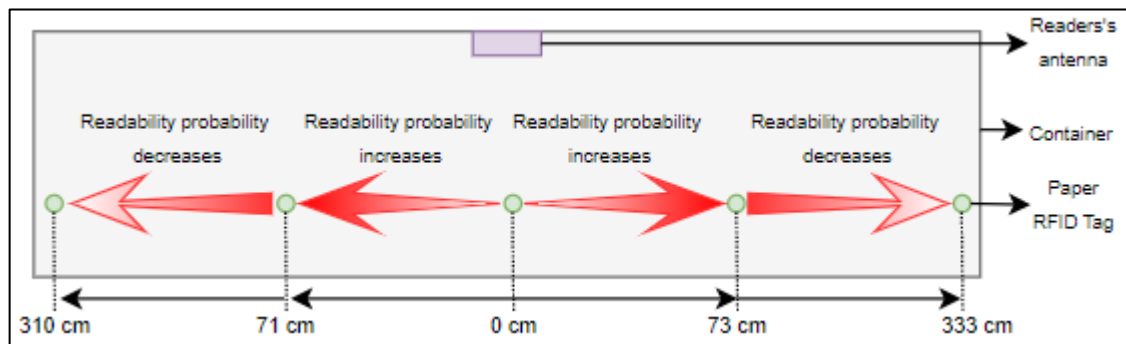


Figure 52: Readability probability for plastic.

In Figure 53, it is shown that the probability for the RFID tag to be detected is high at the centre and the probability decreases when the RFID tag moves away from the center. This was once again expected because the wood also acts like a lens. When the thickness of the wood was increased, the E-field converges at the top of the wood as time increases, as if the E-field is been focused as it propagates through the material. In addition, it was also shown that the E-field does increase as the thickness of the material increases. Hence, this dielectric lens increases the E-field by focusing the E-field at a particular focal-point as it propagates through the material. This means the reader's antenna has a higher probability of detecting the RFID tag when it is placed directly in front of it and the

probability will decrease when the RFID tag is moved away from the reader's antenna. This was discussed in detail in Section 5.3.2.3.

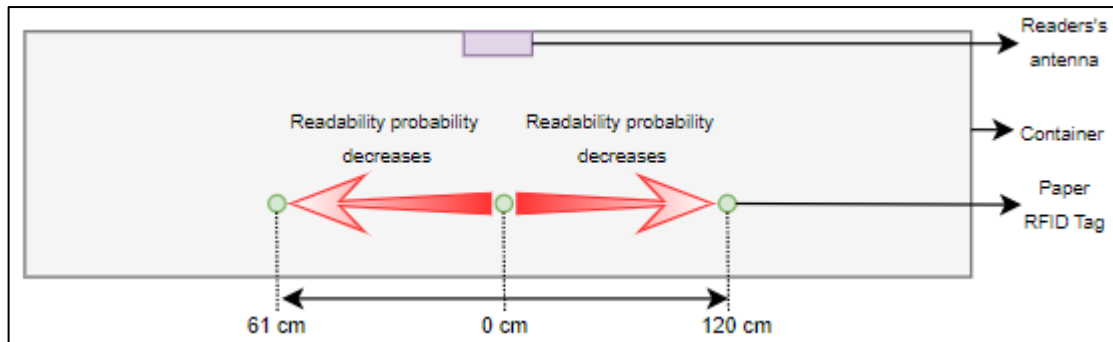


Figure 53: Readability probability for wood.

From Figures 54 to 56, it can be shown that the RFID system performs better in the steel container than in free space. The steel structure of the container aids in reflecting the EM waves inside the steel container. This reflection brings about the super positioning of the EM waves. This means the reflected EM waves undergo constructive and destructive interference, unlike in free space. Constructive interference occurs when two EM waves combine in-phase and produce an EM wave that has twice the amplitude of the two individual EM waves. Destructive interference occurs when the two EM waves combine out-of-phase and cancels each other out resulting in an EM wave with a zero amplitude. Hence it is advised that the RFID tags are placed where the EM waves constructively interfere with each other. Placing of the RFID tag in a horizontal orientation also achieves a higher readability percentage than the vertically orientated RFID tag. In addition, the use of the metal RFID tag increases the readability when compared to the paper RFID tag. The reason why a horizontally orientated RFID tag performs better than a vertically orientated RFID tag is due to the axial ratio of the RFID reader's antenna. As discussed in Section 4.3 the axial ratio of the antenna designed was 0.34 dB. It is also known that if the axial ratio is less than 3dB at 90 degrees for theta and phi, then the antenna is said to be "circularly polarized". However, this is technically not correct. The axial ratio for a perfect circularly polarized antenna is unity (0dB) [75]. This means that the two orthogonal E-field components are of equal magnitude. Even though the axial ratio of 0.34dB is close to 0dB, the polarization is not actually circular but rather elliptical. This means the two orthogonal E-field components are not of equal magnitude. Hence, it is known that the power received by the RFID tag is made up of the electric and magnetic field components. Since the E-field components are not of equal magnitude for an elliptically polarized EM wave, the power that is received by the RFID tag therefore will vary. Therefore, the power received by the RFID tag is dependent on the orientation of it with respect to the reader's

antenna. From the results in Figures 54 to 56, it can be shown the E-field is strongest when the RFID tag is horizontally orientated and weakest when the RFID is vertically orientated with respect to the reader's antenna.

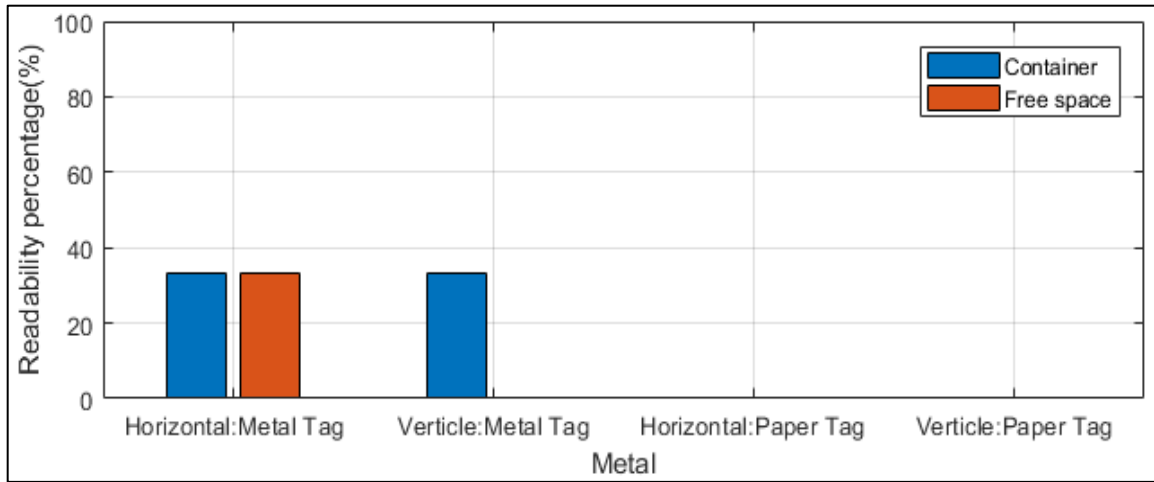


Figure 54: Graph of RFID tag orientation vs readability percentage for steel.

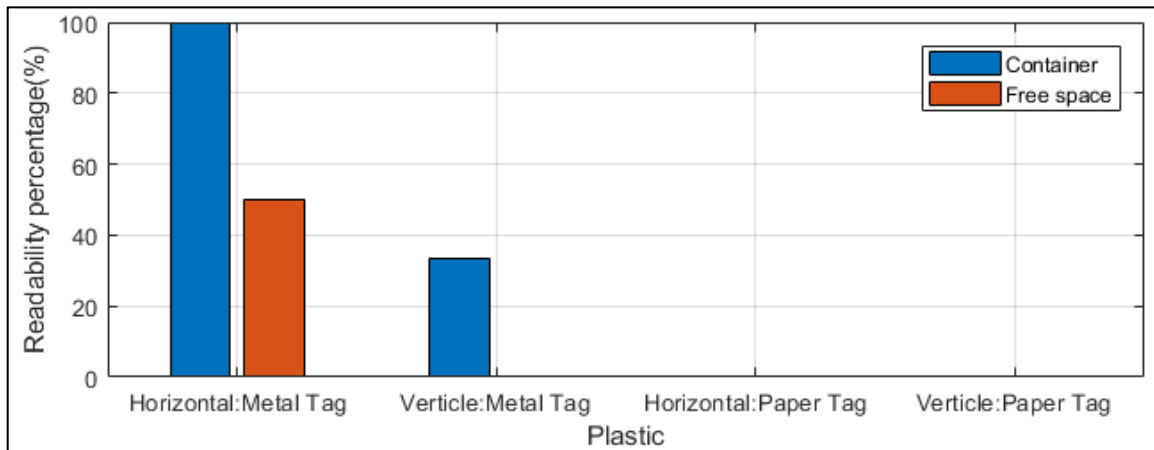


Figure 55: Graph of RFID tag orientation vs readability percentage for plastic.

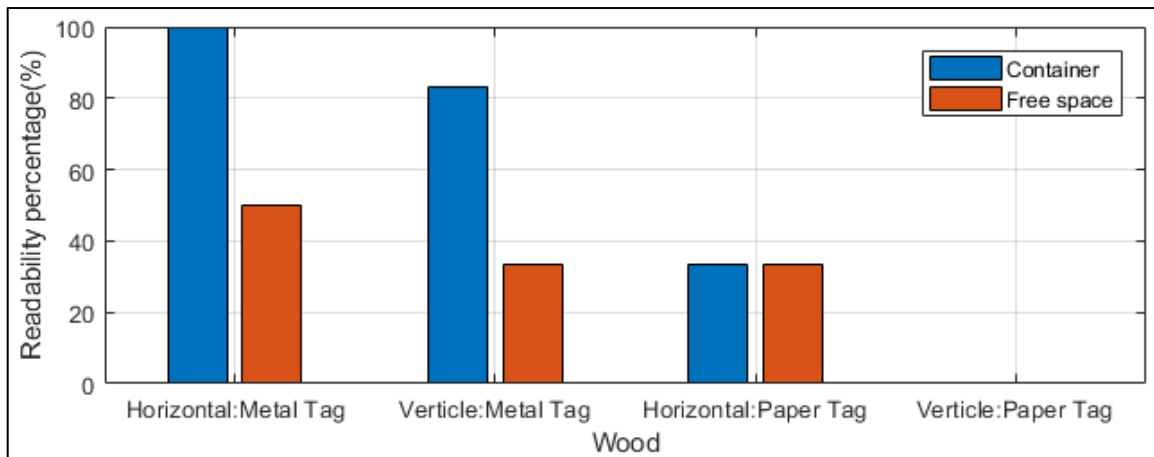


Figure 56: Graph of RFID tag orientation vs readability percentage for wood.

In the instances when the RFID tag was not detected at positions 1,2,5 and 6 the RFID tag was then moved closer to the RFID reader's antenna until it was detected. The worst-case distance measured occurs when a paper RFID tag was used. Figures 57 and 58 shows the distance away from the RFID reader's antenna, when the RFID is detected, in both the positive and negative z-plane for their respective orientation. From Figure 57, it can be shown that wood achieves the best range in both the negative and positive z-planes. This is followed by plastic and then steel. Wood also achieves the best range when the RFID tag is vertically orientated. This is once again followed by plastic and then steel. In addition, the horizontally orientated RFID tag achieves a greater range than the vertically orientated RFID tag. From both Figure 57 and 58 the range for the negative z-plane is always less than the range of the positive z-plane. The reason for this is the directivity of the RFID reader's antenna is not centred at 0 degrees, but rather it is offset to the left at, as shown in Figure 59. This means that the negative z-plane might receive less power than the positive z-plane due to the offset.

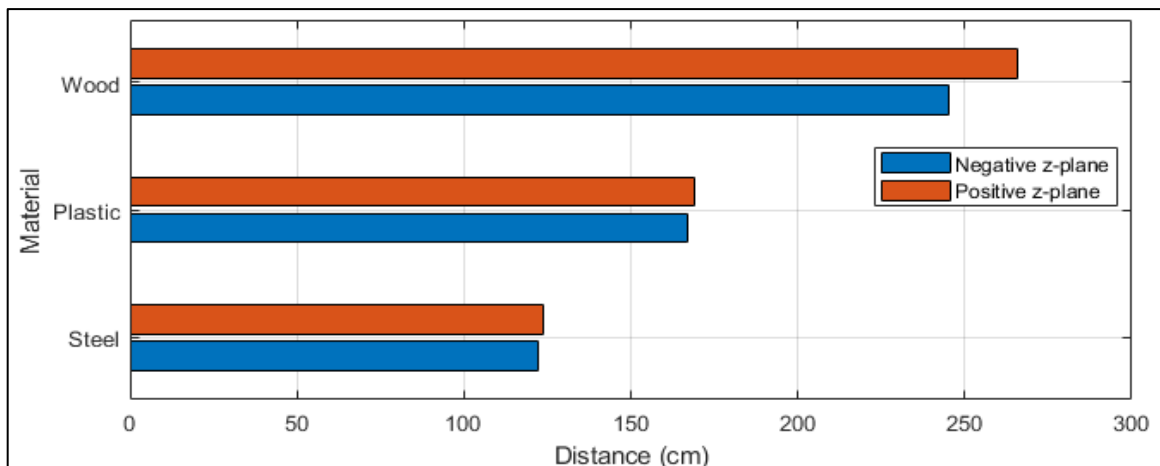


Figure 57: Graph of distance vs material using a paper RFID tag in a horizontal orientation.

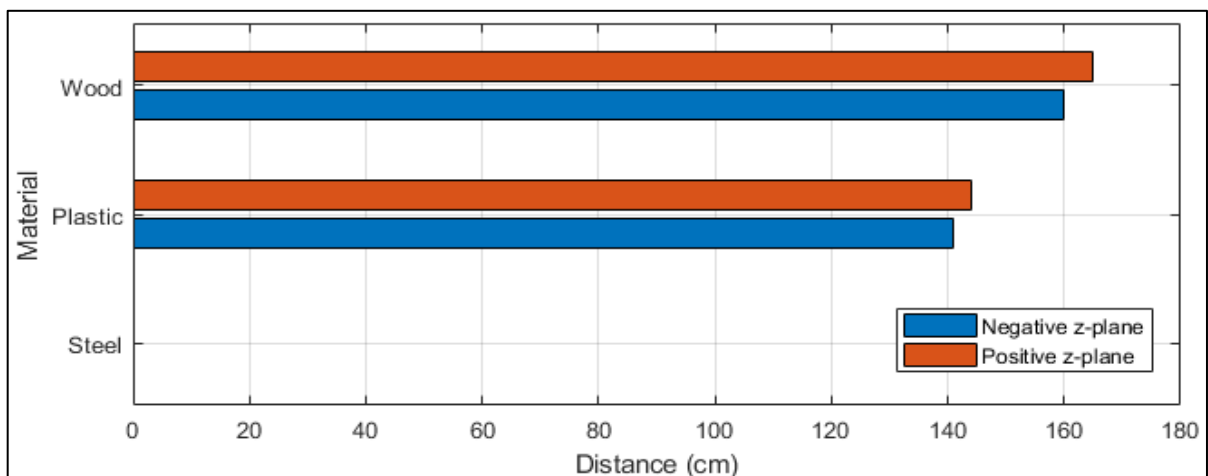


Figure 58: Graph of distance vs material using a paper RFID tag in a vertical orientation.

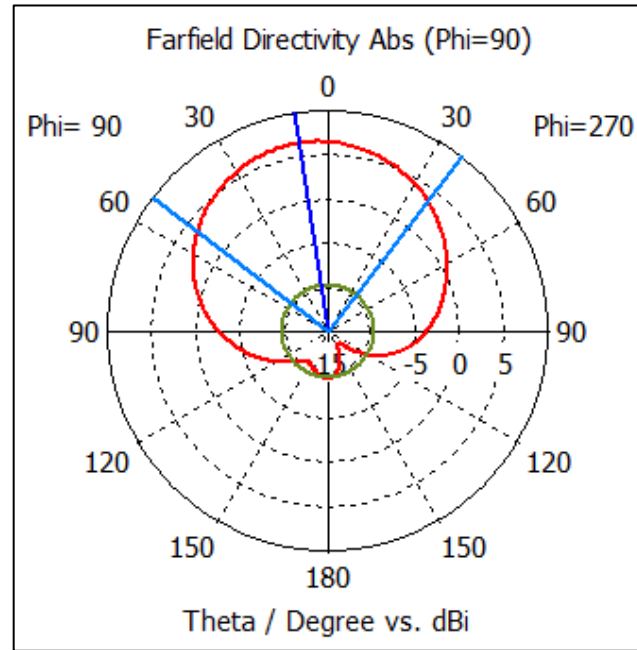


Figure 59: Directivity of the proposed antenna.

6. DISCUSSION AND CONCLUSION

6.1. Research work objectives

This research work investigates how to design and implement a low-cost high-performance vehicle mounted ultra-high frequency (UHF) radio frequency identification (RFID) system to keep track of cargo whilst in transit. The vehicle mounting include – inside or on cargo vehicle enclosures, the shipping containers, and so forth. The UHF RFID system comprised of a UHF RFID reader, multiple UHF RFID circularly polarized antennas and RFID tags. This thesis focused on two objectives. The first objective was to design a low-cost high performance circularly polarized microstrip patch antenna. This was required in order to reduce the overall cost of the UHF RFID system. The second objective was to investigate how the interference caused by different materials affects the performance of the UHF RFID system inside a metal enclosure. In order to ascertain if there is an improvement in the performance of the UHF RFID system, it was benchmarked against free space.

6.2. Summary of all results and validation

Chapter 4 detailed the design of a UHF circularly polarized microstrip patch antenna. Since multiple antennas will be used, it was necessary to develop an antenna that was low cost. By developing a low-cost antenna, it will reduce the overall cost of the entire vehicle mounted UHF RFID system. The overall size achieved was 200mm x 200mm with a thickness of 6.4mm. FR-4 PCB material was chosen because it is a low-cost PCB material. Simulations were then carried using the software tool and the results were recorded. The simulation results showed that the proposed antenna can achieve a bandwidth of 38.73 MHz (886.23 MHz to 924.96 MHz) and an axial ratio of less than 3 dB from 915 MHz to 919 MHz. The maximum gain and directivity achieved was 2.68 dBi and 6.56 dB respectively. The proposed antenna was then fabricated and tested. The fabricated antenna achieved a bandwidth of 57.527 MHz with a minimum reflection coefficient of -27.97 dB at 914.045 MHz. Previous papers did show improvements in their respective designs, in terms of the gain, axial ratio and bandwidth as compared to the antenna designed in this thesis. However, these papers showed that there was always a notably trade-off between having a low axial ratio and a high gain, directivity or bandwidth unlike in this thesis. In addition, the fabricated antenna was implemented at a much lower cost when compared to the commercial UHF circularly polarized antenna.

Chapter 5 looked at how different materials (steel, plastic and wood) of varying thickness degrades the performance of the UHF RFID system. The investigation first started by

using a simulation tool to ascertain the performance of the UHF RFID system. From the simulation results it was concluded that steel offers the worst performance followed by plastic and then wood. It was also noted that plastic and wood exhibit signs that they act as a dielectric lens when EM waves pass through them. Therefore, when plastic was used the lens separates the E-field along the centre, thereby resulting in two separate E-field side lobes. This new resultant e-field also increased by 4.7% (from 0.4917 V/m to 0.5148 V/m) as the thickness of the plastic material increased. Hence, it was concluded that when plastic was placed away from the receiver it was best to use thicker plastic since this does cause a slight increase in the power received at the receiver. When wood was simulated the e-field tends to converge at a focal point as it propagates through the material as the thickness increases. The e-field increase by 62.75% as the thickness was increased from 2 cm to 20 cm and the field varied from 0.757 V/m to 1.232 V/m respectively. Therefore, when this material is used it is best to place it when it is in line with the receiver. These results were then validated using prior research papers. Two papers were used to validate the results. The results from the first paper showed the wood performed the best followed plastic and then metal. It was also noted that placing the RFID tag closer to the material greatly improved the results and it was also concluded that the metal box used in the experiments influences the behaviour of the RFID system in a positive manner. This was also proven to be true in the practical results obtained. The second paper investigated the effects of placing different types of metals in front of a RFID tag. The experiment used mild steel of two thicknesses. One was 1.5mm thick while the other was 1mm thick. The results concluded that the effect of the thicker mild steel negatively affects the performance of the RFID system. The RFID tag placed on the 1mm thick mild steel could be read at 77% of the total 3780 data points while the RFID tag placed on the 1.5mm thick mild steel could only be read at 45% of the total data points. Practical testing was then carried out. These tests were done inside a steel container and also in free space. As expected from the simulations steel performed the worst followed by plastic and then wood. The testing was done using two types of tags (metal and paper RFID tag) and two orientations of the RFID tags (horizontal and vertical). The performance of the UHF RFID system was better inside the steel container than in free space. This was due to the steel container reflecting EM waves. This therefore brings about the super positioning of EM waves unlike in free space. In addition, a horizontally orientated RFID tag performs better than a vertically orientated RFID tag this was due to the nature of the polarization from the reader's antenna. It was also found out that wood achieves the largest range in the positive and negative z-plane, as shown in Figures 57 and 58 when the RFID tag was not detected at positions 1, 2, 5 and 6 as shown in Figures 38.

6.3. Research contribution

The following contributions were made:

1. **Cost benefits** – The contribution made in terms of reducing the cost of the UHF RFID system was discussed in Chapter 4. This section details the design of a low-cost high performance circularly polarized microstrip patch antenna. Table 6 shows that the antenna designed offers a respectable amount of performance in all six parameters. It was also noted that unlike previous antenna designs where comprises existed, the antenna proposed in this thesis achieved a low axial-ratio whilst still offering a relatively high directivity, gain and bandwidth. Table 7 also shows the total cost of designing the proposed antenna as compared to a commercial antenna.
2. **Tracking of containerized cargo while in-transit** – the contribution made in terms of tracking of containerized cargo was investigated in Chapter 5. This chapter used different materials in order to simulate the cargo inside the container. Investigations were carried out to see how the interference caused by these materials affect the performance of the UHF RFID system. The results from these investigations were noted in Section 5.4.

6.4. Recommendations

The following recommendations are shown below:

1. **Number of RFID antennas** – the practical investigation carried out used only one RFID reader's antenna in a 650 cm x 236 cm x 220 cm container. It was noted that when there were no materials obstructing the RFID tag the RFID reader's antenna detected the RFID tag at every position. However, when the materials were placed in front of the RFID tag the reader's antenna did not detect the RFID tag at certain positions. Therefore, it was concluded during practical testing that in order to provide sufficient coverage in the container a number of circularly polarized RFID antennas are required for a 650 cm x 236 cm x 220 cm container. The number of antennas required will be dependent on the cargo that is loaded in the container.
2. **Placing of materials inside the container**
 - a. **Using a metal RFID tag**

From the results noted in this thesis, the following recommendations are made regarding the placement of cargo that is made of steel (metal), plastic and wood inside the container. The use of steel is best used when it is placed directly in line

with the RFID reader's antenna with a maximum thickness of 16mm. However, a greater range can be achieved by reducing the thickness of the steel to 8mm. When using plastic or wood it was noted that the RFID reader's antenna detected the RFID tag at the worst-case positions 1,2,5 and 6 as shown in Figure 38. This shows that these materials do not have a restriction in terms of where they can be positioned within the container.

b. Using a paper RFID tag

The use of the paper RFID tag on steel cargo should only be placed directly in line of the reader's antenna. It is not recommended to place steel cargo to the sides of the reader's antenna. When using plastics, it was noted placing the plastic directly in front of the reader's antenna is not recommended. Plastics should be placed to the sides of the reader's antenna. However, it was noted that when the plastic was placed far away from the reader's antenna, the reader's antenna failed to detect the RFID tag. Therefore, it is recommended to first ascertain the limits of the detection region for plastic cargo before loading other cargo. When using wood, it is recommended to place them directly in line of the reader's antenna. It was noted the reader's antenna failed to detect the RFID tag when it was moved away from the reader's antenna.

3. **Orientation of RFID tag** – from the results it is recommended to place the RFID tag (anti-metal or paper) horizontally with respect to the reader's antenna orientation and not vertically.

6.5. Future research work

1. This thesis only looked at one component to improve the cost of a RFID system. There are still other components such as the RFID reader and the RFID tag that can still be optimised in order to reduce the cost of the system.
2. Multiple RFID tags can be investigated as compared to a single RFID tag.
3. Only three materials were chosen in this thesis to be investigated, namely, wood, plastic and metal. Other materials can also be investigated in order to determine how they affect the performance of the RFID system.
4. More data points can be tested with respect to the practical testing. With a robot [23] more data can be gathered at a quicker and more accurate rate inside the metal enclosure.
5. Only one direction of the RFID signal was taken in account in Section 5.3. Which was from the RFID tag to the RFID reader's antenna. However, further investigations can

be done to demonstrate how the signal propagates from the RFID reader's antenna to the RFID tag.

6. Further investigations can be carried out on larger shipping container such as the 12m long containers.

7. REFERENCES

- [1] K. Finkenzerler, RFID Handbook: Fundamentals and Applications in Contactless Smarts Cards, Radio Frequency Identification and Near-Field Communication, United Kingdom: John Wiley & Sons, Ltd, 2010.
- [2] "Zetes," n.d. [Online]. Available: <https://www.zetes.com/en/technologies-consumables/rfid-in-supply-chain>. [Accessed 08 September 2019].
- [3] "itu.int," [Online]. Available: <https://www.itu.int/en/Pages/default.aspx>. [Accessed 28 February 2020].
- [4] S. Hofmayr , "Analysis and comparison of the potential of RFID-technology in European and U.S. retail supply chains".
- [5] "Behance," 15 July 2018. [Online]. Available: <https://www.behance.net/gallery/67918923/RFID-Tag>.
- [6] R. Store, "medium," [Online]. Available: <https://medium.com/@rufumarcom/your-guide-to-uhf-rfid-tags-8a6fb7400596>. [Accessed 01 May 2020].
- [7] "Passive RFID Tag (or Passive Tag)," [Online]. Available: <http://www.technovelgy.com/ct/technology-article.asp?artnum=47>. [Accessed 2 March 2019].
- [8] B. Ray, "Active Vs. Passive RFID For Location Tracking," Airfinder.com, 28 March 2018. [Online]. Available: <https://www.airfinder.com/blog/active-vs-passive-rfid>. [Accessed 15 March 2019].
- [9] M. Kaur, M. Sandhu, N. Mohan and P. S. Sandhu, "RFID Technology Principles, Advantages, Limitations and Its Application," *International Journal of Computer and Electrical Engineering*, vol. 3, no. 1, pp. 154-155, 2011.
- [10] S. I. Bakhtar and R. S. Dhekekar, "Use of RFID for Safety at School/Hospital Campus," *International Journal of Scientific and Research Publications*, vol. 2, no. 5, p. 3, 2012.

- [11] S. Lewis, "A basic introduction to RFID technology and its use in the supply chain," 2004.
- [12] A. . T. Mobashsher, M. T. Islam and N. Misran, Current Trends and Challenges in RFID, IntechOpen, 2011, p. 90.
- [13] C.-H. Li, K.-W. Lao and K.-W. Tam, "A Flooding Warning System based on RFID Tag Array for Energy Facility," in *IEEE*, Macau, 2018.
- [14] P. V. Nikitin and K. V. Rao, "Performance limitations of passive UHF RFID systems," in *IEEE*, Albuquerque, 2006.
- [15] M. Yu, T. Deng and J. Fu, "Application of RFID and GPS Technology in Transportation Vehicles Monitoring System for Dangerous Goods," in *2nd International Conference on Remote Sensing, Environment and Transportation Engineering*, Nanjing, China, 2012.
- [16] R. Zhang, "Applying RFID and GPS tracker for signal processing in a cargo security system," in *IEEE International Conference on Signal Processing, Communication and Computing (ICSPCC 2013)*, KunMing, China, 2013.
- [17] F. Xi, "Design and Implementation of Logistics Safety Monitoring System based on RFID Technology," in *International Conference on Information Hiding and Image Processing*, Manchester, United Kingdom, 2018.
- [18] J. K. Siror, S. Huanye , D. Wang and W. Jie, "Application of RFID Technology to Curb Diversion of Transit Goods in Kenya," in *Fifth International Joint Conference on INC, IMS and IDC*, Seoul, South Korea, 2009.
- [19] E. Xiaozheng and L. Wenfeng, "The Design and Application of RFID Tag System for Logistical Unit," in *International Conference on Wireless Communications, Networking and Mobile Computing*, Dalian, China, 2008.
- [20] L. Jun'e , Z. Xiaocui and L. Bingwu, "The application of RFID technology in the inventory management," in *International Conference on Signal Processing Systems*, Dalian, China, 2010.

- [21] M. Holmqvist and G. Stefansson, "Mobile RFID - A Case from Volvo on Innovation in SCM," in *Proceedings of the 39th Hawaii International Conference on System Sciences*, Hawaii, 2006.
- [22] D. M. Dobkin and S. M. Weigand, "Environmental effects on RFID tag antennas," *IEEE MTT-S International Microwave Symposium Digest*, pp. 135 - 138, 2005.
- [23] K. Arora , H. Mallinson , A. Kulkarni, J. Brusey and D. McFarlane, "The Practical Feasibility of Using RFID in a Metal Environment," in *IEEE Wireless Communications and Networking Conference*, Kowloon, China, 2007.
- [24] A. J. Mercer, R. K. James, G. Bennett, P. Patel, C. Johnston and J. Cai, "Performance Testing of RFID Systems with RF-Harsh Materials," in *IEEE International Conference on RFID-Technologies and Applications*, 2011.
- [25] D. Dobkin, "The RF in RFID: Passive UHF in Practice," Newnes, 2008, pp. 85-88, 330–332.
- [26] C. A. Balanis, *Antenna Thoery, Analysis and Design*, Hoboken, New Jersey: John Wiley & Sons, 2005.
- [27] G. A. Deschamps and , "Microstrip Microwave Antennas," in *Third USAF Symposium on Antennas*, 1953.
- [28] H. Gutton and G. Baissinot, "Flat Aerial for Ultra High Frequencies". France Patent 703113, N.a N.a 1995.
- [29] R. B. Waterhouse , *Microstrip Patch Antennas: A Designer's Guide*, New York: Kluwer Academic, 2003.
- [30] M. H. Ariff, I. Ismarani and N. Shamsuddin, "Design and development of UHF RFID reader antenna for livestock monitoring," in *IEEE*, 2014.
- [31] V. L. Subrahmanya, *Pattern Analysis of: The Rectangular Microstrip Patch Antenna (M.S thesis)*, University College of Boras, 2009.
- [32] A. K. Varshney, P. S. Reddy, R. Mondal and P. P. Sarkar, "Design of Highly Compact Circular Microstrip Patch Antenna Using Slot in the Ground Plane for Potential WiMAX Application at 2.5GHz," *International Journal of Microwave and Optical Technology*, vol. 15, no. 1, pp. 1-9, 2020.

- [33] M. Mabaso and P. Kumar, "A Dual Band Patch Antenna for Bluetooth and Wireless Local Area Networks Applications," *International Journal of Microwave and Optical Technology*, vol. 13, no. 5, pp. 393-400, 2018.
- [34] M. Mabaso and P. Kumar, "A Microstrip Patch Antenna with Defected Ground Structure for Triple Band Wireless Communications," *Journal of Communications*, vol. 14, no. 8, pp. 684-688, 2019.
- [35] A. E. Hamdouni, A. Tajmouati, J. Zbitou, A. Errkik, M. Latrach and L. Abdellaoui, "Design of CPW Antenna with Fractal Radiating Patch and Slots on the Ground Planes for UWB Applications," *International Journal of Microwave and Optical Technology*, vol. 14, no. 3, pp. 160-165, 2019.
- [36] P. Kumar and J. L. Masa-Campos, "Dual polarized microstrip patch antennas for ultra-wideband applications," *Microwave and Optical Technology Letters*, vol. 56, no. 9, pp. 2174-2179, 2014.
- [37] K. Sharma, D. K. Upadhyay and H. Parthasarathy, "High-Gain Dual-Polarized Resonant Cavity Antenna with Slotted Circular Patch FSS," *International Journal of Microwave and Technology*, vol. 12, no. 4, pp. 239-248, 2017.
- [38] P. Kumar, "Single Feed Dual Polarized Patch Antennas for Ultra-Wideband Applications," *International Review of Electrical Engineering*, vol. 14, no. 4, pp. 284-290, 2019.
- [39] M. S. Ibrahim, "2x2 Circularly Polarized MIMO Antenna at Ka-band for Fifth Generation Applications," *International Journal of Communication Antenna and Propagation*, vol. 9, no. 2, pp. 100-109, 2019.
- [40] M. I. Ahmed, M. F. Ahmed and A. A. Shaalan, "SAR Calculations of Novel Textile Dual-Layer UWB Lotus Antenna for Astronauts Spacesuit," *Progress In Electromagnetics Research*, vol. 82, pp. 135-144, 2018.
- [41] K. R. Rathod and B. K. Mishra, "Low Cost Dual Band Circularly Polarized Textile Antenna Using Electro-textile and Polyester Fabrics," *International Journal of Microwave and Optical Technology*, vol. 14, no. 1, pp. 15-22, 2019.

- [42] A. Kruekaew and C. Phongcharoenpanich, "Linear/Circular Polarization Switchable Antenna for UHF RFID Reader," in *International Symposium on Intelligent Signal Processing and Communication Systems*, 2011.
- [43] D. Duraj, K. Nyka and M. Rzymowski, "Dual Polarization Antennas for UHF RFID Readers," in *20th International Conference on Microwaves, Radar and Wireless Communications*, 2014.
- [44] Z. N. Chen, X. Qing and H. L. Chung, "A Universal UHF RFID Reader Antenna," *IEEE Transactions on Microwave Theory and Techniques*, vol. 57, no. 5, 2009.
- [45] C.-Y.-D. Sim and C.-J. Chi, "A Slot Loaded Circularly Polarized Patch," *IEEE Transactions on Antennas and Propagation*, vol. 60, no. 10, 2012.
- [46] S. Sarkar and B. Gupta, "A Dual Frequency Circularly Polarized UHF-RFID/WLAN Circular Patch Antenna for RFID Readers," in *International Conference on RFID Technology and Applications (RFID-TA)*, pp. 448 - 452, Pisa, Italy, 2019.
- [47] D. M. Pozar, "Microstrip Antennas," *Proc. IEEE*, vol. 80, no. 1, pp. 79-81, 1992.
- [48] R. Garg, P. Bhartia, P. Bahl and A. Ittipiboon, *Microstrip Antenna Design Handbook*, Artech House, 2001.
- [49] M. Shakeeb, "Circularly Polarized Microstrip Antenna," 2010.
- [50] R. Garg, P. Bartia, I. Bahl and A. Ittipiboon, *Microstrip Antenna Design Handbook*, Norwood: Artech House Inc., 2001.
- [51] S. Verma and J. A. Ansari, "Analysis of U-slot loaded truncated corner rectangular microstrip patch antenna for broadband operation," *International Journal of Electronics and Communications*, vol. 69, no. 10, pp. 1483-1488, 2015.
- [52] "antenna-theory," [Online]. Available: <http://www.antenna-theory.com/basics/efficiency.php>. [Accessed 11 January 2020].
- [53] X. Y. Huo, J. H. Wang and M. E. Chen, "Circularly Polarized Microstrip Antenna with Two Asymmetric Circular Slots for RFID Application," in *International Conference on Microwave Technology and Computational Electromagnetics*, pp. 184 - 187, Qingdao, China, 2013.

- [54] C.-H. Yeh, B.-S. Chen, C.-C. Chen and C.-Y.-D. Sim, "L-Shaped Probe Feed Patch Antenna with Circular Polarization Radiation for UHF RFID Applications," in *IEEE MTT-S 2015 International Microwave Workshop Series on RF and Wireless Technologies for Biomedical and Healthcare Applications (IMWS-BIO)*, pp. 214 - 215, Taipei, Taiwan, 2015.
- [55] K. Nuangwongsa and K. Miyai, "Corner Truncated Patch Circularly Polarized Antenna for UHF RFID Applications," in *International Conference on Electrical Engineering/Electronics, Computer, Telecommunications and Information Technology (ECTI-CON)*, pp. 433 - 436, Chiang Rai, Thailand, 2018.
- [56] M. I. Sabran, S. K. A. Rahim, M. S. A. Rani and M. Z. M. Nor, "A Single Band Dual-Fed Circular Polarization Microstrip Antenna for RFID Application," in *IEEE International RF & Microwave Conference*, pp. 137 - 140, Seremban, Negeri Sembilan, 2011.
- [57] J. M. Lee, N. S. Kim and C. S. Pyo, "A Circular Polarized Metallic Patch Antenna for RFID Reader," in *Asia-Pacific Conference on Communications*, pp. 116 - 118, Perth, Australia, 2005.
- [58] C. Phongcharoenpanich and S. Dentri, "Circularly Polarized UHF-RFID Antenna using Defected Rectangular Plate on the Ground Plane," in *IEEE Asia-Pacific Conference on Antennas and Propagation*, pp. 1 - 2, Singapore, 2012.
- [59] J.-H. Lu and H.-M. Chin, "Planar Circularly Polarized Circular Antenna with Clover Slot for RFID System," in *International Symposium on Antennas and Propagation (ISAP)*, pp. 420 - 421, Okinawa, Japan, 2016.
- [60] C. Phongcharoenpanich , K. Lertsakwimarn , R. Sukkamat , N. Mhudtongon , S. Kosulvit and P. Akkaraekthalin, "Design of circularly polarized unidirectional antenna using probe-excited circular ring antenna above the square reflector with inserted metallic slabs," in *International Symposium on Antennas and Propagation (ISAP)*, pp. 962 - 963, Okinawa, Japan, 2016.
- [61] "Taggit SA," n.d. [Online]. Available: <https://taggitsa.co.za/>. [Accessed 17 September 2019].

- [62] "Pay Scale," [Online]. Available: https://www.payscale.com/research/ZA/Job=Electronics_Technician/Salary. [Accessed 06 January 2020].
- [63] "mantech," [Online]. Available: <https://www.mantech.co.za/ProductInfo.aspx?Item=82M1296>. [Accessed 03 May 2020].
- [64] C. J. Cela, "3. The Finite-Difference Time-Domain Method (FDTD)," University of Utah, Utah, 2012.
- [65] M. N. Sadiku, "Maxwell's Equations," in *Elements of Electromagnetics*, New York, Oxford University Press, 2011, p. 406.
- [66] A. Taflove and S. C. Hagness, *Computational Electrodynamics: The Finite-Difference Time-Domain Method*, Norwood: Artech House, Inc, 2000.
- [67] I. Giannakis, A. Giannopoulos and C. Warren, "gprMax: Open source software to simulate electromagnetic wave propagation for Ground Penetrating Radar," *Computer Physics Communications*, vol. 209, pp. 163-170, 2016.
- [68] D. Liu, R. Wang, K. Yao, X. Zou and L. Guo, "Design and Implementation of a RF Powering Circuit for RFID Tags or Other Batteryless Embedded Devices.," *MDPI*, vol. 14, no. 8, pp. 14839-14857, 2014.
- [69] J.-Y. Jung, H. Kim, H.-S. Lee and K.-W. Yeom, "An UHF RFID Tag with Long Read Range," in *European Microwave Conference*, Rome, 2009.
- [70] Z. N. Chen, D. Liu, H. Nakano, X. Qing and T. Zwick, *Handbook of Antenna Technologies*, Singapore: Springer Nature, 2016.
- [71] A. L. Bleda, G. Santa, A. J. Jara, R. Maestre and A. G. Skarmeta, "Evaluation of the electromagnetic absorption in furniture for the integration of UHF-RFID tags," in *IEEE International Conference on RFID-Technologies and Applications*, Sitges, Spain, 2011.
- [72] J. Meli`a-Segu`ı and R. Pous, "Human-object Interaction Reasoning using RFID-enabled Smart Shelf," in *International Conference on the Internet of Things (IOT)*, 2014.

[73] T. 7, "Times-7 | Multiplexer vs Power Divider," Times-7.com, 24 June 2018. [Online]. Available: <https://www.times-7.com/blog/2018/06/24/multiplexer-vs-power-divider/>. [Accessed 15 June 2019].

[74] "An Intro to RFID Readers Basics and Features," atlasRFIDstore.

[75] W. L. Stutzman and G. A. Thiele, Antenna Theory and Design, Hoboken, New Jersey: John Wiley & Sons, Inc, 2013.